TECHNISCHE UNIVERSITÄT WIEN
Vienna University of Technology

Dissertation

Fission Track – Laser Ablation Inductively Coupled Plasma Mass Spectrometry for the Spatially Resolved Isotope Ratio Measurements of Uranium microparticles in Safeguards Environmental Samples

Ausgeführt zum Zwecke der Erlangung des akademischen Grades einer

Doktorin der Naturwissenschaften

unter der Leitung von

Associate Prof. Dipl.-Ing. Dr.techn. Andreas Limbeck
Institut für Chemische Technologien und Analytik
TU Wien

PD Dr. Sergei Boulyga
SGAS, Abteilung für Safeguards,
Internationale Atomenergiebehörde

und

Ernesto Chinea-Cano M.Sc
SGAS, Abteilung für Safeguards,
Internationale Atomenergiebehörde

eingereicht an der Technischen Universität Wien

Fakultät für Physik

von

Naida Dzigal, M. Sci in Physik
Matrikelnummer: 1228695

Wien, 6. März 2017

Abstract

The aim of this work is to implement a fission track based micro-artefact identification methodology as a tool for characterizing environmental samples of SG interest, followed by their analysis by laser ablation mass spectrometry. The main outcome is the advancement and improvement of the micro particle handling strategies for the fission track method and related techniques.

As part of this work, an in-depth evaluation of current sample preparation techniques used at analytical laboratories for the identification and extraction and handling of micron-sized dust particles was conducted. A shock-wave based particle dispersion device was designed, constructed and compared to existing sampling methods. This device was thereafter used in the preparation of fission track samples. Fundamental improvements to the FT methodology, including the SSNTD selection, the etching optimization and a 3-point based relocation algorithm were implemented. The latter was used as part of a correlative microscopy methodology devised for the backtracking of detected FTs to their originating particles of interest (POIs). After this, a semi-automated laser-micro-dissection technique was used for the isolation of POIs. An investigation of the capabilities of a ns laser ablation quadrupole ICP-MS for the analysis of uranium isotopes of in micron-sized particles was completed. This resulted in a novel approach to the data evaluation strategy for transient MS signals.

Abstrakt

Ziel dieser Arbeit war es, eine Mikro-Artefakt-Identifikationsmethodologie zu entwickeln und implementieren als Methode zur Charakterisierung von Mikropartikeln in sogennanten Safeguards Environmental Swipe Samples (Safeguards Wischproben). Dem folgte die Analyse durch Laserablations-Massenspektrometrie. Das wichtigste Ergebnis ist die Weiterentwicklung und Verbesserung der Mikropartikel-Handhabungsstrategien für die Spaltspurenmethode (FT) und ähnliche Techniken.

Als Teil dieser Arbeit wurde eine eingehende Bewertung der aktuellen Probenvorbereitungstechniken durchgeführt, die in weltweiten analytischen Laboratorien zur Identifizierung, Extraktion und Handhabung von mikrometergroßen Staubpartikeln verwendet werden. Eine stoßwellenbasierte Partikeldispersionsgerät wurde konstruiert, und mit bestehenden Probenahmeverfahren verglichen. Dieses Gerät wurde danach bei der Herstellung von Spaltspurproben verwendet. Grundlegende Verbesserungen der FT-Methodik, einschließlich der SSNTD-Auswahl, der Ätzoptimierung und eines 3-Punkt-basierten Verlagerungsalgorithmus wurden implementiert. Letzteres wurde als Teil einer Korrelatmikroskopie-Methodik verwendet, die für die Rückverfolgung von detektierten Spaltspuren zu ihren Ursprungspartikeln entwickelt wurde. Danach wurde eine halbautomatisierte Lasermikrodissektionstechnik zur Isolierung von POIs eingesetzt. Eine Untersuchung der Fähigkeiten eines ns-Laserablations-Quadrupols ICP-MS für die Analyse von Uranisotopen in Mikrometer-Partikeln wurde abgeschlossen. Dies führte zu einem neuartigen Ansatz zur Datenbewertungsstrategie für transiente MS-Signale.

Acknowledgements

As is customary to most PhD dissertations, the acknowledgements are left for the very end as one of those things that you need to tick off a requirements list. In that fashion, one usually happens to end up writing it at 3 am on an extremely cold and snowy night, imagining oneself bathing in sunlight on a beach of a distant island. This time is no exception and yet, without their help, this dissertation, that has become ever-consuming of all aspects of my life, could never have inspired the dream of swimming with dolphins I have continuously had for the past months.

Having said that, I cannot think of a better comparison of this PhD than my journey to Uhuru Peak on Mt. Kilimanjaro. "Pole, pole" ("slowly, slowly" in Swahili) is what our guide made us repeat after him each and every day. "Think only of the next step and you will climb to the top of Africa", he would say. Summit I did – on June 14th, 2013, and achieved a dream. Looking back, it changed the way I approach everything: with enough preparation, mental strength and at my own pace, I can do anything.

I am first and foremost deeply indebted to my mother, a single mother of three and a PhD graduate herself (although in Electrical Engineering). Her sweat has motivated my sweat; her tears have fuelled my tears. "Education and the continuous pursuit of knowledge is everything and no one can take that away from you", she would always say. I see and I do mama.

Secondly, I would not be half the person I am without my little sister. Her dedicated work ethic, perceptive talks and interminable energy have made me question whether we share the same gene pool as I am less and less able to keep up with her over the years. I guess we'll find out once I have gotten this out of the way. The same goes for my brother, the third musketeer: I cannot wait to have more time for both of you again.

Thirdly, my day-to-day supervisor throughout, Ernesto Chinea-Cano of the IAEA, a brilliant scientist and extra-ordinary type of human being I have aspired to be like since the second time we met in 2012. Rome was not built in a day and you have taught me that everything takes time. Today I know how right you always were: the axis of this project was formed years ago together with Uri Admon and to both of them I owe having a firm basis to build upon.

Fourthly, thanks to my family at the IAEA: Olivier Bildstein, Sergei Boulyga, Maria Hedberg, Joseph Hiess, Amirul Islam, Alla Kist, Andreas Koepf, Alexander Knott, Stefanie Konegger-Kappel, Zsuzsanna Macsik, Jane Poths, Ariana Rugova-Alihajdaraj, Laure Sangely, Axel Schwannhäuser Guillaume Stadelmann, Thippatai Tanpraphan, Beata Varga, Stephan Vogt, Madrim Warsosumarto, Stephen Walsh and Darek Wegrzyneck. Special thanks to Yusuke Kuno, the SGAS Director, who encouraged me to further the fission track project. Steffi, Zsuzsi and Alex know too well the struggles we PhD students go through: thank you all for your advice and never-ending supply of coffee and sweets. To my Women-in-Nuclear family: thank you for inspiring me to continue pursuing a career in science ladies!

To Gabrielle Voigt, a statuesque figure and Bavarian woman who held all the strings, even those you may not realise she possessed, I am humbled by your informal mentorship and would like to reiterate my appreciation for the opportunity to start this 4-year journey back in late 2012. What a guardian you have been.

And last but not least, Andreas Limbeck and the Division of Instrumental Analytical Chemistry at the Vienna University of Technology took me in when I was left orphaned. Maximilian Bonta and Felix Horak, thank you guys for the discussions, chocolate boxes left to surprise me on my desk and especially your insights during kitchen coffee sessions. To Andreas Limbeck's kindness and openness I am forever grateful and most definitely deeply indebted.

A final shout-out to all my friends: thank you all for motivating me to push through this, keeping me grounded along the way: I could not have done it without you by my side.

Foreword

This manuscript is based on the work conducted as part of 9 publications and poster presentations (see publication list at the end of this work). It should serve as a complete guide to all developments conducted as part of this PhD towards the improvement of the Fission Track method for safeguards, written as a single monograph (All the material found here has been previously published). Without the help, guidance and countless discussions with Ernesto Chinea-Cano, Andreas Limbeck, and Stephen J. Walsh none of the publications would have seen daylight in their current state. For this reason, I am hugely indebted to all of them and thank them for their support, but also hope we will continue collaborating on similar projects in the future.

Chapter 1: Introduction

Where Science Met Politics: Nuclear Weapons and WWII

As the finale of WWII was being played out, it became clear that the political alignment and social structures of the world would never be the same again after 1945. The detonation of Little Boy and Fat Man in Hiroshima (6th of August 1945) and Nagasaki (9th of August 1945) in their role of forcing The Empire of Japan to surrender to the Allies is to this day still debated. For the purpose of preventing a similar scenario to WWII, the United Nations Organisation was finally established on October 24th 1945 with the primary goal of preserving international peace and security [1].

Even though the role of nuclear bombs in ending WWII is questioned to this day, one thing is clear: they started a novel trend of deterrence where the state with nuclear weapons always had the upper hand in an international dispute. This technology was the result of the Manhattan Project, a secret military project that started in 1942 for the purpose of beating Nazi Germany and making the first US nuclear weapon [2]. After the explosions in the cities of Hiroshima and Nagasaki, the rest of the world became acquainted with the power and impact of nuclear weaponry, soon thereafter calling it the most dangerous weapon known to mankind. During the bombings, approximately 130,000 people were killed and hundreds of thousands were injured – but the consequences of radiation were apparent in survivors for decades, spreading onto the next generation. The destructiveness of nuclear weapons was evident and the world had to come together to prevent such destruction in the future.

The Birth of Safeguards

The detonations of Little Boy and Fat Man were extremely unfortunate events, so as President Eisenhower took the stage during a meeting of the United Nations' General Assembly in 1957, he instigated the establishment of the Atomic Energy Agency with the

primary goal of serving the peaceful pursuits of mankind in the nuclear field. Such an organisation had dual responsibilities:

1. to promote the safe and peaceful use of nuclear energy and

2. to provide assurances that nuclear energy is not being misused for non-peaceful purposes [3, p. 15]

This organisation became to be known as the International Atomic Energy Agency (IAEA) and its principal objective was defined as to help in the acceleration and expansion of the peaceful uses of atomic energy throughout the world, but at the same time ensuring, to the best of its abilities, that the transfer of such knowledge does not further any military purpose [4]. The IAEA thus proceeded to conclude agreements with the State or States concerned which refer to the application of safeguards under article [3, p. 15].

Safeguards applied by the IAEA are an important element of the global nuclear non-proliferation regime on every scale. For example, states and governments need not necessarily be the initiators of weapons-grade enrichment or other rogue activities and the implementation of timely inspections can act as an asset not only to the international community, but also to the state in question. All IAEA Member States recognise the need for verification, as well as for the timely detection of rogue activities and this is where the safeguards system plays an instrumental role in the IAEA, the United Nations and therefore in the preservation of world peace.

Initially the prevalent concern of the IAEA of non-peaceful use of nuclear technology was being discussed in the 1960s and 1970s where nuclear energy technology was emerging as a result of the world electricity dilemma – [5, p. 253] notes that *"the introduction of any major technological innovation may entail new problems and uncertainties equal to, or greater than, those which the innovation is supposed to resolve".* [5] sees the importance of verification in the nuclear industry as a prevention mechanism for proliferation, but also

Figure 1: At a machine tool factory, an IAEA inspector takes a swipe sample (as part of the Iraqi nuclear program dismantlement). Photo credits: Pavlicek, IAEA, http://www.iaea.org/newscenter/multimedia/photogallery/photo-gallery-iaea-action-team-inspectors-december-2002

recognizes the important role nuclear energy will have in the upcoming decades in replacing fossil fuels in electrical energy production. The dangers of nuclear weaponry were evident in 1945 and in the nuclear arms race that followed, so the introduction of nuclear energy was met with great concerns about safety and security. If countries cannot do without nuclear energy, they have to learn how to deal with accompanying ethical obligations. The international community is primarily concerned with the "bootleg bomb scenario" where [5] outlines that with increased nuclear power plants proliferation, it will become easier for nations to construct nuclear bombs because the same material used in power plants can be used in bombs and the technical expertise for constructing bombs is readily accessible (and is not as complex as one might think). Exactly this is the safeguards problem: "how to insure that nuclear materials will not be diverted to nuclear weaponry?" [5, p. 254] [6, p. 179]

As it so happens, there is no generally accepted strategy, but rather a set of methods. All aspects of the IAEA safeguards department deal with one of the following: collecting samples for bulk or particle analysis; the characterization of these samples using different instruments in the laboratories; and the long-term statistical analysis and collection of these data. An interim short report on IAEA Safeguards in 1981 showed that safeguards is a fluid

and unpredictable mission that had to be adjusted each time a new nuclear technology was discovered. Specifically, this means that the safeguards analytical techniques used for the assessment of U enrichment in nuclear fuel rods cannot necessarily be used for the characterization of trace element composition of uranium ore samples. This grow in analytical needs requested the construction of a Safeguards Analytical Laboratory (SAL) for the characterization of an ever-growing number of nuclear material samples in the 1970s. SAL was commissioned in 1976 and has included techniques such as emission spectrography and thermal ionization mass spectrometry (TIMS). At the same time, since the number and type of different samples steadily increased together with the expansion of the nuclear industry and growth of safeguards activities, the IAEA requested its Member States to offer their analytical capabilities for verification purposes [7]. This NetWork of Analytical Laboratories (NWAL) had as its main objective to provide measurements for the evaluation of the facility operator's accounting data by the Safeguards Analytical Laboratory and to assist in the evaluation of these results through paired comparison [7].

The establishment of the IAEA NWAL was originally, in the 1970s, for the purpose of only analysing nuclear material samples (such as spent fuel) [8], but since 1998 the scope expanded to include inspectors sweeping surfaces (taking environmental samples) after these were shown to be a useful source of information during the dismantling of the Iraqi Nuclear Program (1991-1998) [9] [10]. The number of environmental samples has been growing steadily since 1998 and the analysis of such samples falls under the practice named particle analysis and characterization.

Safeguards in Practice

As one of the objectives of the IAEA, it was agreed that safeguards would be applied to verify a State's compliance by implementing a comprehensive safeguards agreement (CSA). The State therefore complies to accept safeguards on all nuclear material in all its peaceful nuclear activities and to verify that such material is not diverted to the proliferation of

nuclear weapons or other nuclear explosive devices [3, p. 11]. In this regard, the technical objective is specified: *"the timely detection of diversion of significant quantities of nuclear material from peaceful nuclear activities to the manufacture of nuclear weapons or of other nuclear explosive devices or for purposes unknown, and deterrence of such diversion by the risk of early detection"* [3, p. 11]. Furthermore, [3] notes that in order to "*address fully the verification of a State's compliance with its undertaking under a CSA, a second technical objective is pursued, viz. the detection of undeclared nuclear material and activities in a State"*. The verification is a lengthy process where IAEA inspectors travel to nuclear facilities and take samples of nuclear material directly from where these are handled, as well as swipes of the environment at the facility and all are then sent to a worldwide network of labs for testing. The origin of the samples is undisclosed for the purpose of unbiased measurement and each sample is measured by two independent labs. The results are collected in a database at the IAEA Headquarters in Vienna.

Environmental Sample Analysis (ESA) [10]

While the active implementation of safeguards was in its early stages, the so-called bulk analysis of samples was the only type of analysis conducted. At that time, sampling or swiping of the environment within nuclear facilities was not conducted and therefore the samples that inspectors sent back to Vienna were limited in what they could test and thus detect. Bulk analysis allows for an average enrichment of, for instance, a uranium ore sample to be identified and an outlier of a 20% enriched particle can be statistically justified. By taking samples of the whole environment – from the hands and wardrobes of managers to the dust in laboratory corners, IAEA analysts are able to construct a more comprehensive picture of the undertakings of a certain facility by simply increasing the number of sampling locations and therefore samples taken. In conclusion, bulk, or destructive analysis of nuclear material samples is used to support nuclear material accountancy for the correctness of States' declarations whereas the primary goal of environmental sample analysis is to search

for evidence of undeclared materials and activities for the completeness of States' declarations.

By that logic, the environmental sampling for safeguards (ESS) programme of the IAEA has been implemented since 1998 as a strengthening measure to detect undeclared nuclear materials or activities in safeguarded States. A collection of various analytical techniques has been deployed in the network of analytical laboratories (NWAL) in the Member States [10]:

1. Bulk analysis of U, Pu and other elements in an inspector's sample at ultra-low levels of detection and

2. Precise isotopic ratio analysis of U or Pu containing particles as small as 1 μm in diameter.

The IAEA laboratories in Seibersdorf, Austria, have in the past decades, expanded the instrumentation supporting such analyses to include the following techniques:

1. Thermal Ionisation Mass Spectrometry (TIMS)

2. Large-Geometry Secondary Ion Mass Spectrometry (LG-SIMS)

3. Inductively Coupled Plasma Mass Spectrometry (ICP-MS)

4. Multi-Collector Inductively Coupled Plasma Mass Spectrometry (MC-ICP-MS)

5. Femtosecond Laser Ablation Inductively Coupled Plasma Mass Spectrometry (fs-LA-ICP-MS)

6. Focused Ion Beam Scanning Electron Microscopy Time-of-Flight SIMS (FIB-SEM-TOF)

The accuracy and sensitivity of sample characterisation is essential not only for verification purposes, but also as a trust-building measure within the international community. That is why such high priority must be given to the preservation of the unbiased handling of each and every sample – from the preparation of inspectors' sampling kits, to the collection of samples at facilities and finally to the prevention of cross-contamination during the analysis and reporting.

Finally, the importance of single environmental hot particle characterization is seen in the wealth of information that it carries: the analysis of a single particle can deliver clues about its radiological, chemical and metallurgical past, including hints about its release-scenario [11]. The ability to locate, handle and analyse single, isolated particles is essential in the arenas of nuclear forensics and environmental research and these should be *analysed individually rather than as agglomerates, because the latter invariably display averaged values, such as speciation or radionuclide dispersion in environmental samples or enrichment levels in safeguards samples* [11].
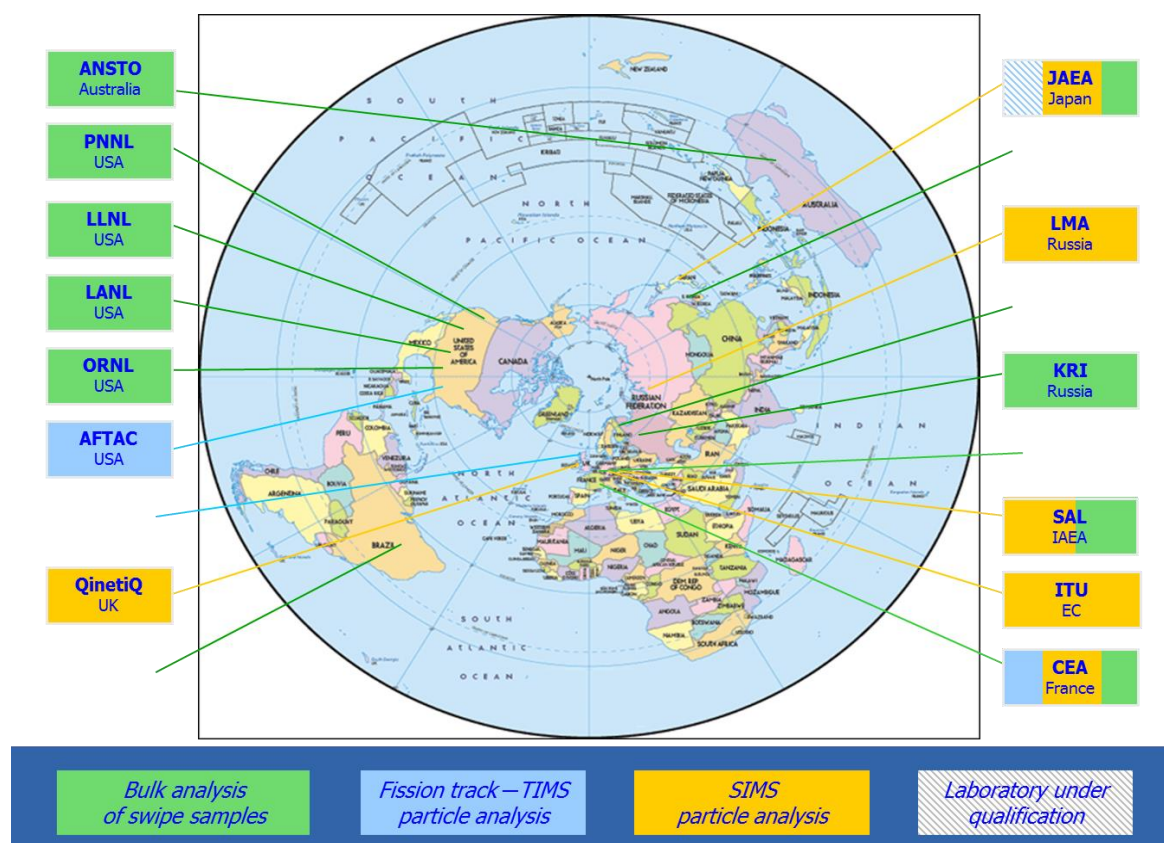
Figure 2: NWAL Capabilities for Environmental Sampling (Donohue, 2006)

Scope and Aim of This Work

The aim of this work was to implement the FT-LA-ICP-MS method in SGAS and demonstrate it can be used as a routine tool for the analysis of individual micro-artifacts of SG interest. The main expected outcome is the advancement of the particle handling strategies, automation of steps and overall improvement of environmental sample analysis for safeguards. This contribution seeks to empower further the IAEA's capabilities in detecting undeclared nuclear activities and to strengthen the IAEA's resources towards the goal of verification and trust-building activities amongst Member States.

The following topics will be covered in the next chapters:

1. **Chapter 2** is an in-depth discussion of current sample preparation techniques used at analytical laboratories for the extraction and handling of micron-sized dust particles from environmental swipes. It includes the details of a shock-wave based particle dispersion device that was designed and constructed as part of this work. It finishes with a comparison of the shock-wave disperser to existing sampling methods, justifying our use of the shock wave disperser in this work;

2. **Chapter 3** includes fundamental improvements to the fission track (FT) methodology. The sample preparation introducing a catcher and harvester is a fundamental achievement of this work. Detectors were chosen based on considerations regarding the manufacturing process and material, but also due to their geometry for the purpose of etching optimization.

3. **Chapter 4** discusses a correlative microscopy methodology which was devised for the backtracking of detected FTs to their originating particles of interest (POIs). This chapter furthermore includes details of a semi-automated laser-micro-dissection technique used for the isolation of identified POIs;

4. **Chapter 5** is an investigation of the capabilities of a ns laser ablation (ns-LA) as a sample introduction device to a quadrupole ICP-MS for the isotope ratio analysis of

uranium containing micron-sized particles. It also gives insight to a novel treatment of transient signals for the purpose of an operator-independent evaluation of isotope ratios in POIs.

5. **Chapter 6** is a discussion of the significance of these results for safeguards and related fields. The suggested methodology for POI isolation is readily applicable to other than LA single particle analytical techniques (e.g. LG-SIMS, TIMS, SEM-EDX).

Highlights may be summarized as follows:

1. It is, to the author's best knowledge, the first attempt at evaluating and summarizing the current state of sample preparation techniques used and it proposes a novel sample dispersion technique for micron-sized particles; "On the Dispersion of Particles on Flat Substrates for Microprobe Analysis Techniques" (Journal of Nuclear Materials Management, December 2015)

2. It identifies current trends in technology, thus bringing major improvements to the identification and tagging of particles of interest in ESA; "Correlative Microscopy Techniques for the Analysis of Particles in Safeguards Environmental Samples" (Journal of Physics: Conference Series 644, June 2015)

3. It evaluates the use of multiple fission track detectors (SSNTDs) for the purpose of POI identification and sets a new classification for FTs hence facilitating the automated recognition of FTs; Fission Track Detection using Automated Microscopy" (Journal of Nuclear Engineering and Radiation Science, March 2017)

4. It achieves the complete analysis from environmental swipe sample screening to isotope ratio analysis, within 12 days, making it suitable for routine particle sample analysis for safeguards; "Revisiting the Fission Track Method for the Analysis of Particles in Safeguards Environmental Samples" (Talanta, February 2017)

5. It proposes a new method for statistical treatment of transient signals for the purpose of an operator-independent and automated evaluation of isotope ratios in micron-sized uranium particles; "Simple robust estimation of uranium isotope ratios in individual particles from LA-ICP-MS measurements", (JAAS, March 2017)

Chapter 2: Aliquoting

2.1 Environmental Sample Analysis Overview

An overview of a typical inspection sample flow is given in the following paragraphs.

Each nuclear forensic laboratory receives coded swipes. The analysts that way do not know anything regarding the history of the swipe or material it contains. Evaluators who manage analysis data have this information so they are able to track and follow up on the environmental conditions in which it was packed (the inspection kits are prepared in a clean laboratory environment), but also to ensure that the background particle count of the swipe is as low as possible. It is necessary to be assured that there are no safeguards significant particles on the swipe prior to its use at a nuclear facility. Therefore, by controlling the conditions in which a swipe was packed, the IAEA can ensure that the final inspection particle analysis results contain only analytical data on particles collected at a nuclear facility under inspection.

Figure 3: Environmental sampling kit for inspectors

The swipe used for sampling is a 10 x 10 cm^2 cotton cloth (Texwipe 304). The composition of these wipers is well characterized in terms of trace elements, especially radioactive elements uranium and plutonium. The inspector kits are produced in a Class-10 clean area with sufficient quality assurance to prove
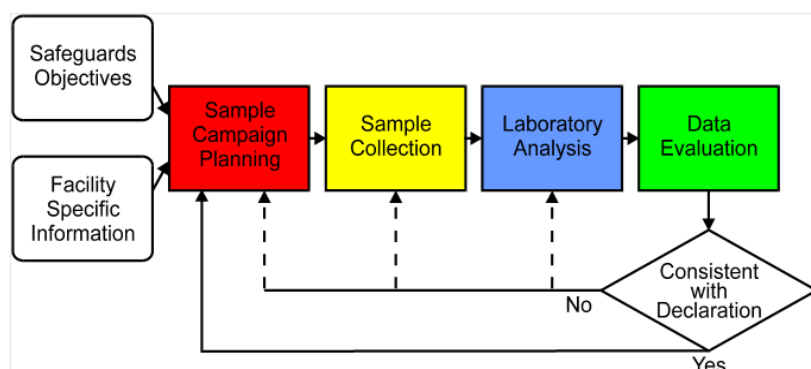
Figure 4: Sampling cycle for Safeguards Inspections

that the swipes were not contaminated with actinide elements or radionuclides before use [12, p. 32A]. A standard kit contains 6 wipers and minigrip plastic bags for the purpose of double-bagging each swipe, 2 pairs of clean-room latex gloves, a pen and a sample information form. The kits have a shelf life of 2 years due to the potential degradation of clean-room latex gloves. The inspectors are instructed to open these sample kits only at the inspection facility and use them to swipe different objects, parts and areas, whilst keeping the unused kits and the final samples under their control [12, p. 32A]. Replicate samples are also made in order to confirm the results by more than two different labs or techniques.

2.2 Step 0: Sample Pre-screening (Gamma Spectrometry)

After an inspection, the swipe contains safeguards particles of interest and upon receipt by an analytical lab it is first sent for radiometry measurements in order to determine whether the amount of material is low enough to be handled safely in a clean laboratory environment. High-resolution gamma spectrometry can be used to provide an initial determination of the isotopic composition of uranium and/or plutonium, as well as detection and quantification of trace fission and activation products in the sample (e.g. reprocessed uranium) [13, p. 1292]. In the case of the IAEA, X-Ray fluorescence analysis is conducted at the
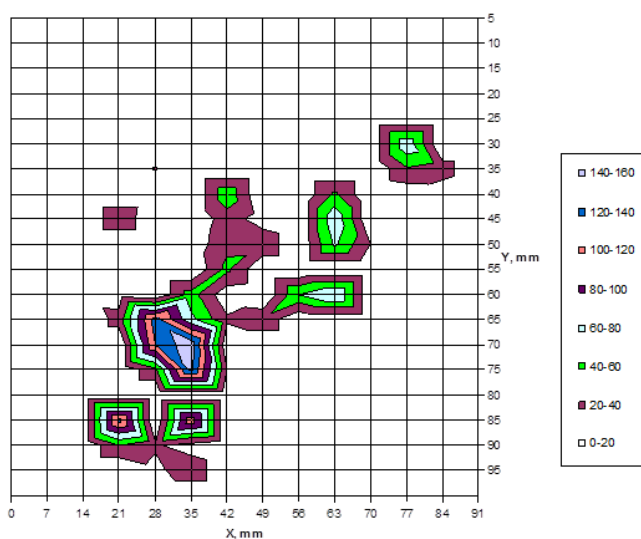
Figure 5: X-ray fluorescence map of a single environmental swipe

Figure 5: Environmental swipe sample (with unique code on upper left)

Environmental Samples Laboratory using a TRIPOD based on a 100 W X-Ray tube excitation and Si(Li) detector. A robotic arm is used to scan the entire surface of the swipe and the typical measurement time for a single cotton cloth is about 4 hours. The detection limit for uranium is $Det(U) = 35\ ng/cm^2$. Figure 5 shows a typical map of U concentration versus the location on a swipe (figure 6). This particular swipe contained a total amount of 2 µg of U.

These measurements provide insightful information to the sampling operator as to what region the particles of interest may be located in on the swipe, making the sampling process from a swipe thereafter not completely blind. Furthermore, by estimating the total U or Pu content of a swipe, this step assures the handler that the swipe in question will not contaminate a clean laboratory environment.

Gamma radiation in general can be recorded using various detectors by exploiting its ionization characteristics. These instruments include ionization chambers, Geiger-Müller counters, proportional counters, scintillation detectors and semiconductor detectors, but preference is given to materials that are of high atomic number and high density for their detection capabilities [14, pp. 26-27]. The gamma spectrum from a sample is characterized by gamma peaks that sit on the Compton continuum of other gamma emitter isotopes, peaks from interactions such as pair production and the Compton effect etc. Due to the complexity of this spectrum, it needs to be evaluated by spectrum evaluation software (the likes of Genie 2000 from Canberra, GSANAL from Bitt, Maestro by Ortec and MicroSAMPO from Aarnio). It is further important to note that background, self-absorption, real coincidence and dead time corrections need to be carried out on each peak area so that the corresponding radionuclides can be identified [14, p. 27]. The background measurement is carried out prior to a measurement of the sample in addition to an energy calibration. The energy calibration curve is not linear, but in of quadratic form, meaning that for a reliable estimate one needs more than 3 points to determine it. By including the uncertainty in each, a total of 6-8 points is desired for an examined energy range and this has to be adjusted to the type of detector

used. A helpful tool for estimating the calibration curve can be found on the aforementioned software packages or by using theoretical models based on Monte Carlo calculations [14].

2.3 Bulk vs Particle Analysis

After the X-ray fluorescence analysis, the swipe is sent for bulk and/or particle analysis. In short, bulk analysis provides average isotopic composition information of elements in the whole sample and particle analysis provides information on individual particles in the sample. It is important to note that a whole swipe is typically analysed during a bulk analysis request and only a small fraction of the material can be analysed in a particle analysis request.

The first step of bulk analysis is usually the dissolution of a cotton swipe in an acid which is then divided into two solutions: one solution is spiked with ^{233}U and/or ^{242}Pu for quantitative analysis and the other is not spiked for the purpose of isotopic ratio analysis. Afterwards, each solution is chemically divided into subsamples containing U, Pu, Am etc separated from the matrix. The isotopic ratios for each element are measured with TIMS and/or ICP-MS and evaluators receive an average isotopic composition of the whole swipe material.

Particle analysis on the other hand is designed around the notion of extracting particles of interest from the swipe and characterizing a number of them. Each particle on its own contains a vast amount of information on its origin, morphology, elemental content, isotopic signature and hints towards a specific production process, especially if it is man-made. One can say that a particle is a sample in itself. For this reason the operator needs to be aware of the following:

1. X-ray fluorescence measurement resolution is several magnitudes worse than the average particle size (10 μm) and thus such a map can only serve as an indicator for the location of large concentrations of safeguards interesting particles;

2. The detection limit for X-ray fluorescence measurements is not enough to discover particles with e.g. picogram or femtogram amounts of fissionable material. Therefore, these maps may miss out on detecting the presence of particles that may contain safeguards relevant information. E.g. potentially a single 300 pg particle of enriched U physically isolated in what appears to be a white area on the radiography map would be overlooked;

By estimating the number of particles on a typical swipe, one is able to deduce the time it would take to analyse each and every one of these. Even if one disregards in their estimation all the sample preparation steps, the analysis of a whole swipe containing 1 million particles would take:

1. For SEM-EDX characterization: $1000000 \, particles \times 10 \, \frac{seconds}{particle} = 115 \, days$ of continuous spectra acquisition.

2. In the LG-SIMS or TIMS analytical march, the typical number of particles analyzed for their isotopic ratio is about 100 per sample, per day. So again, the analysis of all particles would take approx. 10000 days.

Obviously, the outlined problems are an exaggeration and analysts do not microprobe each and every particle of a sample for their reports. A branch of statistics deals with the theory of sampling from a population (i.e. ways to pick specific particles from the population of 1 million) in order to characterize it to a certain degree of certainty (usually 95% confidence). Otherwise, the above estimations would sound like impossible challenges even with the analytical capabilities of today. It is for this reason that a method for particle screening is essential to implement as part of the sampling process and in such a way avoid wasting valuable analysis time on particles that contain no safeguards relevant information. Ideally, such a method would be able to pinpoint towards each and every particle of U or Pu in a sample.

The analytical march used for single particle analysis may be divided into the following steps: particle aliquoting; particle dispersion; sample assembly; sample irradiation; detector etching; FT identification; designation of POIs; POI isolation; POI micro-analysis. In this work, substantial improvements have been made to each of these steps.

Technique	Purpose	Lateral Resolution
Optical Microscopy*	Morphological investigations	1 - 2 μm
Scanning Electron Microscopy (SEM)	Morphological investigations	5 - 10 nm
SEM Energy Dispersive X-Ray Spectroscopy (SEM-EDX)	Chemical/Elemental analysis	2 - 8 μm
SEM Wavelength Dispersive X-Ray Spectroscopy (SEM-WDX)	Chemical/Elemental analysis	2 - 8 μm
Bench-top X-Ray μ-Beam techniques	Elemental, structural analysis. Imaging	5 - 10 (mono-capillary) 10 - 50 (poly-capillary)
Accelerator Based Techniques	**	10 nm to 100 μm
Secondary Ion Mass Spectrometry (SIMS)	Isotopic and molecular analysis	50 μm
Large Geometry SIMS (LG-SIMS)	Isotopic and molecular analysis	5 μm
Focused Ion Beam SEM-SIMS (FIB-TOF-SIMS)	Elemental analysis***	< 1 μm
Laser Ablation Inductively Coupled Plasma Mass Spectrometry (LA-ICP-MS)	Isotopic and molecular analysis	20 - 50 μm
Laser-Induced Breakdown Spectroscopy (LIBS)	Elemental analysis	50 - 100 μm

Table 1: Microprobe Techniques for particle analysis
* Optical Microscopy is not a micro beam technique per-se, however it is commonly used prior to microprobe analysis for the investigation of samples or as a complementary step;
** Accelerators are widely used for an extremely wide range of investigations;
*** SEMs that are equipped with a TOF-SIMS also come with elemental analysers (EDX);

2.4 Importance of Dispersion (Particle Separation)

Once the particles have been extracted from the environmental swipe and dispersed on a substrate, numerous microprobe techniques are used to investigate their properties. It is important to disperse the particles on a flat and smooth surface. Depending on the nature of the information wanted, the analyst will select a suitable micro-probing technique. shows

details of some microprobe analysis techniques and their lateral resolution. We see that there exists a full arsenal of these that can be used to characterize micro artifacts. To make use of the intrinsic capabilities of any micro-analytical technique, the particles should be separated by at least the resolution of the technique.

2.5 Step 1: Extraction of Particles from a Swipe for Particle Analysis

To begin with, the methods of particle extraction can be understood as a sub-sampling or aliquoting step and these can be destructive or non-destructive to the swipe [15]. By destructive, one means that no further sub-sampling of the swipe can be done to obtain the same analytical results. There exist two main methodologies [16]:

1. Wet extraction methods: ultrasonification, filtration, centrifugation and chemical etching;

2. Dry extraction methods: thermal (low temperature plasma, chemical and oven ashing) as well as inertial impact collection.

In ultrasonification, the swipe is immersed into water, ethanol, or heptane (or a mixture of these) and the particles are induced to detach from the fibres via vibrations. The swipe is removed from the liquid and the suspension is evaporated [17, pp. 1-2] [18, p. 584] [12] [19]. Centrifugation is done by placing the swipe in a liquid vial, which is then placed into an ultra-centrifuge after some time [19] [20] [21]. Other wet extraction methods include the rinsing off the swipe using a carrier liquid followed by filtration through membranes of a micron and sub-micron pore size [22].

Figure 7: An intertial impactor used at the IAEA Seibersdorf Clean laboratory

In thermal methods, the swipes are ashed to get rid of the swipe material and other organic matter from a couple of hours to days at temperatures in the range of

400-600˚C [15] [23]. Since thermal treatment can be followed by chemical ones, elevated temperatures are not desirable because of the formation of refractory particles [15], but this used to be the practice [10]. Sometimes, the swipe is cut into smaller pieces for treatment [22] [10] [24] [25].

One non-destructive method for particle extraction has seen an increase in use recently: a suction-type device that pulls particles off a swipe. In SG literature, this device is called an inertial impactor (see figure 7), since it is connected to a reverse air-flow that "vacuums" particles off the swipes [21] [24] [26] [27] [28] [29] [30] [12] [21] [31] [32] [28] [29] [30]. It houses a substrate (typically a glassy carbon disc), previously coated with a sticky substance, as an impaction medium. Regardless of its widespread use, it has known limitations [26] for sample preparation. This will be discussed in more detail in the following sections.

Low temperature ashing (plasma ashing) can be used after some of the extraction techniques described in this section. It removes excess organic and biological (matrix) materials that could produce interferences in later analysis [33, p. 2157] [29, p. 123] [34, p. 350]. [33] demonstrated that using cold plasma ashing (CPA) had the following advantages:

1. a highly significant reduction of the background (between 26 and 46% for all elements) and

2. a significant increase of the signal-to-background relationship by a factor 1.5−2.5 (for all elements) as well as a much better detection of trace elements [33].

Finally, for investigations of particles in a scanning electron microscope, the sample can also be covered with a thin layer of graphite, gold or similar material to increase the conductivity of the sample [18, pp. 584-585] [29, p. 123].

2.6 Step 2: Re-sampling of Swipe Particles (Dispersion) [26]

Re-sampling is a way of re-dispersing swipe particles onto a new substrate. Translucent substrates are preferred in optical microscopy, silicon wafers in LA-ICP-MS investigations and glassy-carbon planchets in scanning electron microscopy and LG-SIMS analyses. Depending on the substrate used, one can improve results by minimizing isobaric interferences, or increasing feedback by improving sample conductivity, etc.

Particles from swipes vary typically in size from sub-micron to ~100 μm in diameter with an average of about ~10μm (this includes particles of interest and matrix particles). Each particle carries a wealth of information, and for that reason it is vital to prevent mixing of chemical signatures of particles of interest and other particles. Hence, to avoid collecting data from more than one particle at a time, it is necessary that the particles are separated physically and that the microprobe used is of comparable size: smaller than the inter-particle distance. This parameter can be adjusted during sample preparation and includes a two-step process where the particles are extracted from the original swipe, redistributed onto a new substrate, and then characterized using microprobe techniques. Some procedures are biased toward a certain size range of particles, others suffer from particle clustering or lack of reproducibility. Therefore, to avoid simultaneous analysis of multiple micro-artifacts of varying signatures, possibly belonging to separate production processes, a step to separate particles is imperative.
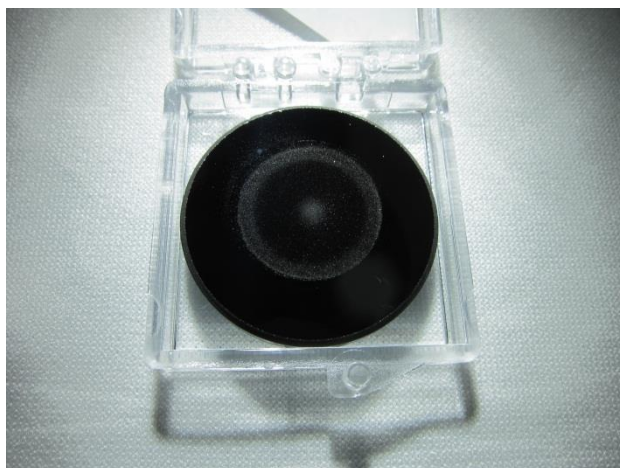
Figure 8: Deposition of particles using an inertial impactor for LG-SIMS samples at IAEA

2.7 Standard Dispersion Methods

Established dispersion methods include sprinkling of particles onto a substrate, mixing the sample with a liquid to create a suspension or slurry solution and pipetting this mixture onto

a substrate, or filtration of particles from liquids or gases. Usually, collection substrates have an adhesive deposited on their surface to collect and fix particles in place so that they do not re-disperse or bounce off the substrate. Currently, the inertial impaction method enjoys a preferential place as the method of choice for particle extraction and dispersion of safeguards particulate materials since both operations can be performed within a glove bag (see figure 7 for an image of an inertial impactor and figure 8 for a particle re-distribution image on a glassy carbon substrate). Using a glove bag further minimizes the cross-contamination risks associated to sample preparation by containing most activities within a closed bubble.

2.8 Dispersion Method Quality Assurance

As part of this dissertation, the applicability of the shock wave disperser was investigated. The dispersion quality of this method was compared to some features of merit of several existing methods by acquiring images of each dispersed sample and processing these using standard FIJI software and plug-ins.

The assessment of the quality of the dispersion was performed using seven criteria listed below in order of increasing complexity:

1. Visual assessment of the particle distribution using 3D surface plots;
2. Line profiling across the diameter of the sample distribution;
3. Assessment of the circular azimuthal average of particle sizes;
4. Assessment of particle density along evenly spread concentric circles around the geometrical center of deposition;
5. Granulometry: a numerical sieving technique for grouping particles by size;
6. Uniformity and completeness of the particle size distribution (after collection and re-dispersion);
7. Nearest neighbor distances;

Furthermore, a shock wave disperser based on the Sod's tube operation was designed and built as an alternative to existing dispersion techniques.

2.9 The Basics of a Shock Wave Disperser (Sod's Tube) [35] [36] [37] [38]

The physics of Sod Shock Tubes is well-known and has been used widely in industrial applications, investigations of shock wave behavior, and research of fluid dynamics and chaos theories.

Essentially, a Sod shock tube is a tube, with a diaphragm used to separate two sections of high and low pressure (figure 9). A shock wave is produced by the sudden removal of the diaphragm either by means of a small explosion (blast-driven) or by building up the pressure in either section, eventually causing the diaphragm to burst. After the explosion, a shock wave propagates through the length of the tube until a state of thermodynamic equilibrium is reached. The high-pressure section is typically called the driver section and the low-pressure region is called the driven section.

Figure 9: Schematics of a basic shock tube.
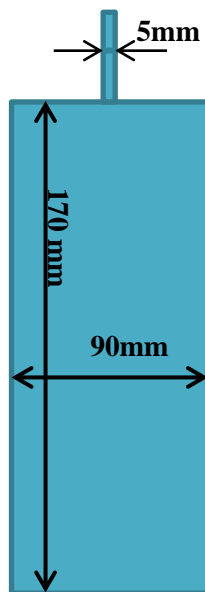
Figure 10: Basic dimensions of the shock tube with cylindrical sample holder
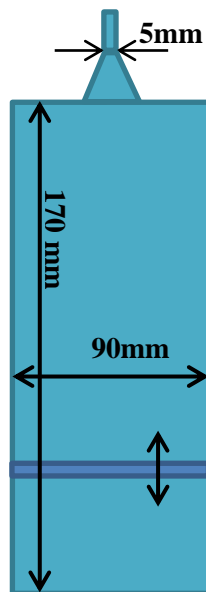
Figure 11: Basic dimensions of the shock tube with conic sample holder. Note sample holder slide (dark blue) which is fixable along the driven section and enables sampling at varying heights.

Figure 12: Prototype of explosive-disperser device

The design of the driven section was optimized to maximize the spreading of particles and to minimize the time needed for the system to stabilize, which had the further advantage of producing a compact dispersion device. The driver section was constructed to have a much smaller volume than that of the driven section (figures 10, 11, and 12) thus minimizing both the amount of sample and the presence of secondary shock waves. Furthermore, the collection substrate was coated with a thin layer of adhesive to reduce particle bouncing and re-suspension by the reflected shock waves.

2.10 Dispersion Simulation

A very basic simulation of the experimental setup was performed using CAD-FEM [39] software. The aim of this simulation was to assess the behavior of the ideal shock wave in the
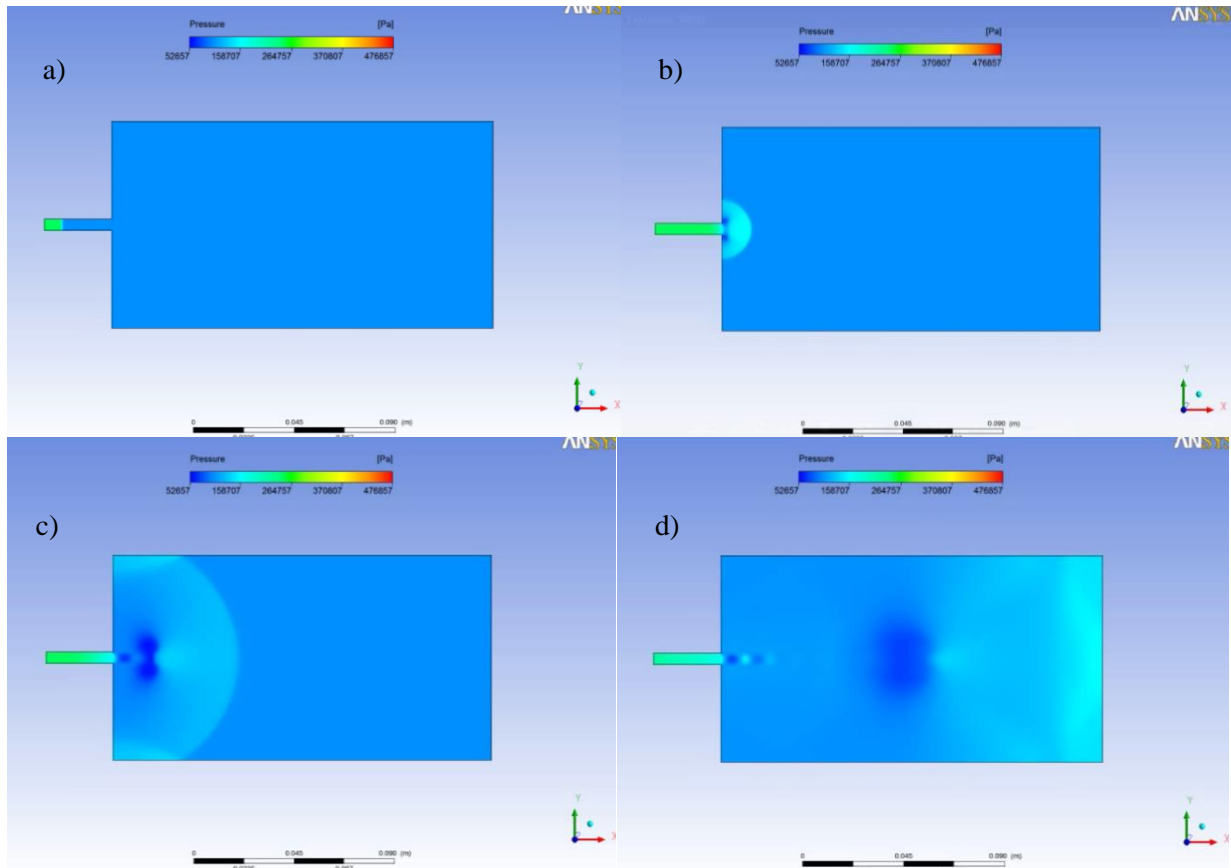
Figure 13: Screenshots from the simulation (pressure in shock tube): a) boundary conditions; b) shock wave reaches end of SOD tube and starts streatching, wavefront distributes pressure evenly; c) pressure wavefront about to reach walls of cylinder; d) wavefront reflected from walls; e) wavefront reaches sample catcher; f) wavefront reflects from sample catcher, pressure wavefront evenly distributed along the sample catcher wall.

dispersion device. Figure 13 includes screenshots from the simulation. It was confirmed experimentally that a pressure >3 atm would break the Mylar® foil material used as a diaphragm. Other simulation parameters include: viscous fluid, inviscid flow, no gravity (in the experimental setup this shock tube would be vertical, not horizontal as in the simulation).

2.11 Investigating Particle Dispersion Techniques: Experimental Setup [26]

To establish the optimum dispersion method for FT analysis, a collection of samples using the aforementioned re-sampling techniques on transparent substrates was made. Images using reflected and transmitted light were acquired of each substrate. The substrates were quartz discs (1" x 1/16", polished, Product No: 16001-1, Ted Pella Inc.). For the acquisition of SEM images, high-quality polished carbon discs of 25mm diameter were used (Hitachi, Japan). The SEM samples were coated with a thin layer of gold to minimize charging effects.

The samples were prepared in a clean room environment. The test material used was IAEA Soil 7 [40, pp. 1-2]. The loading of reference material on the shock wave disperser, the sprinkled, pipetted and slurred samples was consistent ~ 36 ± 1.5 µg (note that depending on the method, not all material was deposited onto the sample collector). High-quality quartz substrates (the aforementioned discs from Ted Pella) were cleaned in an ultra-sonic bath and then depending on the method, were either allowed to dry and left clean or coated with clear varnish (Daler-Rowney Ltd, Bracknell, Berkshire, USA) or with a polyisobutylene (PIB)/nonane mixture (8mg/5ml PIB/nonane, diluted 20x) by means of a spin coater. The substrate was left clean for making pipetted, slurry dispersion, and electrostatic impactor samples but was coated with varnish for shock wave disperser and sprinkling. For the inertial impactor it was coated with a PIB/nonane mixture.

Image Acquisition

Modern imaging instruments are capable of producing large amounts of data. However, post-processing software and computer processors are still limited in processing such large

data sets in a timely manner and hence for this, certain compromises were made as follows:

Optical Images

The optical microscope used was a Zeiss Z2m with its accompanying software to acquire high-quality large-area images of the whole sample with a resolution of ~1.3 μm/pixel (see figure 14 for large area images). Up to 350 individual images taken at 5x magnification (1.268 μm/pixel resolution) were used to build the fused whole sample image. The objective used was an EC Epiplan-Neofluar 5x/0.13 HD M27 with a working distance of 15.1 mm. The images were stitched by the native AxioVision SE64 software that uses stage coordinates and an image overlap of 10 percent. No filtering was conducted to enhance image features and the images were only corrected for background illumination during the acquisition (flat-field correction). Optical microscope images (1-1.2 GB) were acquired in less than fifteen minutes and were subsequently processed using a FIJI plug-in in less than an hour.
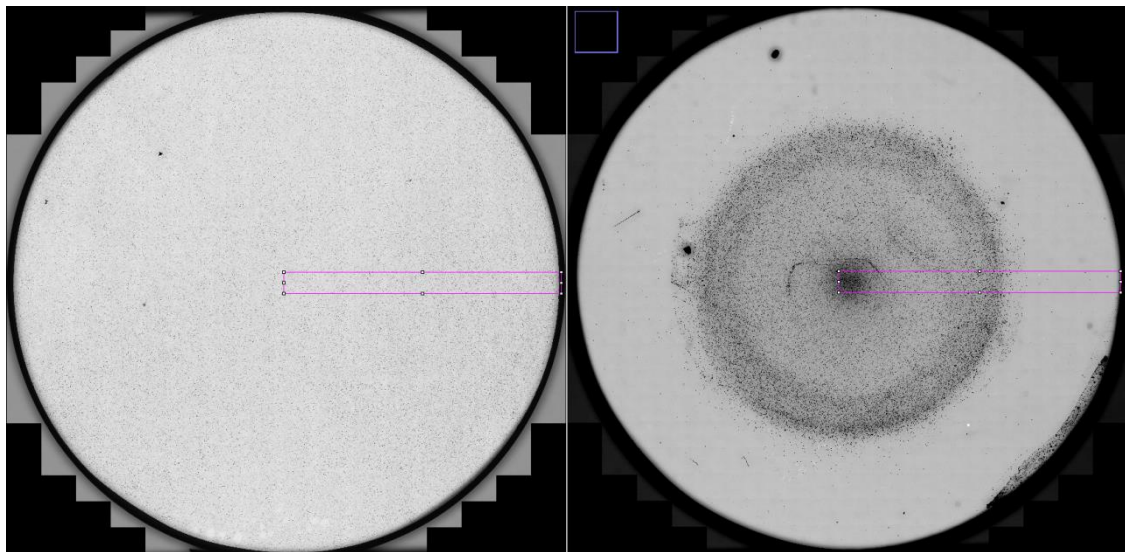
Figure 14: Stripe areas of which SEM images were later taken. Left is a shock wave disperser sample, right is an inertial impactor sample.

SEM Images

The SEM images were taken at TESCAN s.r.o., Brno, Czech Republic, on a Lyra3 FIB-SEM instrument and achieved ~0.3 μm/pixel resolution. Stitched panoramas of individual images

of a 1mm x 13mm stripe along the radius of each sample were prepared (200µm before the geometrical center and 300 µm over the edge, see figure 14 for a depiction of this area). The final panoramas were 300-400 MB in size and took two hours to obtain as well as about twenty minutes to stitch offline. Individual images were of an area 102,4 x 102,4 μm^2 (512 x 512 $pixels^2$). Samples of the inertial impactor and shock wave disperser (with both cone and cylinder heads) were taken for comparison.

Image Processing Software

The image processing software FIJI **[41]** was used to obtain distribution evaluations based on five image processing strategies extracted from data obtained by the following plugins: Interactive 3D Surface Plot **[42]**, Plot Profile **[43]**, Azimuthal Average **[44]**, Concentric Circles **[45]**, Granulometry **[46]**, and Delaunay Voronoi **[47]**. The image size limit for processing by FIJI for all practical purposes was set at 1GB.

2.12 Results and Discussion

In the ideal case, one would measure the size of and count all particles from a sample to determine the particle size distribution. This may be impractical due to limitations of most image processing software, reproducibility of the dispersion method and the spatial resolution achievable by instruments. We made compromises in order to evaluate the dispersion quality of various sampling methods used for a specific analysis.

The discussion on the dispersion quality in the following sections will focus on resolving particles apart by using either optical or electron microscopy imaging techniques. The optical images, as was stated before, attained a resolution of 1.3 µm/pixel whereas the electron images achieved a resolution of 0.3 µm/pixel. These resolutions were deemed acceptable for the task at hand. However, due to the software memory constraints, panoramic SEM images of a maximum area of (1mm x 13 mm) were manageable and therefore used for small arte-fact distribution assessment. On the other hand, whole sample light microscopy images could be processed and were used for large-scale particle distribution analysis.
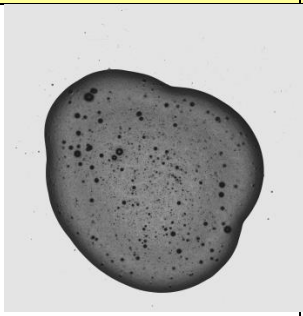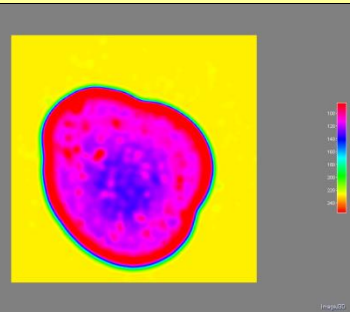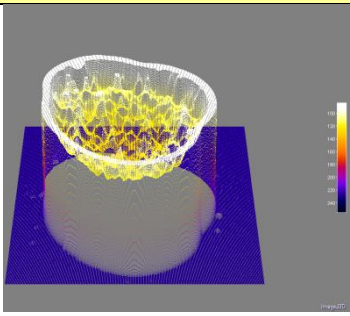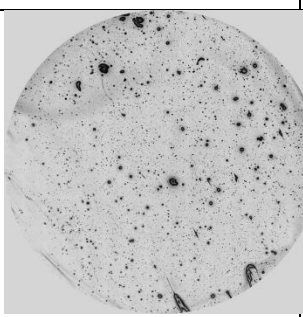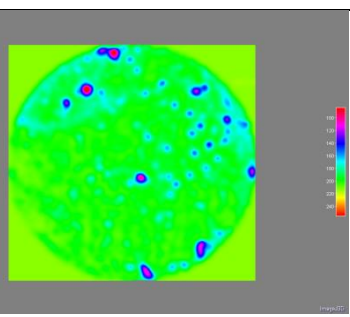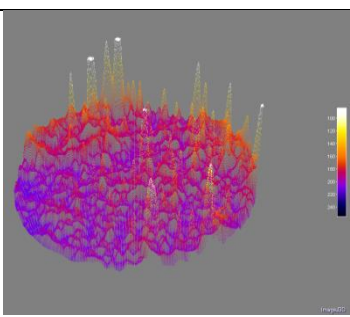
Large-scale particle distribution evaluations also contain optical images of shock wave disperser sample collection substrates at different distances from the cone/cylinder head. This was done to investigate the device and compare the cone and cylinder sample holder heads' dispersion patterns, as well as their evolution with respect to sampling distance.
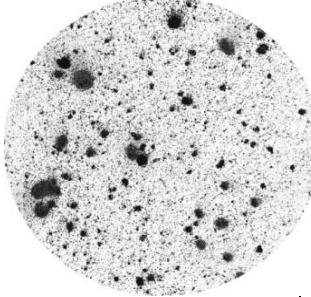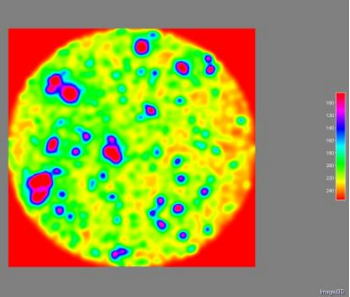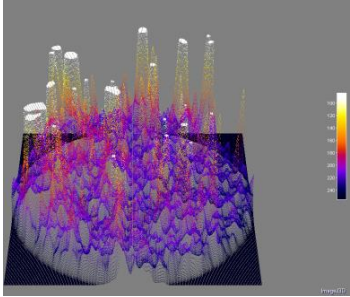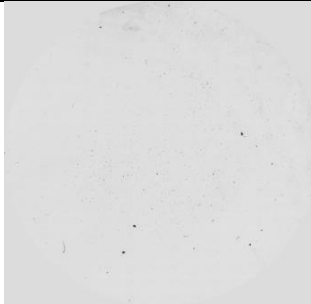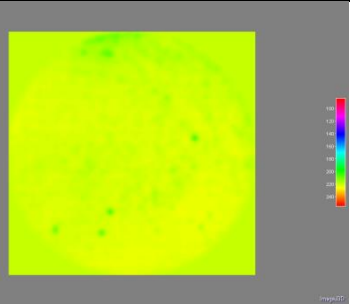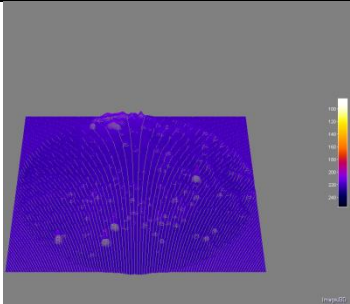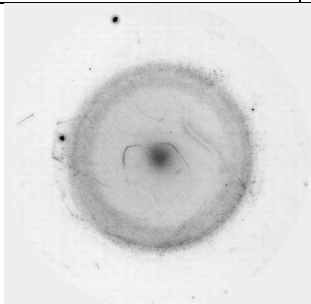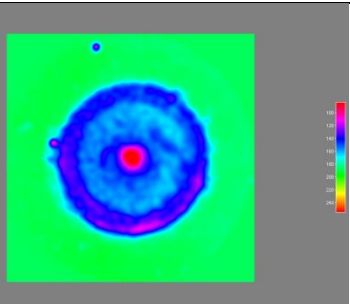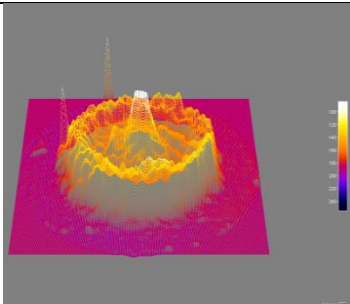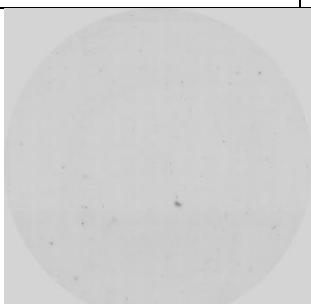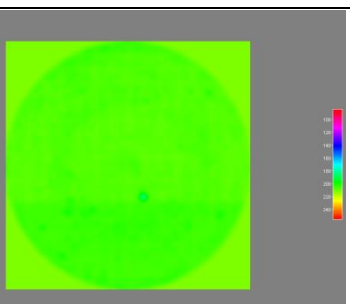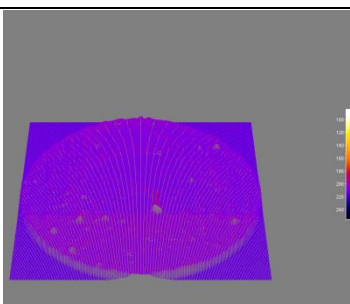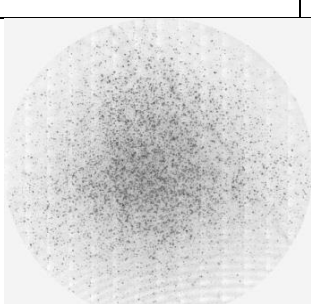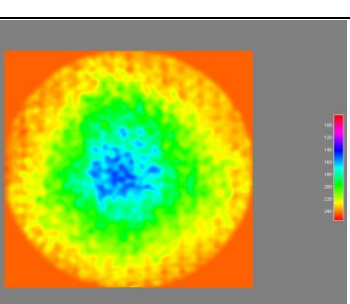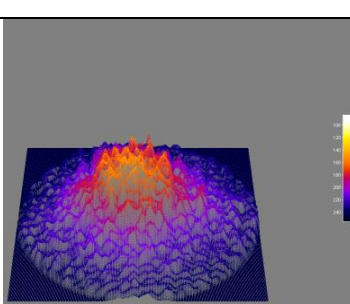
2.13 Large-Scale Particle Distribution Evaluation
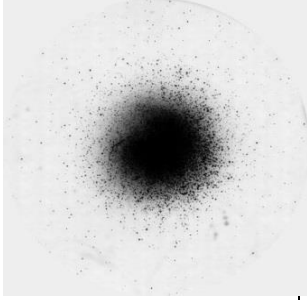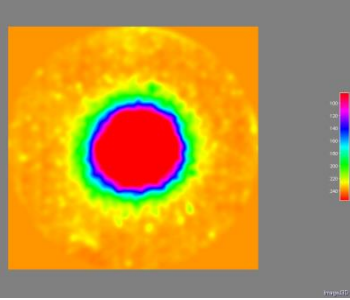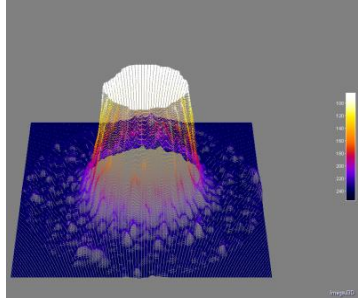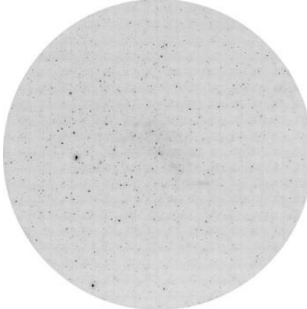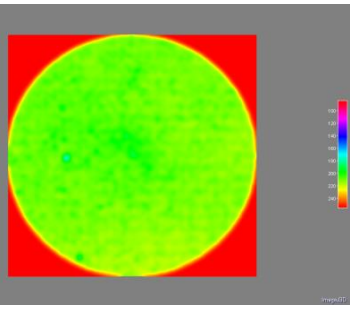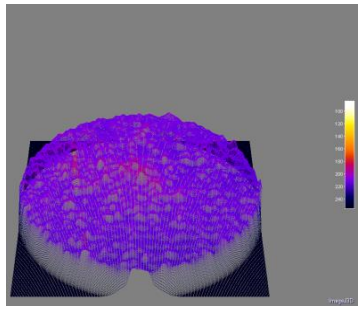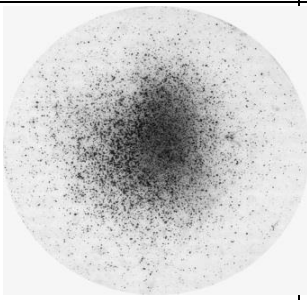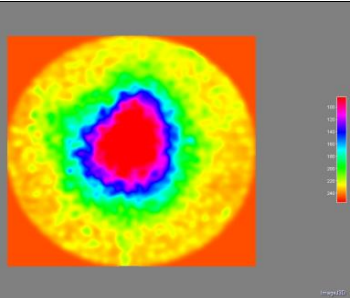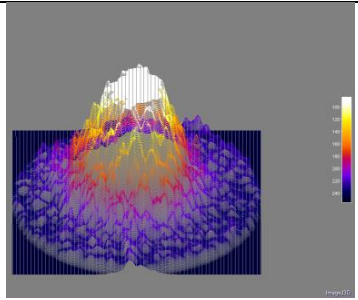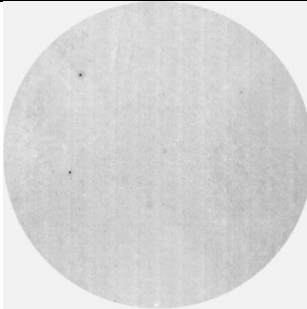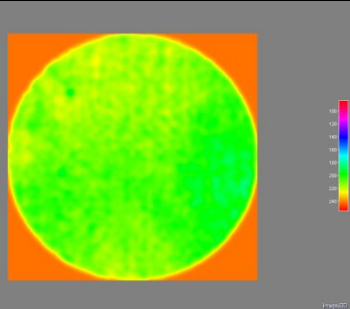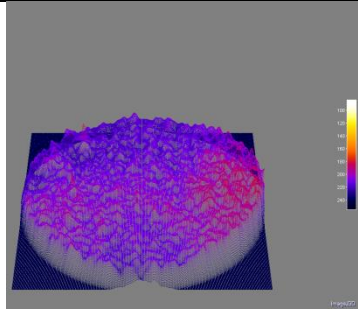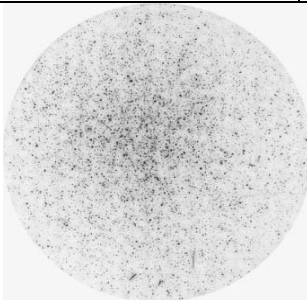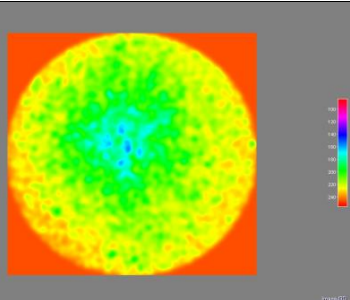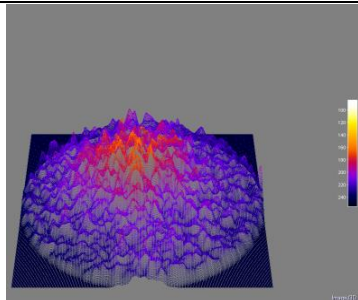
Surface Plots [42]
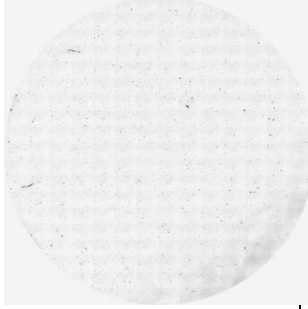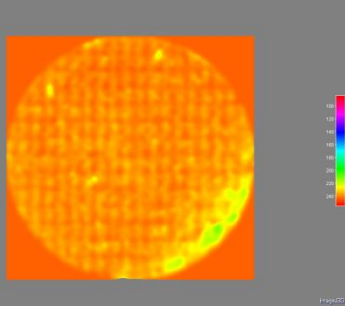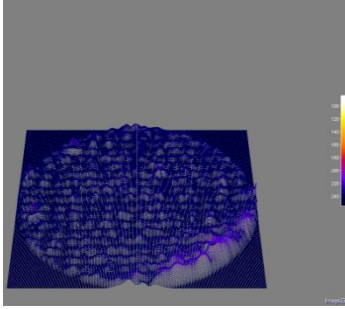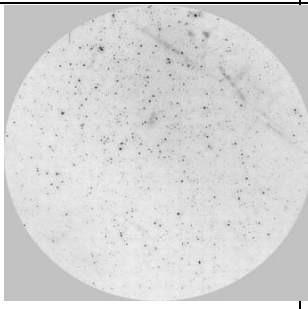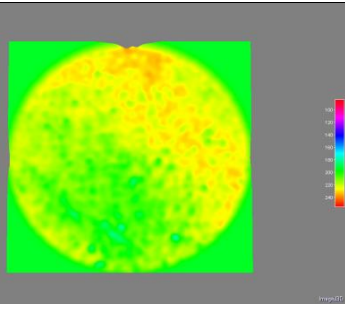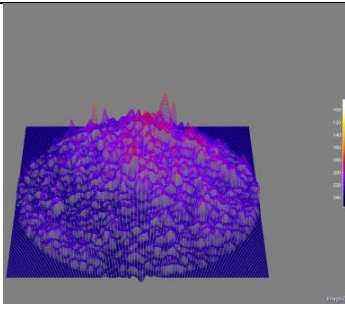
2D and 3D plots were drawn by using the FIJI/ImageJ surface plot plug-in that translates grey level intensities of pixels to 2D and 3D color map surfaces. From the plots shown in table 2, one distinguishes easily between trivial (pipetted, slurry dispersion, and sprinkled) and mechanical (electro-static impactor, inertial impactor, and shock wave disperser) sample preparation techniques by the presence and frequency of particle clusters. White areas (3D surface plot) are particle aggregates composed of clusters of indistinguishable particles.

Method	Overview Image	2D Surface Plot (FIJI)	3D Surface Plot (FIJI)
Pipetted			
Slurry dispersion			

Sprinkled			
Electro-static Impactor			
Inertial Impactor			
Inertial Impactor (blown)			
Cone at 2cm distance (1.4)			

Cylinder at 2 cm distance (1.4)			
Cone at 7cm distance (1.3)			
Cylinder at 7 cm distance (1.3)			
Cone at 12cm distance (1.2)			
Cylinder at 12 cm distance (1.2)			

Cone at 17cm distance (1.1)			
Cylinder at 17 cm distance (1.1)			

Table 2: 2-D and 3-D surface plots of all samples.

Line Profiling [43]

For each of the samples, a line profile across the diameter was taken as an initial assessment of particle dispersion. The result was a grey value function with higher values for white areas and lower values for congested areas with many particles (possibly indicating particles that were touching or overlapping). A flatter function overall indicated a more even distribution of particles. It was found that mechanical techniques produce symmetrical particle distributions around the center of the sample disc. Further statistical strategies needed to be considered since a single diameter of data is not sufficient for drawing definite conclusions. However, the line profile was a good indicator of the inherent symmetric nature of mechanical dispersion techniques. For example, the shock wave disperser method produced Gaussian particle distributions across the diameter of the substrate. Both the cone and cylinder driving sections behaved in a similar way, with the cone samples showing a faster decrease in axial particle loading than the cylinder samples.
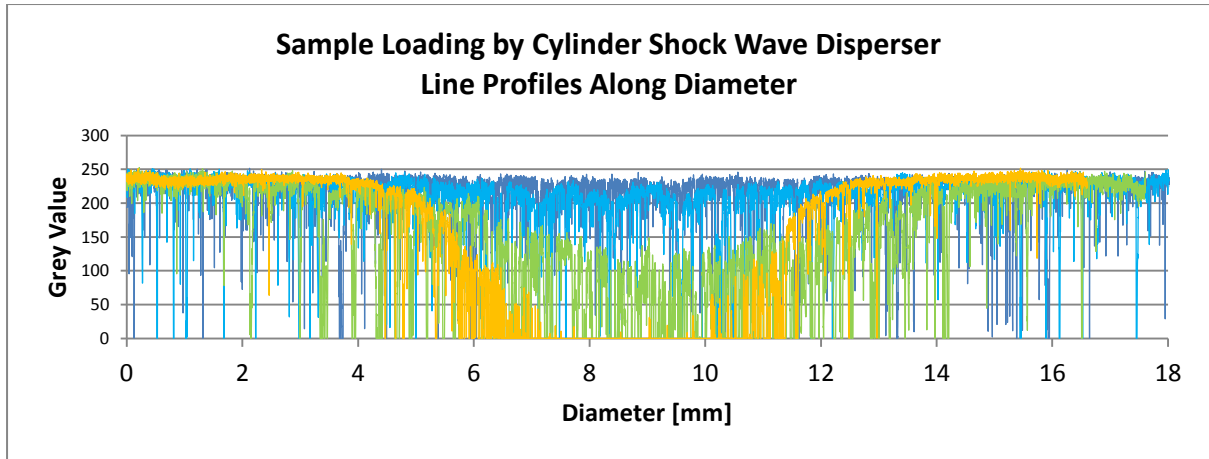
Figure 15: Cylinder line profiles for varying sampling distances from top of shock wave device: at bottom (dark blue, sampling distance at 17cm); step 1 (light blue, sampling distance at 12cm); step 2 (green, sampling distance at 7cm); and step 3 (orange, sampling distance at 2cm).
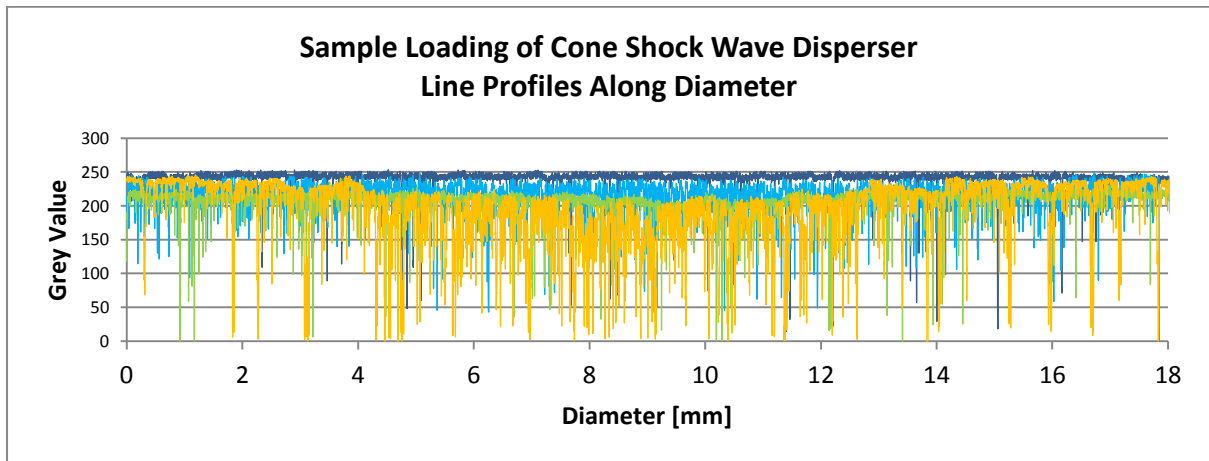
Figure 16: Cone line profiles for varying sampling distances from top of shock wave device: at bottom (dark blue, sampling distance at 17cm); step 1 (light blue, sampling distance at 12cm); step 2 (green, sampling distance at 7cm); and step 3 (orange, sampling distance at 2cm).
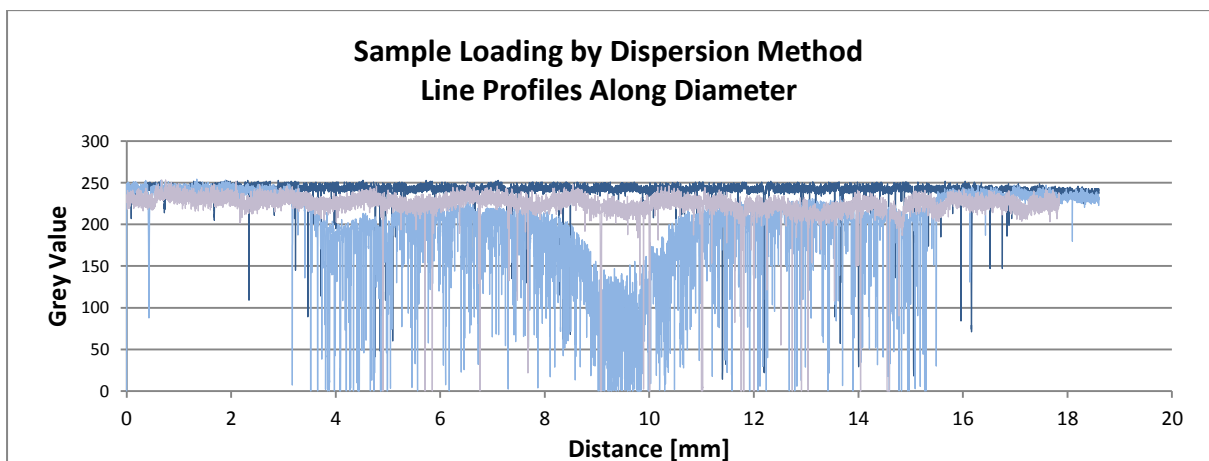
Figure 17: Line profiles comparing the shock wave disperser (dark blue) axial loading to that of the inertial (light blue) and electrostatic impactors (light purple).

Azimuthal Average [44]

The Azimuthal Average plug-in was used to assess the radial density distribution of particle dispersion. These results were an extension of the line profiling in the previous section and are displayed in Figure 18 as normalized integrated intensities vs the angle at which the integration was done (*–180°* to *+180°*). The integration was performed along 100 angular bins (note that the line profiles were taken along diameters). In the ideal case, for a perfectly even distribution of particles, the normalized integrated intensity along a radius will be invariant of the angle.
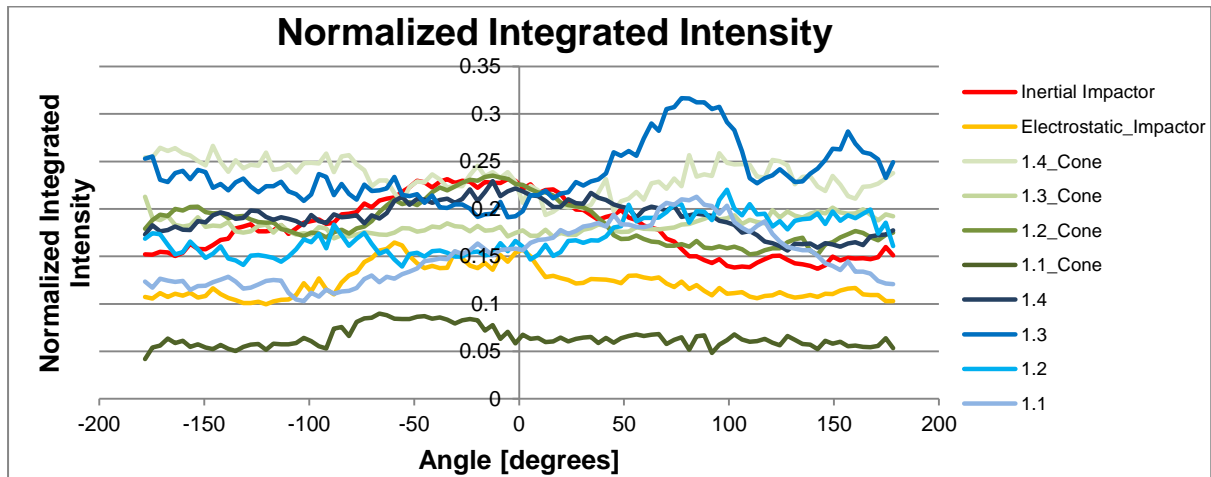
Figure 18: Normalized Integrated Intensity of particles along radii in: inertial impactor (red); electrostatic impactor (orange); shock wave disperser with cone head (green); and shock wave disperser with cylinder head (blue).

Concentric Circles [45]

This plug-in was used in the assessment of particle density along the perimeter of 200 circles, spread evenly around the center of the collection substrate (see figure 19 for a depiction). It is a good tool for estimating the homogeneity of a dispersion method at different distances from the geometrical center of the substrate. In our experiments, the shock wave disperser (at 17cm distance) with a cone head produced the most homogeneous distribution (flattest line in figure 20).
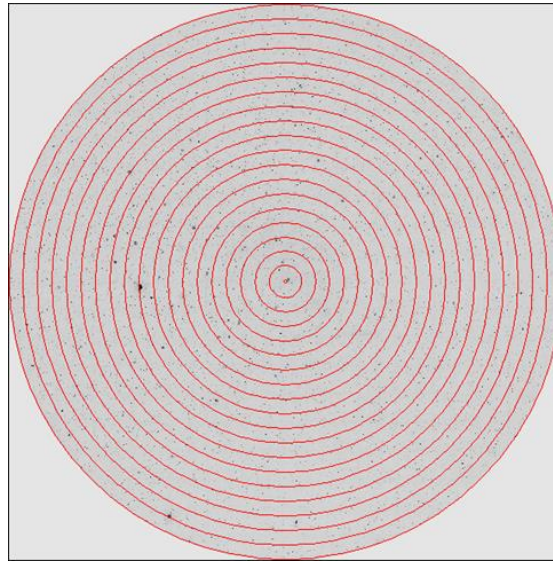
Figure 19: Concentric circles along which variations in the grey level intensity were measured to assess differences in particle distribution along the radii. Note that this depicts 20 concentric circles and the measurements were performed on 200.
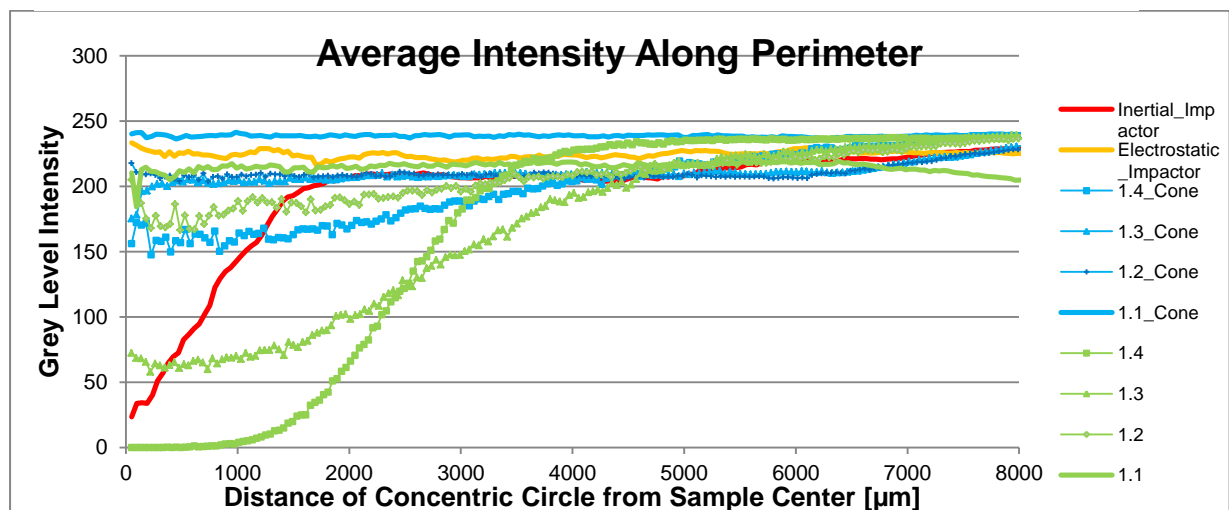
Figure 20: Particle intensity along concentric circle at varying radii along sample: inertial impactor (red); electrostatic impactor (orange); shock wave disperser with cone head (green); and shock wave disperser with cylinder head (blue).

Granulometry [48]

A more rigorous statistical method in the form of a numerical sieving tool was used: granulometry. This virtual tool extracts size distribution from binary images by performing a series of morphological openings with a family of increasing particle groups and plots these into a granulometry function [48]. The function maps each structuring element to the number of image pixels removed during a single cycle. A local maximum in the pattern spectrum at a given particle size thus indicates the presence of many particles of that size. The granulometric function thus can be defined as:

$$G(k) = N(k + 1) - N(k)$$

Where $N(k) = 1 - P_s(k)/P_s(0)$ where $P_s(k)$ is the pixel size distribution function at a certain pixel size k and $P_s(0)$ is just the pixel size distribution function of the original image [48]. See figure 21 for graphs of granulometry functions between different sampling techniques.
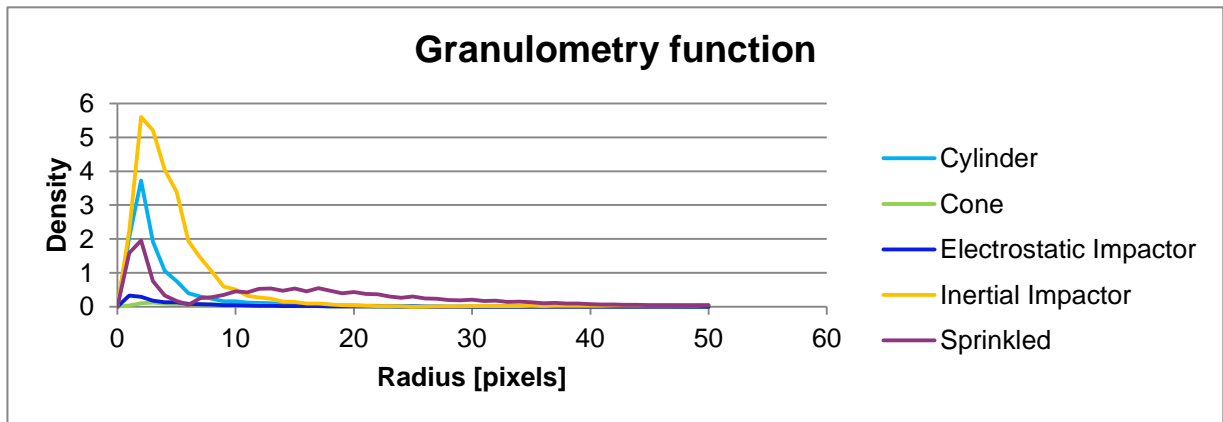
Figure 21: Granulometry function of several sampling methods. Local maxima show a preference of sampling particles of a certain size (inertial impactor method shows biggest preference towards 1-2 μm particles) or clusters. The shock wave disperser method with cone head shows the smallest preference towards particles of any given size and is thus the least biased (particles of all sizes evenly sampled). The sprinkling method has two peaks, the second of these due to particle clustering.

2.14 Small-Scale Particle Distribution Evaluation

To investigate the particle distribution in the small scale, SEM images processed using FIJI in the following sequence: each image was thresholded and particles were identified from the background by their histogram intensity; the edges were detected after an erosion-dilation operation; and lastly, the images were segmented into either background or particle before

any statistics was done. Note that the thresholding was done conservatively and some particles' sizes could have been underestimated. Also, due to the sheer number of particles in a single sample (several tens of thousands), a manual segmentation method is impractical and therefore automatic processes were used (FIJI autothresholding).

After segmentation, the areas of individual particles were calculated and are summarized in table 3. These calculated particle size distributions were compared to measurements by a laser scattering particle size distribution analyzer LA-950 (NA Laboratories, IAEA, Seibersdorf) from HORIBA. From table 3, one can see that the inertial impactor disperses particles in a very narrow size distribution (1.2 μm^2). The particles are assessed for their physical dimensions i.e. their apparent diameter, yet they are dispersed in the inertial impactor method according to their aerodynamic diameter. The shock wave disperser on the other hand sampled on average bigger particles (5.6 μm^2), but these were still smaller than the mean particle radius data obtained from the LA-950 ($\mu=15.9$ μm, $D10=3.05\mu m$, $D90=34.71\mu m$). This may be due to several reasons: smaller sample intake in the laser scattering device, circular-particle size assumptions in the data measurement and evaluation, as well as particle disintegration in the shock wave tube. Still, the data agree very well within $\pm\sigma$.

Particle Area Descriptive Stats	Inertial Impactor	Shock Wave Disperser
Mean Particle Area Estimate	1.218097154	5.562885129
Standard Error	0.030280962	0.124299962
Median	0.342	1.059
Mode	0.171	0.193
Standard Deviation	6.055283933	23.8130959
Sample Variance	36.66646351	567.0635364
Minimum	0.171	0.193
Maximum	386.3	996.369

Table 3. Particle area descriptive statistics for the inertial impactor sample and the shock wave disperser method

A total of just under 40000 particles were used in the statistical evaluation for each sample. Figure 21 shows that the inertial impactor method favors smaller particle sizes (>60% of particles were smaller than 1μm²) and figures 22 and 23 show no particles greater than 9 μm were deposited by the inertial impactor method. This is in very good agreement with theoretical values of a cutoff particle size of ~ 9.5 μm [49]:

$$d_{p50}\sqrt{C_c} = \sqrt{\frac{9\eta D_j(Stk_{50})}{\rho_p U}}$$

Where ρ_p is the particle density, d_{p50} is the particle diameter, U is the flow velocity, η is air viscosity, D_j is the nozzle diameter, C_c is the cutoff particle size (parameters used were $D_j = 6\ mm$ and $U = 4.5\ l/min$).

Furthermore, a plug-in for drawing the Voronoi tessellation diagram was used to estimate the inter-particle distances [50]. The algorithm estimates these by using local maxima of particles as the end-points of a single inter-particle line segment. Only distances between nearest neighbors were used in the calculation. See figure 24 for a normalized distribution of the nearest neighbor distances. Figure 25 shows the logarithmic distribution, revealing a small deviation in inertial impactor values stemming from the outer third ring of the sample where 1% of the particles (172 out of 15662 total particles) occupied a third of the area (see figure 26 top image). Figure 27 depicts the results for the Delaunay Voronoi of the shock-wave disperser method.
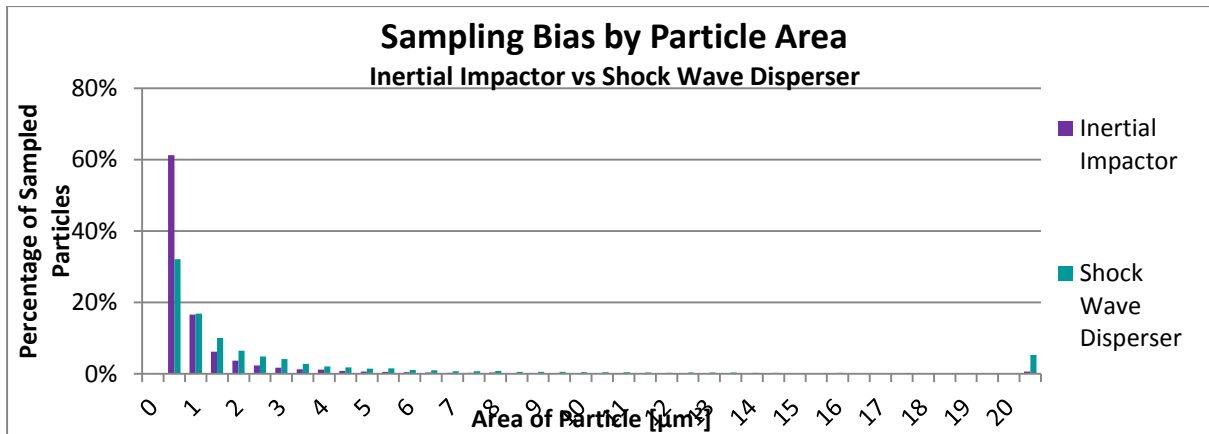
Figure 22: The above graph shows a slight bias for smaller particle area sizes sampled by the inertial impactor in comparison to the shock wave disperser.
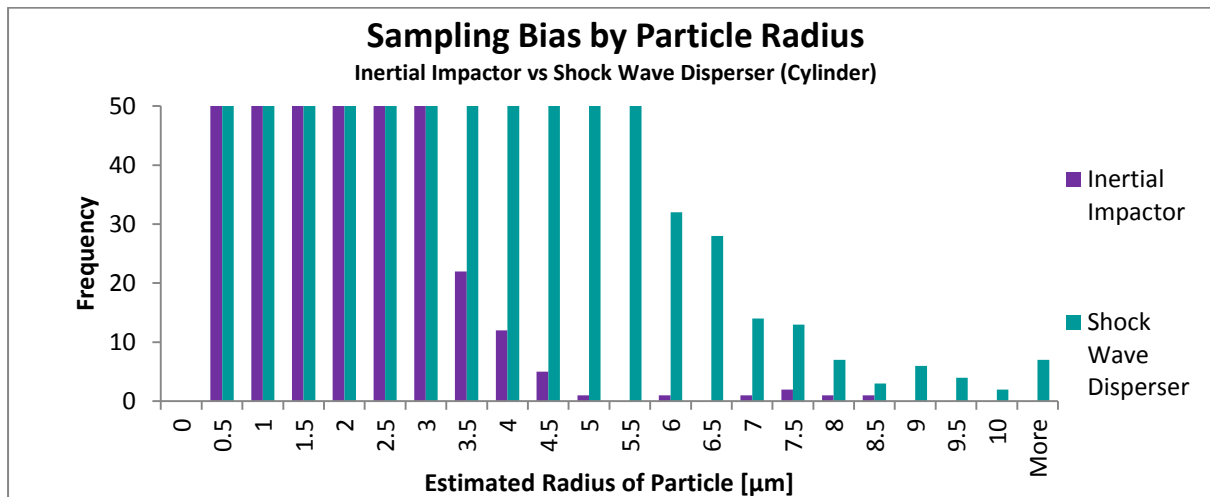
Figure 23: Empirical estimate of the cutoff value for the inertial impactor method was found at <9μm since no particles greater were found in the sample. Note that these radii were calculated from the particle area data by assuming they were spherical i.e. by $4\pi r^2 = 4/3(\pi r^3)$.
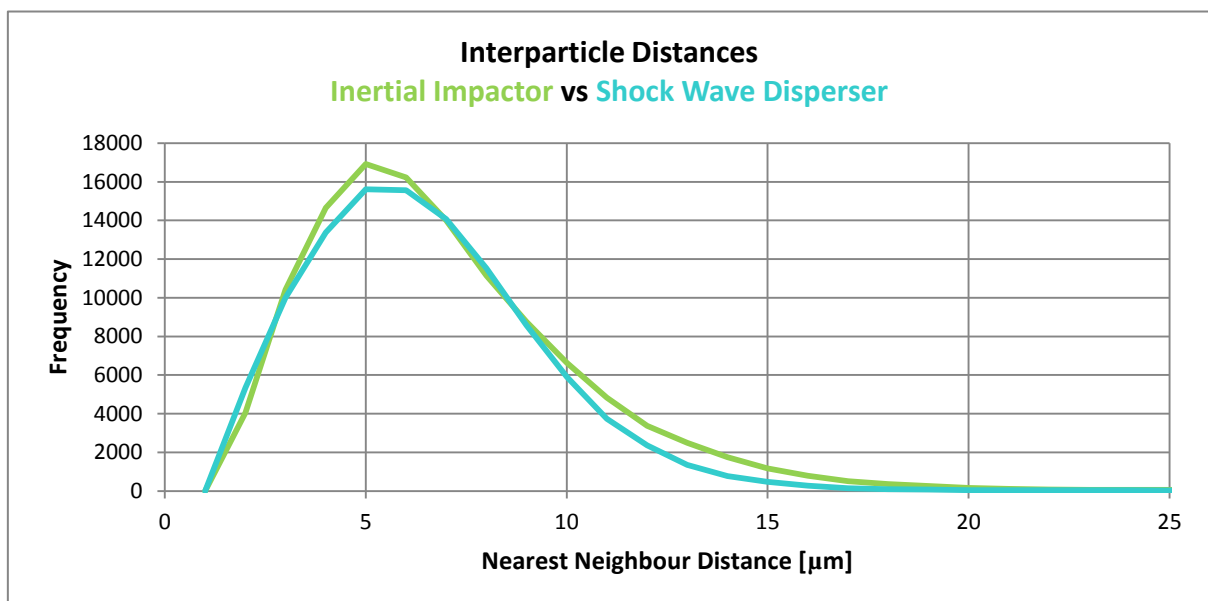
Figure 24: Normalized nearest neighbour distances for inertial impactor sample vs shock wave disperser. Note that both shock wave dispersion methods show almost exactly the same values (only cone head values are shown) and are more densely packed than the inertial impactor sample (number of interparticle distances higher for same area).
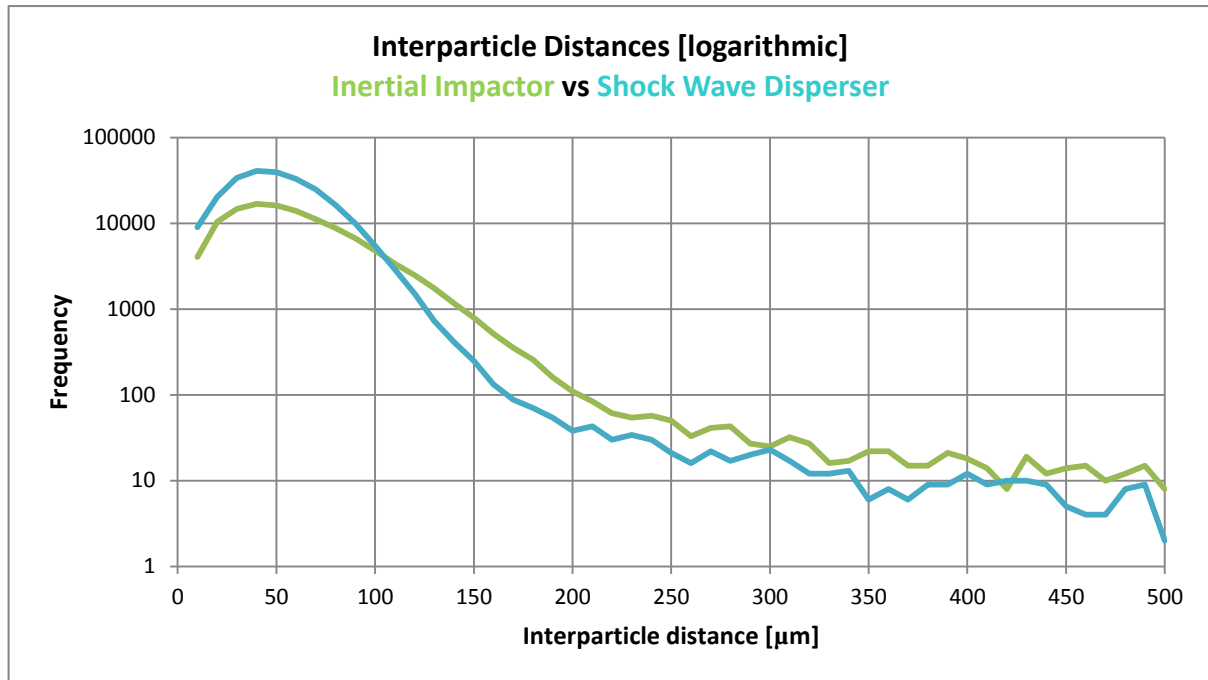
Figure 25: Interparticle distances by sampling method: the shoulder in the inertial impactor values suggests an area where the number of particles is smaller, thus their nearest neighbour values will deviate from expected mean values. See Figure 18 for the voronoi triangulation plot of the inertial impactor sample and observe the outer (right) ring of the sample where in about a third of the area, there are only 172 particles located (from a total of ~16000).

Figure 26: Delaunay Voronoi run on the inertial impactor sample. From top to bottom: segmentation; particle area contouring and triangulation overlay drawing (only centers of mass of particles shown). The mean separation of particles in the outer ring of the inertial impactor sample rises from 40-70μm to about 570μm.

Figure 27: Delaunay Voronoi run on the shock wave disperser sample. From top to bottom: segmentation; particle area contouring; tagging of center of mass of each particle and the resulting triangulation overlay. See figures 28 and 29 for optical images of particles dispersed with this method.

2.15 Evaluation of Dispersion

The image analyses conducted were focused on determining the characteristics of resulting patterns for each particle dispersion method. It was found that trivial methods (sprinkling, slurry dispersion and pipetting) suffered from the lack of reproducibility, as well as effects such as particle clustering, overlapping and grouping on the sample edges (Marangoni effect).

Mechanical methods on the other hand produced reproducible results (as long as parameters were kept fixed). Several statistical tools were used to evaluate the dispersion quality, and whether each method was biased towards collecting particles of a certain size. Using FIJI software along with several plug-ins (surface plots, line profiles, azimuthal averaging, concentric circles and granulometry), the distributions of the mechanical methods (inertial and electrostatic impactor, shock wave disperser) were found to be symmetrical around the geometrical center of the collection substrate, with little or no particle clustering. The shock wave disperser method was the method that dispersed the particles most evenly on the sample collector and showed the least bias in sampling particles based on their size (granulometry function). This method also sampled the greatest number of particles covering the full area of the substrate, with no bias detected for particles of a certain size range (see figure 28 and 29).

In the small scale dispersion analysis, more than 60000 particles were analyzed and their nearest neighbor distances plotted. It was found that by using the inertial impactor method 60% of the sampled particles were about 1-2μm^2 in size. The shock wave dispersion method on the other hand sampled particles in the range of submicron to 1000μm^2 in size, with the mean at 5μm^2 and only a third of the particles sampled were in the range of 1-2μm^2 in size (see figure 30 for a stitched SEM overview image partially used for the evaluation).

Each approach has its advantages and disadvantages – the trivial sampling methods may be faster and make use of less material, but the mechanical ones enable control in the

reproducibility, quality and inter-particle distances. The mechanical methods have issues regarding potential contamination of the laboratory environment and cross-contamination between samples. Because the shock wave dispersion method was most promising in delivering non-overlapping, evenly spread-out particles, we continued using it in the preparation of FT samples in the proceeding chapters. For one, it had the potential to produce the same results in the FT detector: evenly spread out fission tracks that could be assigned to a single particle for further analysis. By minimizing track overlapping, it is easier for the operator to assign a fission track to its originating particle [18, p. 586] as well as to separate particles of U, Pu and Am in order to analyse isotopic ratios separately.
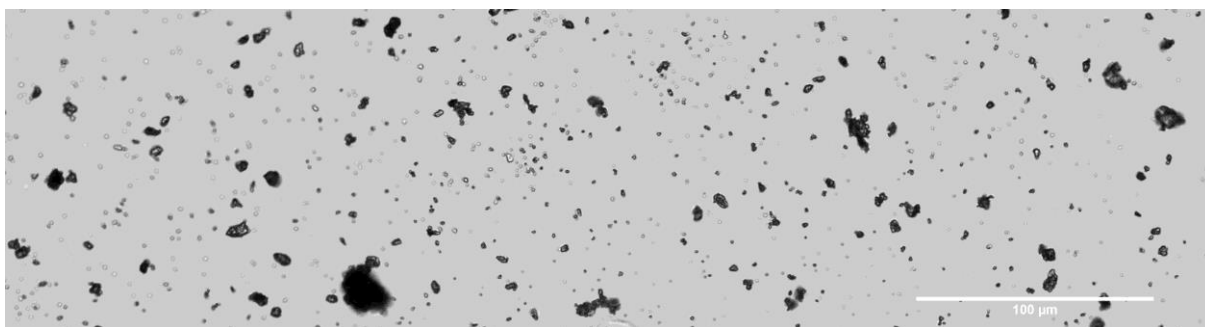
Figure 28: An example of four stitched images where particles were dispersed by means of the shock-wave device. Notice there are no (distinguishable) particle agglomerates.
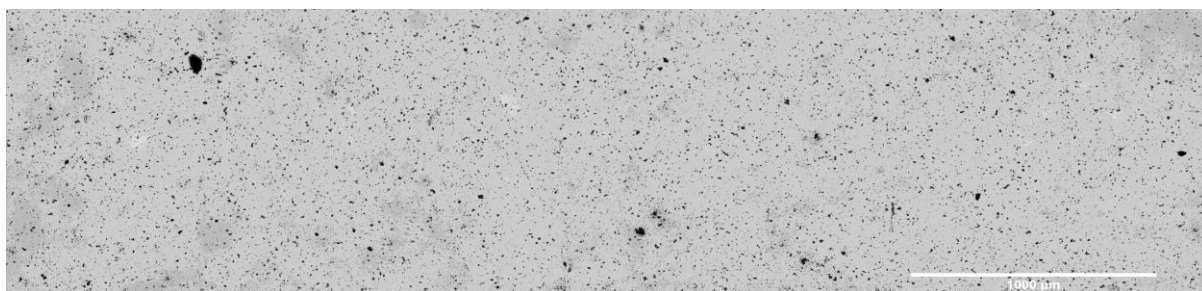
Figure 29: An example of a large area of 20 stitched images of a sample prepared using the shock wave device. This image (as the one above) was taken with the Zeiss Z2m optical microscope.
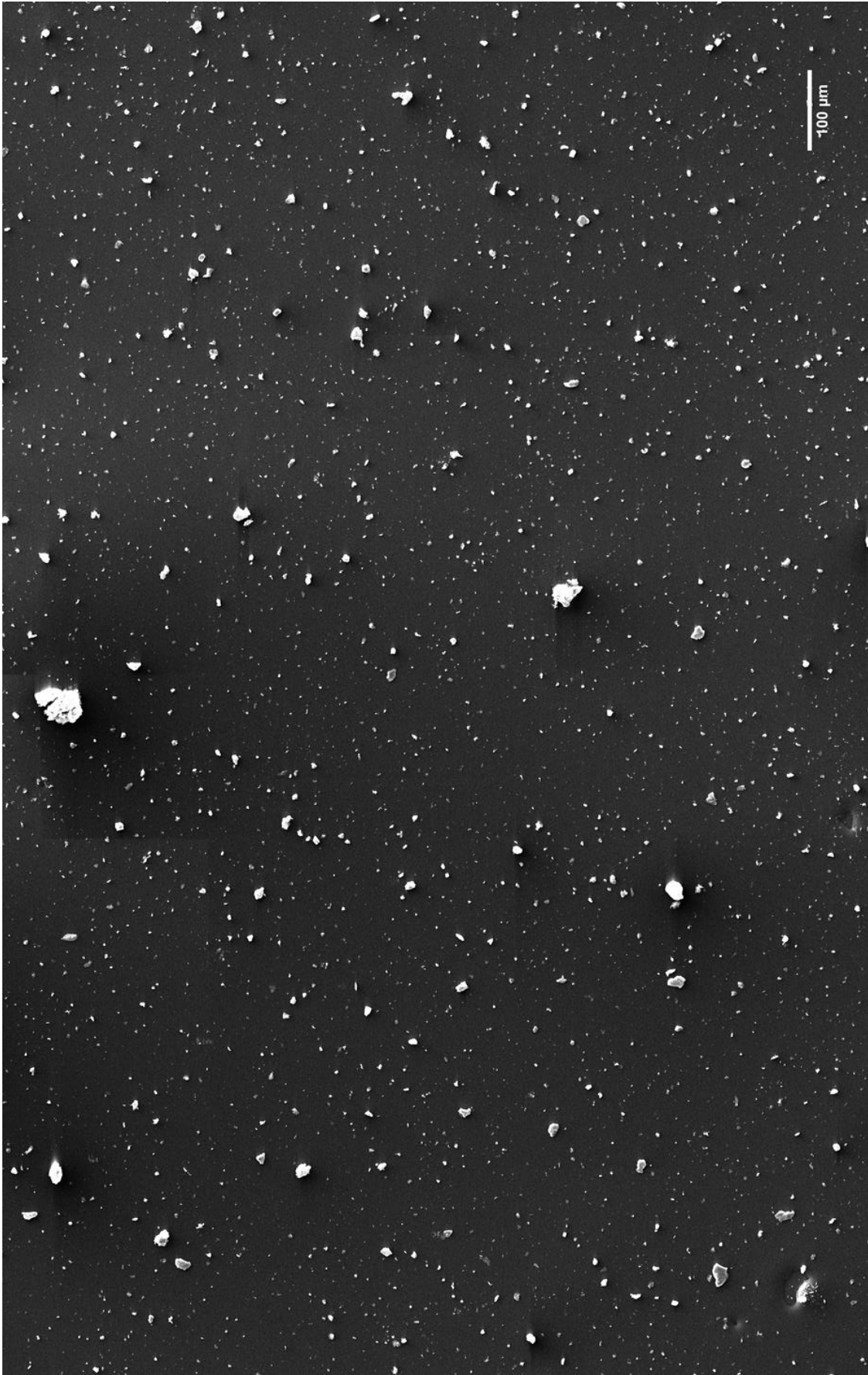
Figure 30: Stitched overview SEM image of particle dispersion using the shock wave dispersion device. The particle size estimation results are as follows: $\mu = 11.255$ μm; $\sigma = 24.361$ μm; min: 0.114 μm; max: 474.173 μm

Chapter 3: Fission Track Analysis

This chapter starts with an overview of the state of the fission track analysis method, followed by an in-depth description of the changes proposed in a recent publication **[16]**. For this reason, the chapter contains a general discussion on the history of the technique. The advantages of certain detectors are outlined, but the greatest attention is given to the promising results of using correlative microscopy.

3.1 Historic Overview of Fission Track Analysis [16]

Historically, the fission track technique and the accompanying etching were discovered in 1894 where H. Baumhauer observed etched figures in apatite after he diluted a sample in sulfuric acid, but did not know that these were fission fragment tracks since radioactivity would only be discovered two years later [51, p. 234]. The first scientist to recognise etchings in crystals as fission-fragment tracks caused by radiation damage by heavily charged particles was D.A. Young in 1958 and from there in 1961 P.B. Price and R.M. Walker found a way to avoid the fading of tracks by means of chemical etching, as well as their enlargement so that these were observable under an ordinary optical microscope [51, p. 235] [52]. Price and Walker observed such tracks in crystals (mica), but after R.L. Fleischer joined them, they together discovered that polymers and glasses could also record etchable tracks of heavily charged particles and thus extended nuclear track applications into nuclear physics [53].

Neutron activation analysis (NAA) was, up to the 1980s, the standard analytical method used in safeguards and dosimetry fields, for managing multi-element analyses with sub-ppm detection limits [54, pp. 50-52]. The basic principle behind NAA is that a mixture of elements comprised in a sample are irradiated with neutrons (in a nuclear reactor core) and these are excited into artificial radioactive elements whose gamma spectrum is later measured. The decay ways (emission of α, β and γ particles) of all elements are extremely well known and thus by collecting a sample's spectra post-irradiation, the radioactive decay

lines can be identified and the intensity of each peak converted back to the original concentration of the parent element in the irradiated sample [54, p. 51].

However, another effect of this method can be used to identify fissile material. Already in the 1960s, nuclear physicists showed that by irradiating fissile isotopes (initially in a nuclear reactor with a high flux of 10^{17} neutrons/cm^2), fission fragments could be detected by the marks they imprint on dielectric materials as they are decelerated. Since they are highly ionizing particles, they leave a trail of damage in a material by breaking chemical bonds and ionizing atoms, thus loosing energy until they are eventually stopped. Fission fragments can also be expelled spontaneously (natural radioactivity).

3.2 What is a Fission Track?
[55] [16]

Only ions (this includes alpha particles and obviously fission fragments) can create etchable tracks in solids (electrons, X-rays and gamma rays cannot). The most suitable detectors for fission track analysis are plastic track detectors such as CR-39, CN, PC and PET [51, p. 254] – compared to
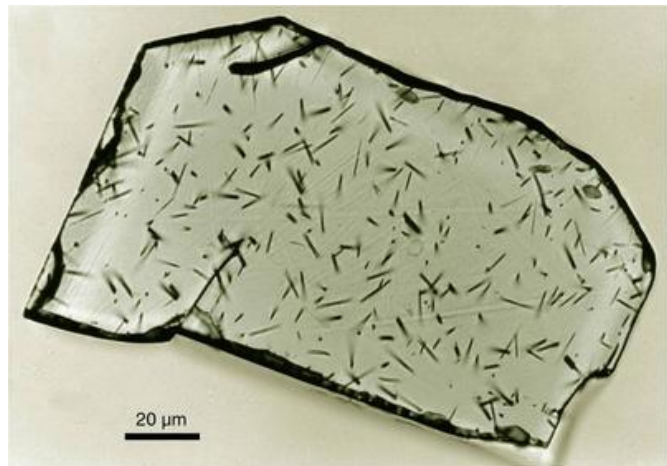
Figure 31: Image of fission tracks from apatite. Notice the tracks are homogeneously distributed and randomly oriented in the detector material. This image is from the University of Bergen FT Group. (http://www.uib.no/en/project/tectonics/57057/fission-track-laboratory)

glasses and minerals they are more sensitive to ionizing particles. In a high polymer, such as a plastic, molecular chains are broken by a passing charged particle and for this only 2eV of energy are actually necessary. This is much less than the required amount to ionize an atom and therefore, one can say that high polymers have a higher sensitivity to damage caused by ionized particles than inorganic solids [51, p. 258].

The application of the fission track technique in safeguards (SG) takes advantage of this ionizing particle interaction by putting dust particles in close contact with detector materials in order to identify the ones with fissionable material [56] [20] [25] [28] [29] [57] [58] [59] [60]. An important distinction in this case is that fission tracks originate from single entities (the fissionable material is not homogeneously distributed as it for instance is within a rock – see figure 31 (FTs from homogeneously distributed fissionable material) and figure 32 (FTs from particles with concentrated fissionable material)). In the latter case, the fission tracks exhibit a stochastically round shape and define both the presence and location of a particle of interest (POI). This circular damage site is commonly referred to as a fission track star in literature [61, p. 1222]. A disadvantage of this method is that the size of a single fission track is in the sub-micron range, making it invisible under an optical microscope without chemical etching [51, p. 258]. If the tracks are not too crowded together, one can count the total number of tracks to know the number of fissions that had occurred in the particle [51, p. 254].
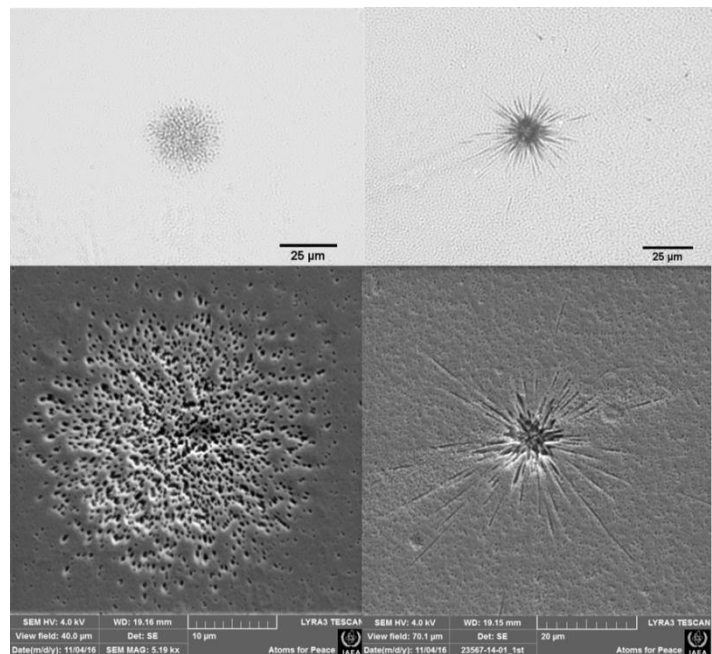
Figure 32: Optical and SEM images of FTs from POIs. (the two left images are of the same FT; the two right images are of the same FT). Notice that the tracks emanate from a single

Fission Track Detectors

A classification of the detector materials used in fission track etching can be seen in figure 33. (from [51, p. 240]). All of these can be used to record tracks of fission fragments [51, p. 250]. As was noted in the previous section, plastic (polymer) detectors are the most sensitive to heavily charged particles compared to crystals and glasses (the most sensitive being CR-39 (or PADC)) [51, p. 241]. Another advantage of plastics is that they are man-made and thus do

not carry background tracks (e.g. cosmic radiation). The use of different detectors for fission track analysis of SG POIs shall be described in the following paragraphs.

Muscovite Mica [51, p. 252]

$$SSNTDs \begin{cases} Crystals \begin{cases} Muscovite\ mica \\ Apatite \\ Zircon \\ Sphene \\ Olivine \\ Phroxene \end{cases} \\ Glasses \begin{cases} Man-made \begin{cases} Tektite \\ Obsidian \end{cases} \\ Natural \begin{cases} Soda-lime \\ Phosphate \\ BP-1 \end{cases} \end{cases} \\ Polymers \begin{cases} Polyallyldiglycol\ carbonate\ (PADC, CR-39) \\ Polycarbonate\ (PC, Lexan, Makrofil, Tuffak, Rodync) \\ Cellulose\ nitrate\ (CN, LR-115, Daicell) \\ Polyethylene\ terephtalate\ (PET, Mylar, Cronar, Lavsan \\ CR-39 - DAP\ Series \\ PETAC-EDC\ Copolymer\ detector \\ Silicone\ nitrate \end{cases} \end{cases}$$

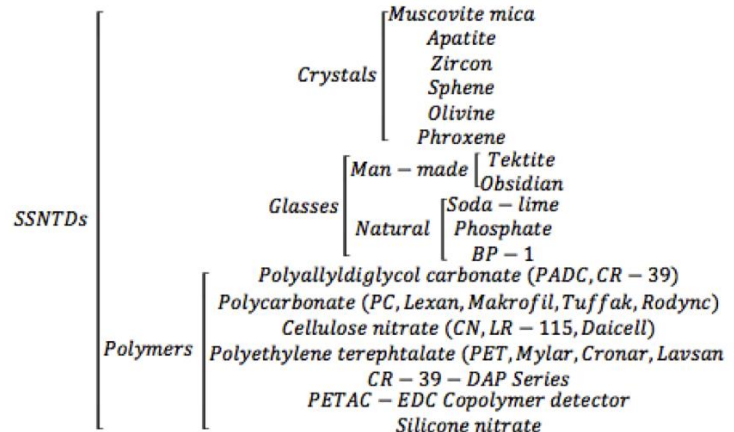**Figure 33:** Classification of Solid State Nuclear Track Detectors

Muscovite mica is a natural track detector for the study of nuclear fission at the low-energy region. It can be cleaved into suitable thickness with a perfect smooth surface and cut to the required area. The lowest atomic number Z of particles recordable by muscovite mica is 10 (Ne) and thus alpha particles emitted from fission sources cannot be recorded in mica. Upon irradiation in a nuclear reactor core, most of the nuclear reaction products from mica cannot form background tracks, which makes it a clean detector for the study of nuclear fission.

In this respect it is better than plastic track detectors such as PC, cellulose nitrate, cellulose acetate, polyethylene terephthalate, and CR-39. The detection efficiency ε of muscovite mica and the critical angle θ_c for fission fragments of U[235] induced by thermal neutrons is $\varepsilon = (93.6 \pm 0.3)\%$ and $\theta_c = 3°41'$ [51, p. 252].

Polycarbonate (Lexan, Makrofol, Tuffak) [51, p. 253] [61, p. 1222]

Polycarbonate is more sensitive than muscovite mica for fission fragments since it can record even Z=2 (He particles). However, this does not necessarily imply that full-energy α particles emitted from U and Pu can be recorded by polycarbonate detectors since they first need to be slowed down within the detector (energy <0.75MeV/u). PC cannot show tracks of natural α

radioactivity of U, Pu and heavier elements and PC is for this reason a clean detector for FT measurements.

At present bisphenol-A polycarbonate (Lexan) is usually used the most in practice for monitoring heavy ions generated in the neutron-induced fission of U, Th and Pu [62]. This material is also extremely cheap [51, p. 253].

Polyethylene terephthalate (PET, Mylar, Chronar, Melinex, Terphane, Lavsan) [51, p. 253] [61, p. 1222]

PET detectors are able to record particles from Li (Z>3). α particles and protons cannot be recorded but this makes PET a clean detector for recording fission fragments of U^{235} and Pu^{239}. [51, p. 253].

CR-39 (also PACD) [51, p. 253]

Poly(diethylene-glycol bis(allylcarbonate) (CR-39) is the most sensitive detector material in SSNTDs and can even record proton tracks [51, p. 246]. It is furthermore the most popular detector for recording α particles and for this has an energy window from 0.1->20 MeV/ (or approx. from 0 to ∞) [51, p. 246] [63, p. 351] [62]. At very high energies, CR-39 can identify charges of projectiles and distinguish the tracks of these from fission fragments [51, p. 253].

Glasses [51, p. 253]

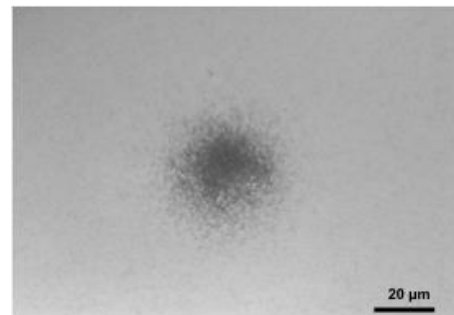Several seconds to minutes are needed to develop fission fragment tracks in soda-lime glass detectors, making it a highly advantageous detection tool. Yet, the efficiency of detection for fission fragments from a thin layer of uranium source is (39.3±0.4)%, which is less than that of muscovite mica and polycarbonate, making this type of detector obsolete for qualitative measurements [51, p. 253].

3.3 Overview of the Fission Track Method for Safeguards [16]

In the previous sections, the use of different detectors for recording FTs was outlined. FTs have optical characteristics that enable their visualization and identification under transmitted or reflected light microscopy. For the changes proposed in this work, translucid SSNTDs were used since they allow the operator to image tracks that are in deeper layers of the detector material (using transmitted light microscopy). See figures 34 and 35 for optical images of FTs under reflected and transmitted light.

As was stated before, FTs are not visible under an optical microscope until they have been chemically etched. POIs are thus found by comparing the location of the FT clusters to their originating particles in the catcher. There are several implementations of the FT method for single particle identification [56] [20] [25] [28] [29] [57] [58] [59] [60]. Most commonly the particles extracted from a swipe are first embedded in a film medium called a catcher (usually a collodion-based mixture that dries out within 24 hours). Then the mixture is placed (or pipetted) onto a detector and after drying dispatched to a nuclear reactor for irradiation. In a reactor, charged fission fragments emerging from a POI ionizes the atoms along its trajectory in the detector

Figure 34: Reflected light image of fission tracks, 2 minutes of etching, 50x magnification. This was an FRM II irradiated sample.
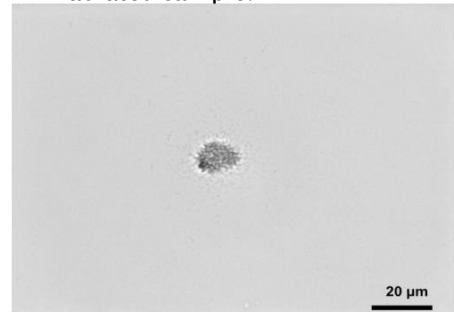
Figure 35: Transmitted light Z-stack image of a fission tracks, 2 minutes of etching, 50x magnification. This is the same FT as in Figure 34. This was an FRM II irradiated sample.

creating a trail of damage [64] [65]. The detection limits in FT analysis are governed by the isotopic composition with respect to fissile isotopes, fission cross-section of the fissile atoms and the energy/fluence of the projectile neutrons [62]. For both U and Pu it is in the sub-fg level [62] [66].

3.4 Improvements to the FT Analysis Method

The existing methodologies suffer from several limitations. In particular, since most of the steps are conducted manually, the method is operator dependent, has low throughput and might bear difficult to account for biases. The state of the implementation does not allow for automation and limits the scalability [62] [66] [16]. In the past couple of years, individual steps were evaluated in order to optimise the FT process as a whole. Therefore, the following was proposed:

1. A new sample assembly construct with three parts: a catcher and detector sandwich for irradiation and a catcher and harvester sandwich for particle segmentation;

2. The use of thick SSNTD materials as detectors;

3. Sample irradiation in a low gamma irradiation channel;

4. An accelerated etching process.

By using three separate parts (catcher, detector and harvester), the three steps of the FT method can be optimised individually:

1. Irradiation: The use of a thin catcher with evenly distributed non-overlapping particles ensures their even and close contact to the detector during the irradiation;
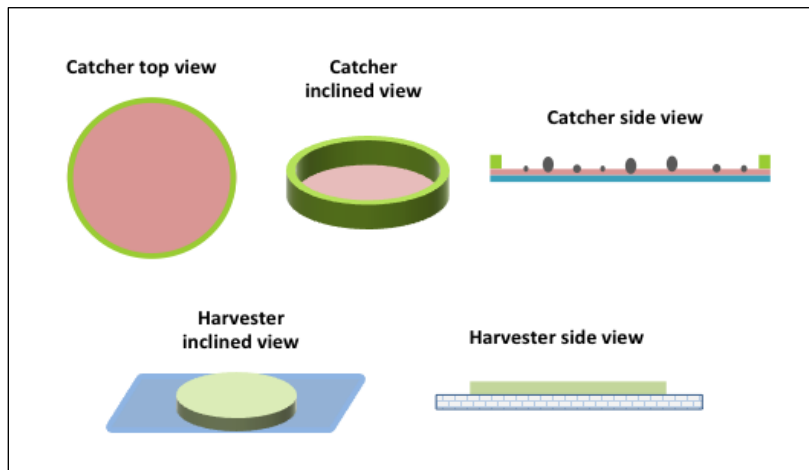
Figure 36: Schematics of catcher and harvester

Particle separation is done by means of a shock wave disperser;

2. FT identification: Detector etching is rapid, ensuring minimum distortion and improved FT to POI assignment;

3. POI harvesting: The thin catcher and sticky harvester materials ensure an up to 100% POI transfer onto a new substrate for microprobing.

These steps are discussed in detail in the following sections.

Catcher and Detector Assembly [16]

The catcher is made out of a thin piece of Mylar foil (Mylar, polyester film, 2.5μm, Breitlander GmbH, Hamm, Germany) or nucleopore filter (Nucleopore Track-Etch Membrane, PC, 0.1μm, Whatman, Tisch Scientific, USA), both 25 mm in diameter. The foils are coated with clear varnish (Daler-Rowney Ltd, Bracknell, Berkshire, USA) by means of a spin coater. The estimated thickness of the sticky layer is~2μm. A 3D printed plastic ring of 24 mm outer diameter was placed onto the coated foil. In this way, the catcher resembles a shallow tambourine (see figures 36, 37 and 38). Coating the foil with a sticky substance was done to minimise particle loses due to bouncing and electrostatic effects. An anti-static gun was also used to handle the mylar foil spreading before coating. Next, the catcher was positioned inside a shock-wave disperser [26]. This specific shape of a thin film ringed tambourine was chosen to permit the laser-based cutting of the identified POIs, as well as to have a flat contact surface between the catcher and particle harvester. The catcher was allowed to dry overnight and was then affixed onto a detector using a droplet of 0.1% sucrose in water solution to ensure a flat, equidistant and intimate contact between the catcher particles and detector.
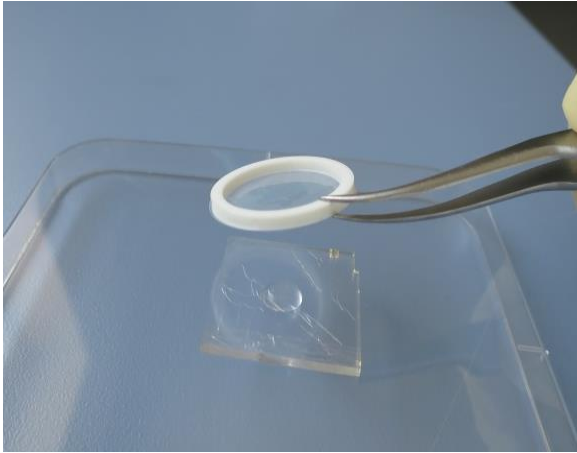
Figure 37: Catcher being attached to the detector using tweezers.
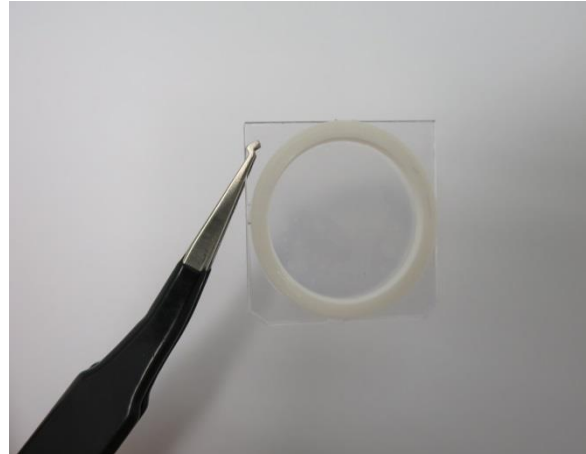
Figure 38: A close-up of the catcher and detector with dispersed particles.

Harvester [16]

This third component, called a harvester, is used to facilitate the removal of all identified POIs in a single collecting substrate by a single operation, simultaneously automating this step. Essentially, a harvester is placed in direct contact to the catcher and is a construct for hosting the POIs after their cutting from the catcher. The isolation of POIs is achieved by gluing the catcher POI-containing cut-outs to the harvester surface as these are being cut out. In practice, the harvester is a relatively thick (~1 mm) translucent, slightly adhesive square or circular piece of cured silicone elastomer. This was made from Sylgard (SYLGARD® 184 Silicone Elastomer Kit, Dow Company, US). About ~10 ml of the mixture was placed into a plastic cup and allowed 3 days to dry in a vacuumed container to minimize environmental particle contamination and minimize the formation of bubbles during the drying. The dried silicone was then cut out into 22 mm in diameter circles and placed onto thin quartz microscope slides 24mm x 40mm (Deckgläser, Menzel Gläser, Germany) (see figure 36 for the

Figure 39: Harvester drying in a sealed vacuumed container.

harvester construction and figures 39 and bottom right of figure 41 for an image). Due to the large adherence of silicone cut-outs to glass, the harvesters were simply placed onto a quartz slide for mechanical stability before cutting.

SSNTDs as Detector Material [16]

From all of the types of detectors for FT analysis described, the Solid-State-Nuclear Track Detectors (SSNTDs) type (PC, PET and CR-39) were used for our experiments. They combine the track recording properties of photographic emulsions and the single particle counting abilities of the semiconductor detectors while keeping permanent records that are unaffected by light and normal atmospheric conditions [62] [51] [65]. In this series of investigations, the detectors used were plastics from a variety of manufacturers. They were either of specialized CR-39 type (1. Landauer, UK; and 2. Radosys Radiation Detection Company, Gilroy, California). or industrial plastics (Semadeni, Vienna, Austria). The most important factor for choosing our SSNTDs was their thickness: 1–2 mm. It was hypothesized that thick detectors would not show extreme etching, mechanical deformation or irradiation effects (colour change) typical in thin foil detectors (such as Lexan). Also, a thick detector provides a degree of stability to the assembly [67]. All detectors were square shaped, translucent and covered an area of 24mm x 24mm.

Assembly Irradiation [16]

A consideration for the selection of the irradiation conditions was to ensure a low gamma background because this affects the bulk and track etching characteristics of any plastic detector [68]. A high gamma flux creates artefacts in the detector, which are difficult to deal with during imaging (specifically: milkiness and structural tessellation). Therefore, the low gamma irradiation channel at the FRM II Research Reactor in Munich was chosen. It is worth noting that these disadvantages from high gamma backgrounds may be avoided with the use of muscovite mica and other mineral SSNTDs.

Prior to irradiation, the assemblies were placed into separate plastic bags and packed airtight within aluminium capsules (V=30 cm^3), which were then lowered into a pool of water to an irradiation position with a neutron flux density of up to 1.3 x 10^{14} cm^{-2}s^{-1}. The standard ratio of thermal/fast neutron flux density at this spot ranges between 330 and 770. Each sample was irradiated for 1 hour.
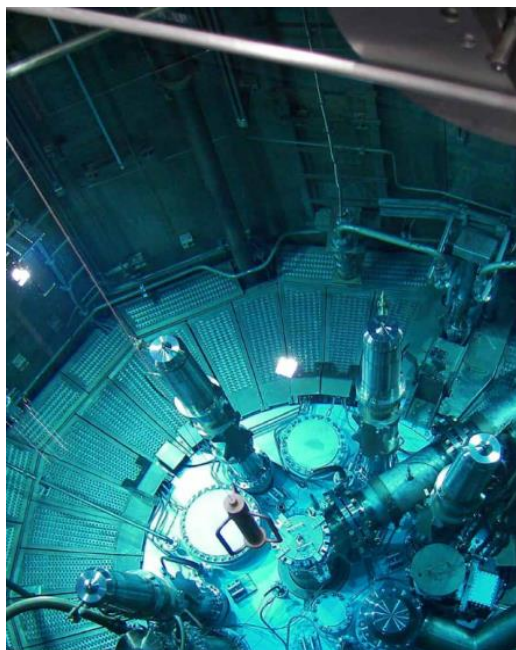
Figure 40: Moderator tank used for sample irradiation at FRM II Munich.
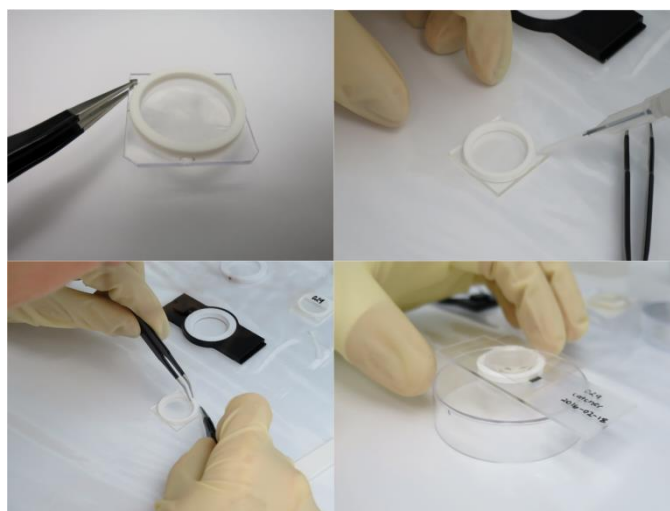
Figure 41: From top left - a) unpacking of catcher and detector assembly; b) pipetting water between the membrane and the detector; c) slow removal of the catcher from the detector; d) placement of the harvester onto the catcher.

Figure 42: Samples with mica (top and bottom left) detectors and a semadeni plastic.
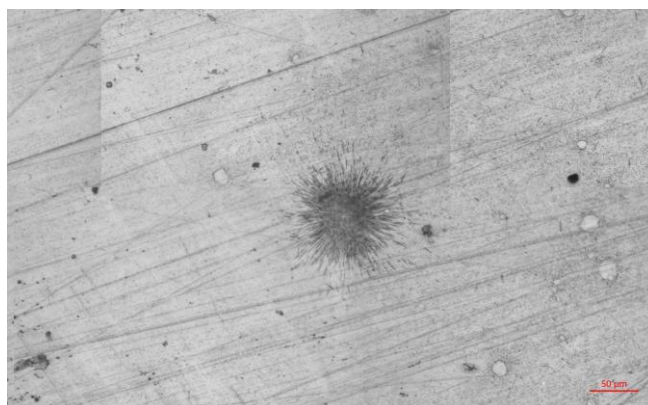
Figure 43: FT with high background.

Detector Etching [16]

The aim of etching is to make visible (under an optical microscope) latent tracks left by fission fragments. In the best case, FTs would be the only artefacts on an image, or at least they would be easily distinguishable from their background. As was stated before, some precautions were taken to minimise the background (compare figures 43 and 34). Etching is a crucial step in that it may result in distorting the detector greatly. This of course affects the relocation accuracy and thus besides using thick detectors, the etching proposed by [69] was employed. The etching time quoted by [69] was 10-13 minutes. For

Figure 44: Etching of SSNTD using a forcepts. Thermostat bath set to 60°C.

these samples FTs were observed after 2 minutes of etching and the detectors were overetched at 7-9 minutes. It was confirmed experimentally that long etching times lead to a higher structural tessellation in the detectors (see the background in figure 43).
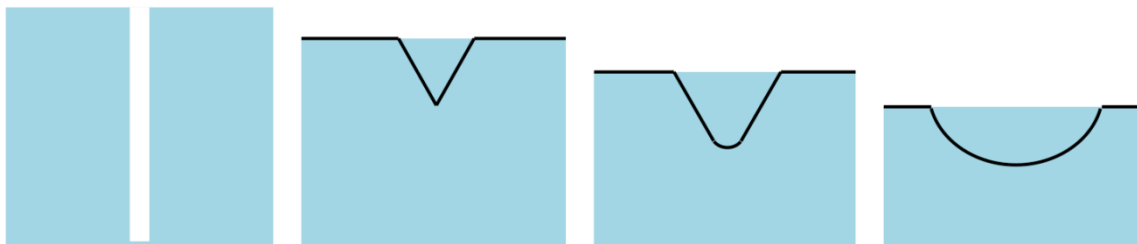
Figure 45: left to right: a latent track; etching started; etching of the track is optimum; the detector was overetched and the track is barely distinguishable from the background.

When a detector is submerged into an etching solution (see figure 44), the etching solution will eat away the plastic layer by layer. The damaged areas will recede at a faster rate than the bulk (see a depiction of this in figures 45 and 46).

Plastics are birefringent materials and defects of the material (surface or other) may be revealed by chemical etching [70]. The damage exposed by etching is not always only from fission fragments: lateral birefringence is also 'seen' by ionizing radiation. During the production process, plastic molecules are 'frozen' in a certain conformation during the melting stage (while the plastic is being moulded or extruded). As a consequence, certain molecules can exhibit different angles of refraction for incoming electromagnetic waves and thus a single material will behave as having several refractive indices. A polarizer can be used to detect this.

For a collection of tracks (depending on the etching time), the side view of developed FTs from a single POI is shown in figure 47. [71] summarizes several papers where the bulk etch rate depends on the SSNTD used: different bulk etch rates were observed for CR-39 detectors from different manufacturers, implying that a stricter classification of this material should be conducted.

The etching conditions are probably the parameter reported with the largest variability between publications [16] [72] [20] [22] [25] [28] [29] [57] [58] [59] [69] [73] [52]. Etching rates are mostly not reported and etching times vary (from minutes to hours). Thermostat temperatures range from room temperature to
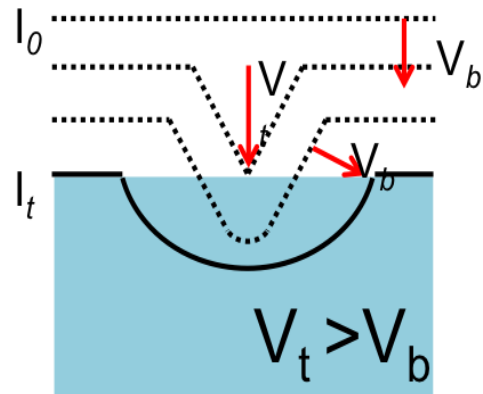
Figure 46: Track etch rate is higher than bulk etch rate $v_t > v_b$
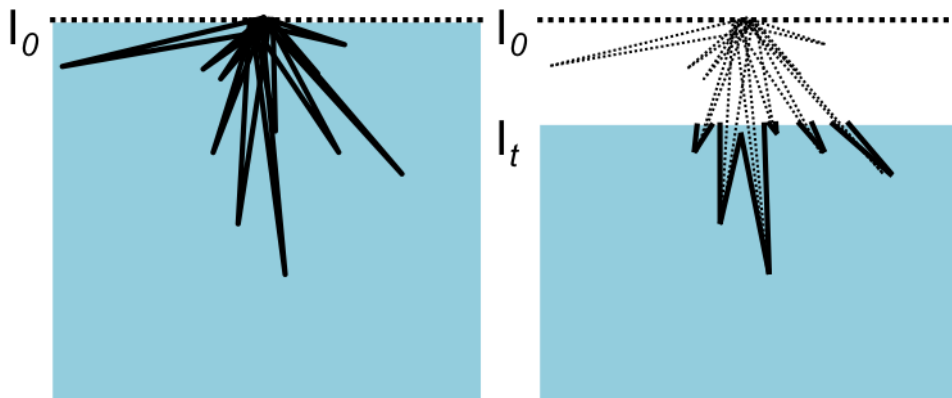
Figure 47: Side view of FTs from a single particle before (left) and after (right) etching.

64

90°C. Higher etching temperatures may cause irreversible changes in the volume of the nuclear track detector (swelling effect) which would decrease the precision of the localization of micrometer particles. The type and concentration of the etchant varies too [16] [20] [25] [29] [57] [58] [59] [22] [69] [52].

Thus, for the reasons outlined in the previous paragraphs, each type of detector requires an optimization step of the etching since there is no consensus on the criteria. [74, p. 788] gives an insight into how to approach optimizing the etching conditions for CR-39 detectors from different manufacturers using different etchants. It was shown that detectors from different manufacturers exhibited varying etch rates, but all etch rates were still of a linear nature. In [16], it was decided that the optimization of the etching conditions would be made subjectively: optimized conditions should produce well-defined track clusters, with reasonable contrast, without introducing too many structural/tessellation artefacts in the background. This was for the purpose of ultimately automating the search for FTs. From the evolution of one FT shown in figure 48 [16], it was concluded that, for the detectors used in this case, the optimum etching time (developed FTs with low background) was 3-4 minutes.

Table 4 summarizes 13 publications' etching conditions for FT analysis using SSNTDs. Note that the applications of SSNTDs in these varies. This includes long-term measurements, synchrotron beams, nuclear activation analysis, fission fragments etc.

Publication	Detector type	Etching solution	Etching time
[59]	PC membrane filter	6 M NaOH at 55°C	1-30 minutes
[75]	CR-39	5 M NaOH/ethanol mixture at 55°C	2- 30 minutes
[71]	CR-39	KOH solutions ranging from 4.7 to 7.6 N at 70°C	minutes to hours
[20]	Polycarbonate membrane filter	6.5 NaOH at 70°C	15 minutes
[76]	Muscovite mica	40% HF at 25°C	20 minutes
[69]	CR-39	6 M NaOH solution with variable Na_2CO_3 mixture at 50, 60 and 70°C	15-210 minutes
[74]	CR-39	5.4 N KOH at 80°C	6h
[58] [28]	Makrofol	6M NaOH at 55°C	15 minutes
[29]	Makrofol	6M NaOH at 55°C	15 minutes
[14]	CR-39	NaOH at 60-70°C	3, 8 and 26 minutes
[77]	Lexan	KOH at 60°C	35 minutes
[78]	CR39	6 N NaOH + 1% ethyl alcohol at 70 °C	40 h
	CR39	6 N NaOH, 70°C	30 h
	CR39	6 N NaOH, 45 °C	268 h
	Makrofol	6 N KOH + 20% ethyl alcohol at 50 °C	8 h
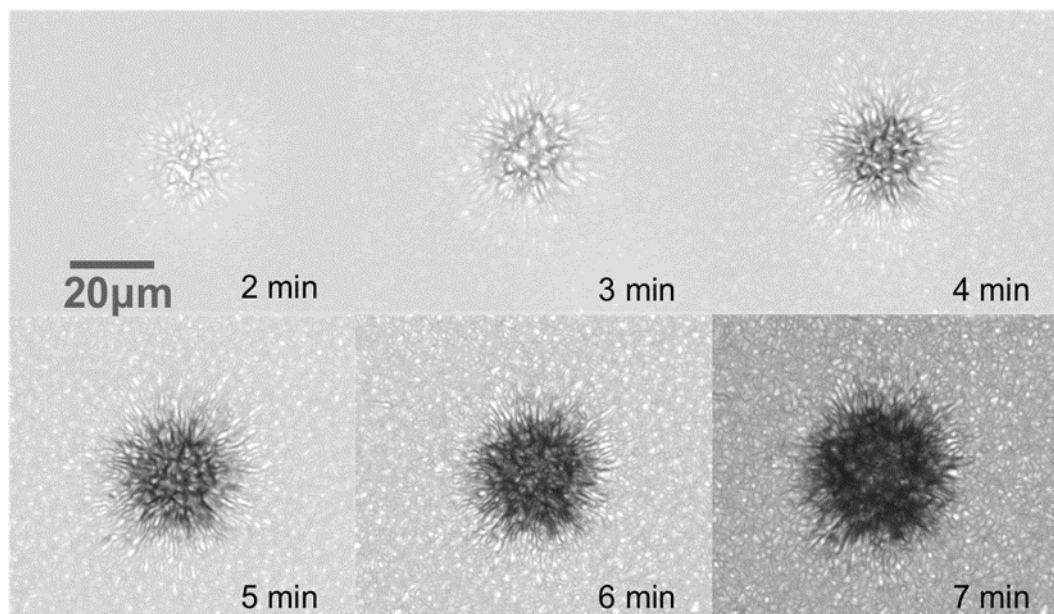
Figure 48: Evolution of FTs with etching. The same FT was relocated in intervals of 1 min of etching and imaged in a Zeiss Z2m microscope at 50x magnification. The images above are the results of morphed Z-projection stacks for which 15 slices (images) at 0.15 μm distances of a single FT star were taken. Note that this particular sample was irradiated at the Atomic Institute (ATI) of the Vienna University of Technology. The SSNTD used was a Semadeni industrial plastic.

The etching conditions used for the detectors in this work were taken from [69]. Each detector was immersed in a 6 M NaOH solution with 4% Na_2CO_3 at 60±0.1°C inside a teflon beaker, in a thermostat bath. While etching, the detector was held by plastic tweezers and
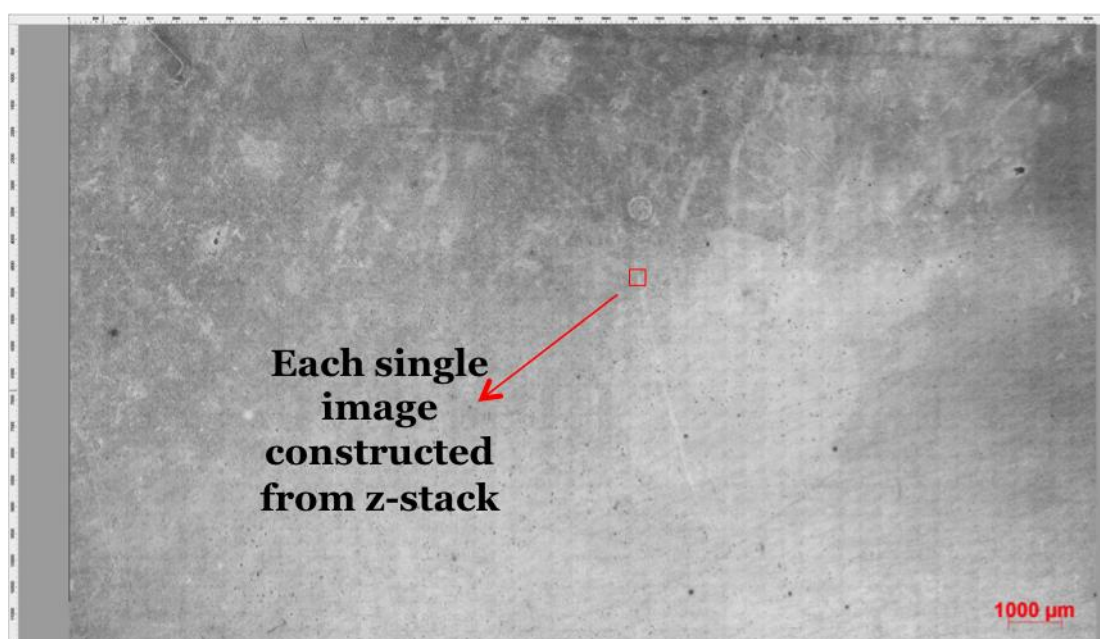
Figure 49: Overview imaged stitched by the native Zeiss software.
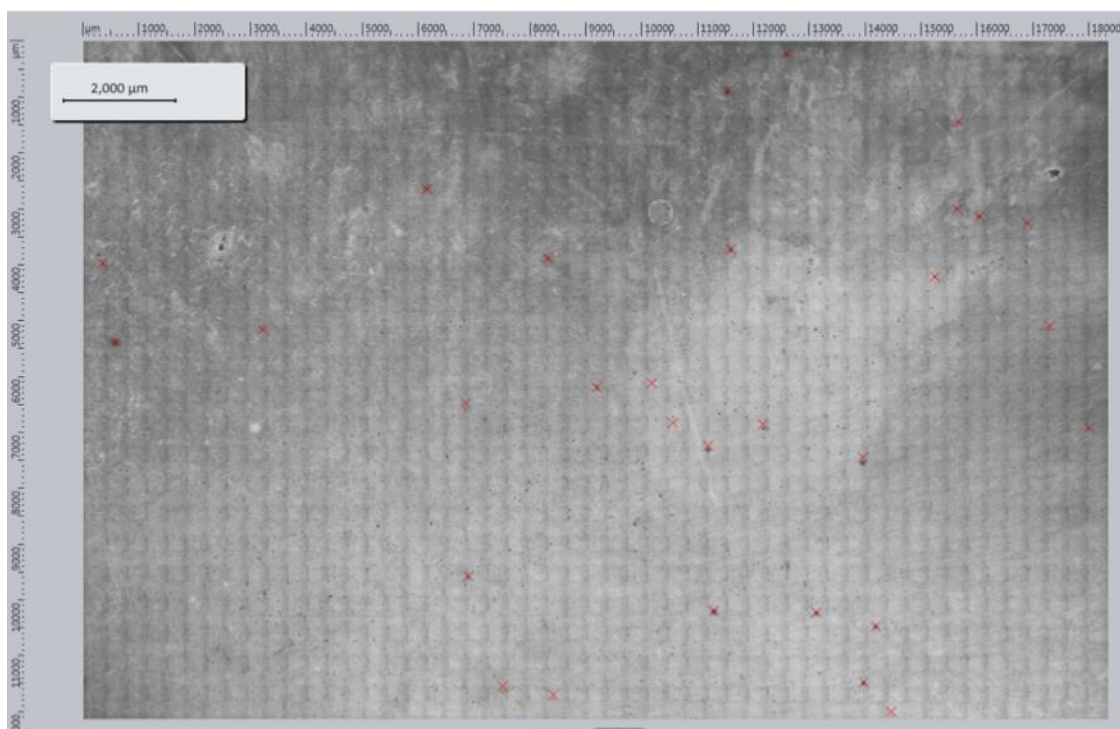
Figure 50: 30 FTs found and marked within a single sample detector.

stirred through the etching solution to keep the etching solution homogeneous and avoid that the etched products deposit on the detector surfaces [78]. Post-etching, the detectors were washed under running osmosis water for 30 seconds and allowed to air-dry. Then, they were scanned using a Zeiss Z2m optical microscope at 5x, 10x and 20x magnification to collect mosaic images (see figures 49 and 50 for overview images of a whole detector). These were stitched together using native Zeiss software (AxioVision) and inspected closely for FTs: each FT coordinate could be traced using the 3-point coordinate system (see Chapter 4 for details of the relocation) marked by laser-imprinted fiducial marks. Note that the detector samples shown in Figures 49 and 50 were over-etched and that these samples were also irradiated at the Atomic Institute in Vienna (higher gamma background in this channel than the one chosen at FRM II Munich). Notice also the low level of structural topographic artefacts in the FT images shown in figures 34 and 35 ("flat background") compared to figure 43 (over-etched).

3.5 Fission Track Classification

In our experiments, a range of different fission tracks was observed. In all types of plastic detectors, particles with very low U-ore content left few tracks, and particles with large U-ore content 'burned a hole' in the SSNTD. See figure 51 for a graph showing FTs from different SSNTDs following this rule. As can be seen from this figure, FTs have characteristics that enable their visualisation and identification, but which also distinguish them from other features [16]. The tracks in plastic detectors form a radial cluster and lengthen and widen with increased etching time until a certain maximum has been reached (over-etching) [64]. In some cases (FTs to the far left of figure 51), it is easier to distinguish individual tracks and thus estimate the number of fissions that occurred in the original POI by their count. This has been done in previous publications in order to assess the U-isotopic content of particles [51] [20] [29] [58] [60] [22]. Nevertheless, there are difficulties in this non-standardized approach due to the lack of reference materials, reference particles or scientific consensus concerning the approach to this issue.

Still, three main types of FTs could be distinguished in the etched detectors using two morphological structures [16]:

1. the inner (omphalos) zone; and
2. the outer (trix) zone.

Low activity FTs (left images in figures 51 and 52) have no omphalos; medium activity FTs have a small omphalos and well-developed trix (overlapping tracks); and high activity FTs have a supreme omphalous and less developed trix [16]. In samples 018 and 037 no medium activity FTs were observed and sample 029 had no high activity FTs (as can be seen in figure 51). Table 5 shows the type of SSNTDs used and etching time for each of the detectors in figures 51 and 52.
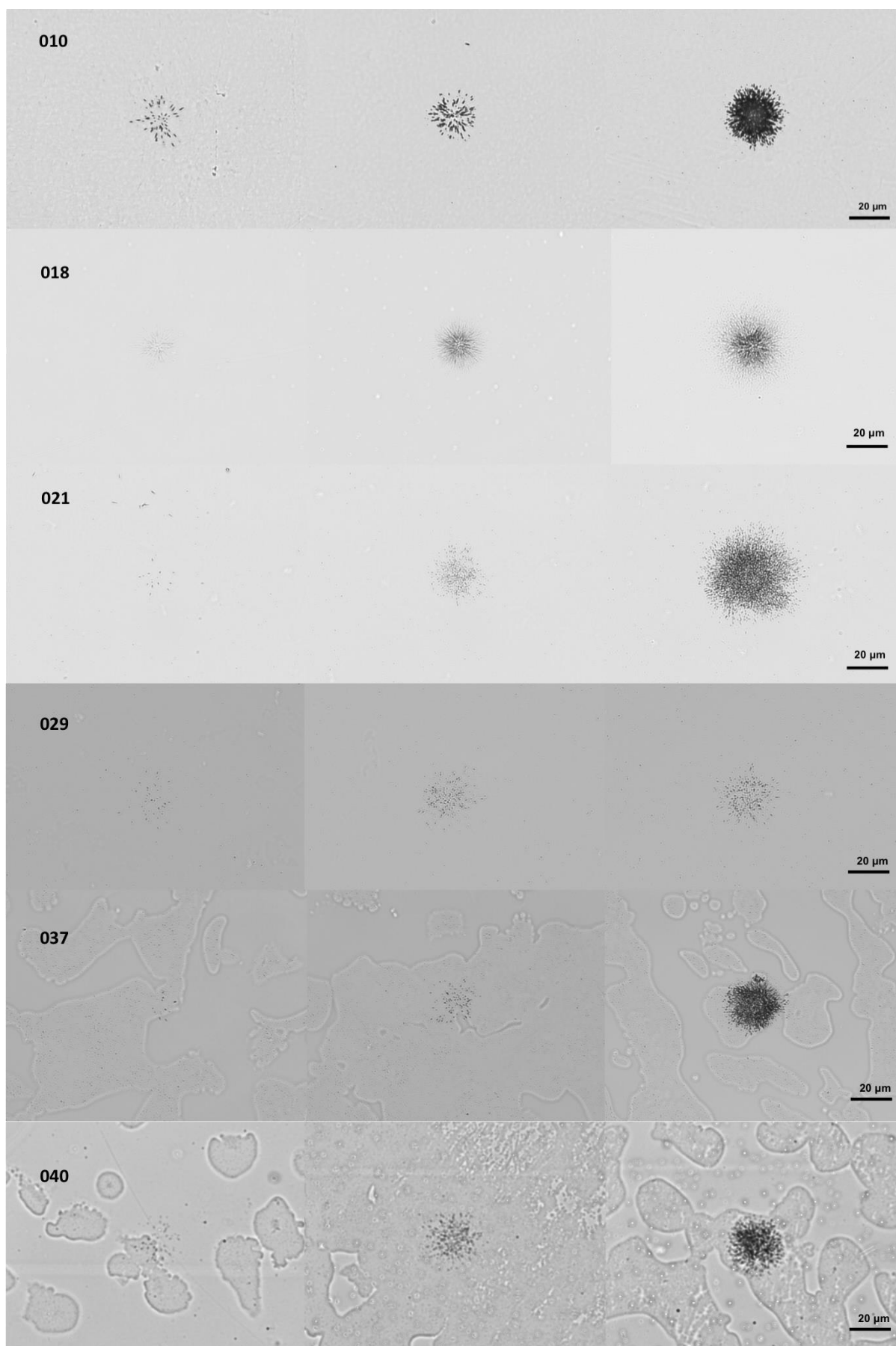
Figure 51: Low, medium and high activity FTs from 6 detectors. Detector number is indicated on the left and FTs are grouped from left to right with increasing LA-ICP_MS signal (see chapter 5)

Sample ID	Detector type (manufacturer)	Catcher type	Etching time
010	Semadeni Industrial plastic	Nucleopore filter	5 minutes
013	Muscovite mica	Nucleopore filter	70 minutes
018	Radosys CR-39	Mylar foil	5 minutes
021	Radosys CR-39	Nucleopore filter	5 minutes
029	Radosys CR-39	Nucleopore filter	4 minutes
037	Landauer CR-39	Nucleopore filter	6 minutes
040	Landauer CR-39	Nucleopore filter	6 minutes

Table 5: Detectors and individual etching times
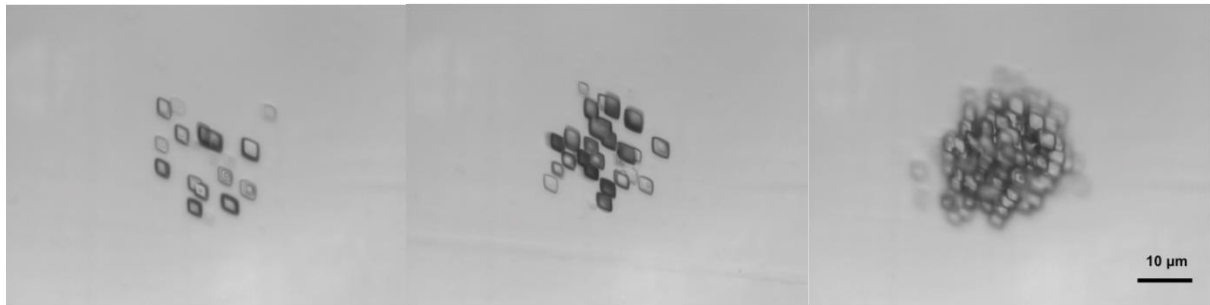
Figure 52: Muscovite mica FTs. These images were taken at 100x magnification (Figure 44 images were taken with 50x lens). Note that the same pattern was observed in mica FTs: low, medium and high activity stars (left to right). Note that this sample was etched in in 40% HF and these images were taken after 70 minutes of etching.

Detector Thickness vs Etching Time

After each minute of etching, the detectors were taken out to measure their thickness using a micrometer. This measurement was only taken for the plastic-type detectors. A difference in the average etching rate was observed for detectors from different manufacturers: sample 010 (9.2 µm/min); samples 018, 021 and 029 (15.8 µm/min); samples 037 and 040 (7.1 µm/min).

3.6 Automatic Fission Track Recognition [16] [55]

There exist reports in the literature [79] [60] of efforts towards attempts at automating the FT pattern recognition procedure. These mostly refer to work in the fields of dosimetry and

geology. Currently, reports on the development on a fully automated FT recognition and relocation algorithm are being published [55].

The growing use of FIJI and ImageJ has had a profound influence on the way digital data is treated in recent years. The same is true for optical image processing: using a set of native FIJI plug-ins, FTs can be distinguished from other image artefacts, therefore automating the FT-to-POI coordinate export. The following FIJI plug-ins are used and the logic goes (see figure 53 for a depiction of each step) [55]:

1. background correction;

2. hysteresis thresholding;

3. masks of ROIs are created and assessed for roundness;

4. these are then skeletonized and based on those two criteria the ROIs are evaluated to be FT stars (or not). The criteria in this step is the number of endpoints (this can be changed by the user);

5. the fiducial points are input into the software and then the coordinates of the FT star centroids are output in reference to these three points.
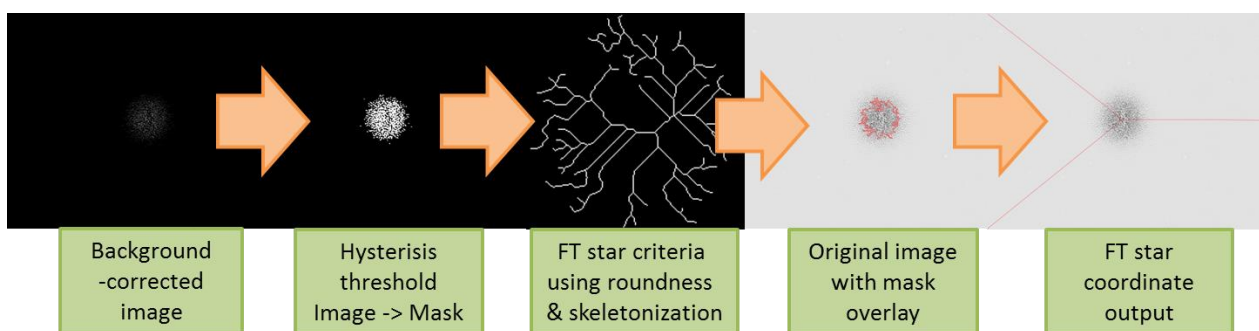
Figure 53: Digital track map creation: the identification of POIs is based on a Fiji script. The whole sample detector is imaged at 20x and each image is analysed separately to find whether it contains fission tracks. [55]

This work is faulty, and will not recognise all low activity stars as FTs, making operator surveillance still necessary. Another problem are false positives (artefacts on the sample that are registered as FTs). No work has been done in this contribution towards automating the recognition of mica FTs. Examples of external efforts and suggestions towards the automatic

image recognition of tracks along with associated difficulties of the software can be found in [79] [20] and [60].

3.7 Measuring FT Coordinates

Once the sample (catcher + detector assembly) has been marked with three fiducial points (see figure 54 for an overview image with these marks), and after the detector has been etched (see figure 55 for an overview image of an etched detector), it is the task of the operator to convert these images into a file containing three reference points and the coordinates of all FTs (POIs) identified. A list of FT coordinates is made and exported.

Figure 54: Overview of catcher and detector assembly with three fiducial marks.
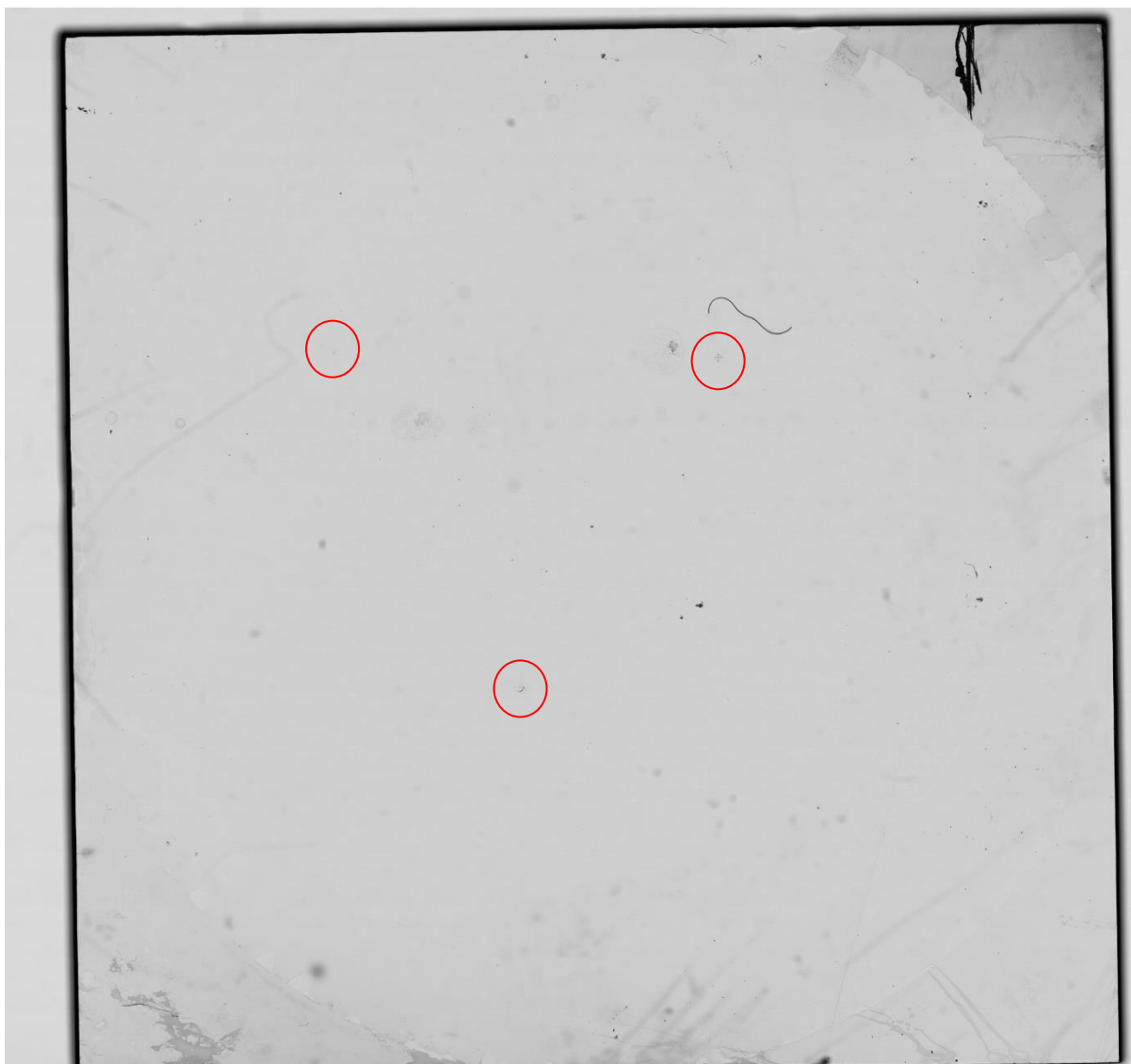
Figure 55: Etched detector overview image.

Another observation made during these experiments is that FTs from very small particles remain hidden or are etched away extremely quickly. See figure 58 for an example of an FT imaged at 3 mins that was no longer observable in the SEM after 7 minutes of etching. The optical image was taken with polarized light, highlighting a number of tracks in the SSNTD.
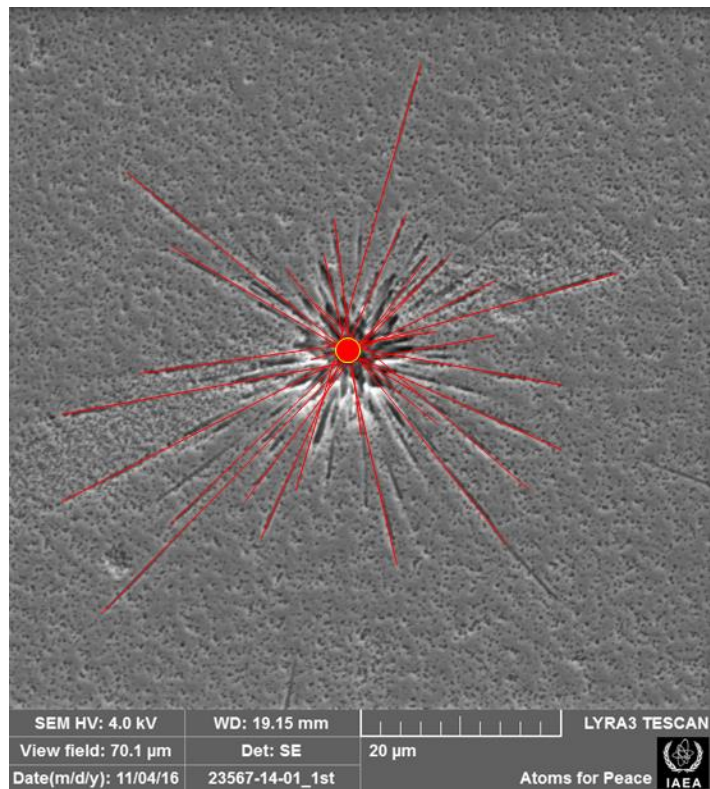
Figure 56: Calculating the source of FTs.
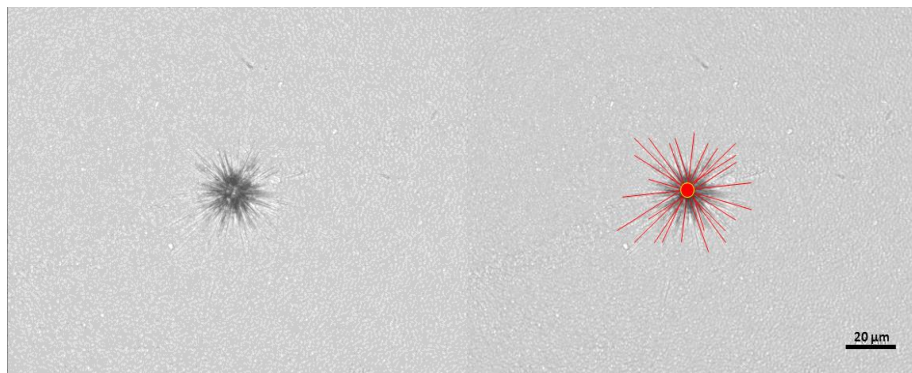
Figure 57: Calculating the source of FTs in an optical image.

Figure 58: SEM (left) and optical (right) images of the same FTs. See lower left image for a typical FT BSE image.

Chapter 4: Isolation of Particles-of-Interest

The list of FT coordinates, serves as an ex-situ reference for identifying POIs in the catcher (see figure 59 for an example of identified FTs in a square detector field and figure 60 for the logic of creating a digital reference map). Our methodological setup was developed for isolating POIs for external microprobe analysis (LA-ICP-MS, TIMS, SIMS, μ-XANES and NEXAFS at synchrotron facilities). The cutting out of particles is conducted using a laser micro-dissection (LMD) device (figure 61).
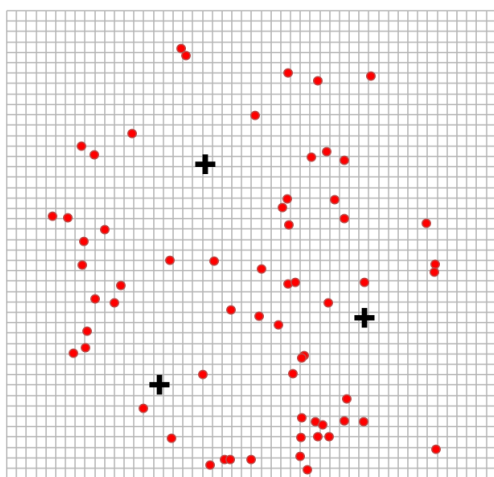
Figure 59: identified FTs (red) with three fiducial marks (black crosses) in a detector. These are used as a reference for cutting out POIs.
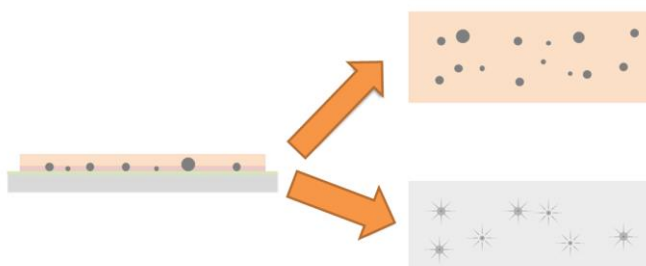
Figure 60: Digital track map creation: the etched FT detector is a reference for POI locations in the sample catcher.

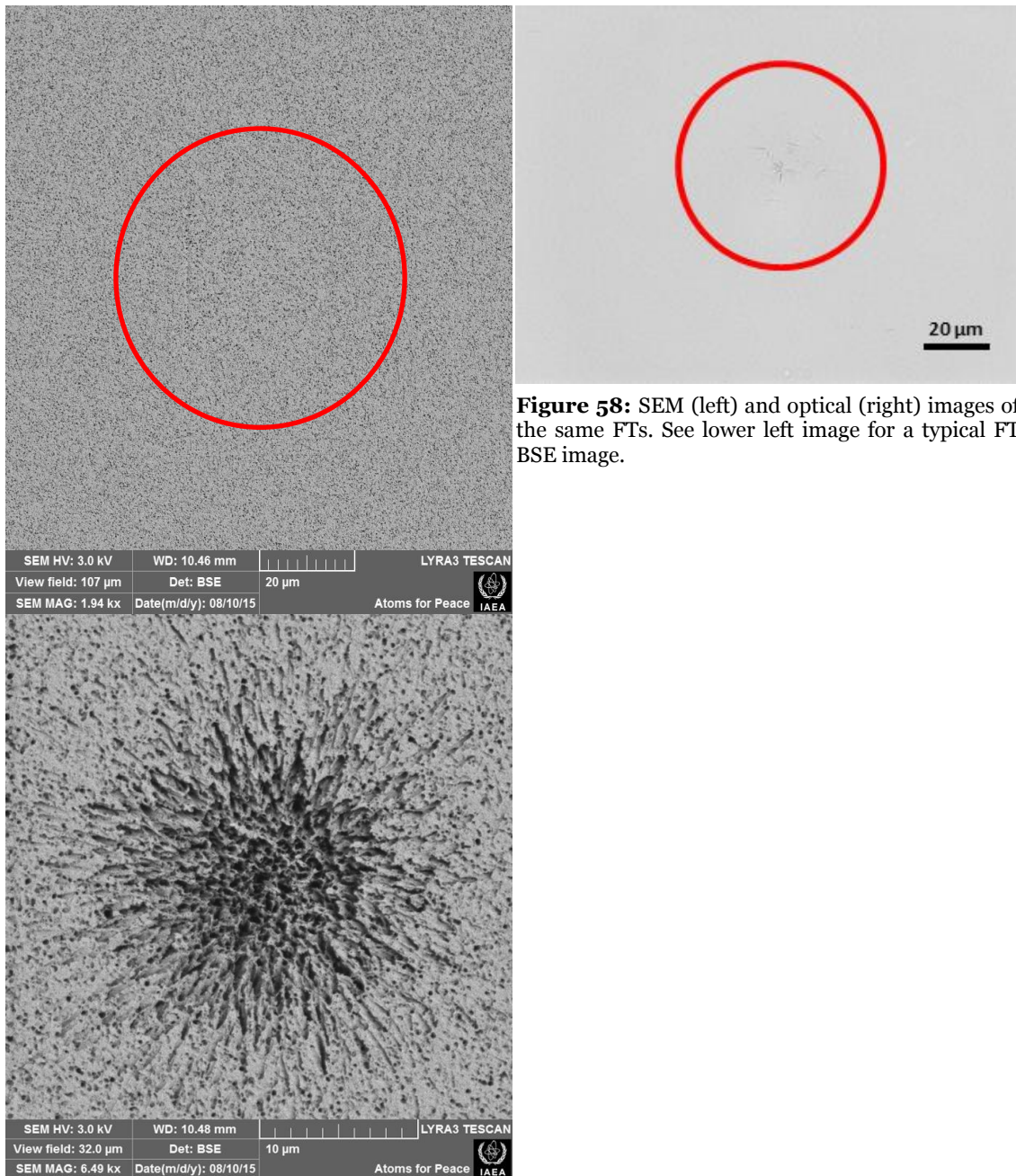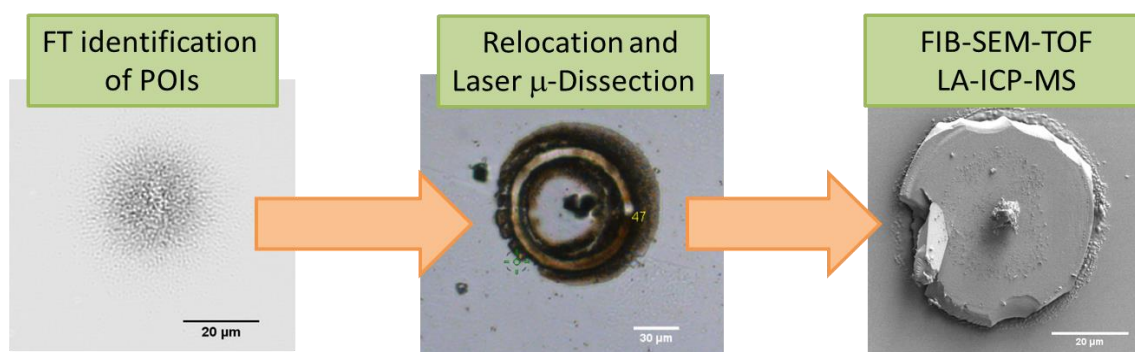**Figure 61:** Analysis Flow from FT star to POI isolation. Upon return from an irradiation facility, three fiducial markers are imprinted onto the detector-catcher assembly after which the detector is detached and developed to reveal a set of fission track stars (1st image on left). The detector is then imaged at 20x and the coordinates of the FT stars, in reference to the fiducial markers are registered. This map is used as a relocation table for the particles from which the tracks originated in the catcher. Once laser micro-dissected (2nd image above), the particles can be analysed using several analytical instruments at the IAEA Laboratories in Seibersdorf (3rd image above is before FIB-SEM-TOF).

This chapter starts with an introduction to the application of LMD in other fields, followed by a brief rationale for using it in particle analysis. Next, the relocation logic is explained and followed by specifics of the procedure for cutting POIs. Selected experimental work discussed in this chapter was published in a scientific journal in 2015 [80].

4.1 Laser Micro-Dissection

Laser Micro-Dissection (LMD) or Laser Capture Micro-Dissection has gained importance in the biological, molecular, botanic and medical sciences since the 1970s as a tool for single cell isolation and manipulation [81] [82] [83] [84] [85]. It has numerous advantages over manual tissue micro-dissection methods: it is simple, requires no moving parts, involves no manual microdissection or manipulations, enables single step transfers, and is completed as quickly as taking a photograph of the micro-dissected tissue [82]. The impact it had on the research quality in biological and related fields is hard to compare to any other tools other than the mass spectrometer: to-date, more than 61 000 journal articles have been written (Google Scholar search for "Laser Microdissection", Dec 18th, 2016).

By the same token, LMD can be used in materials science as a device for the isolation of particulate material dispersed on a thin substrate [86]. In particle analysis, micron-sized artefacts are generally cut out manually (see figure 62). Then, the cut-outs would be lifted using a glass or micro-needle and transferred to a new substrate for further analysis. This is extremely laborious work and it can take a full day to isolate and transfer 10 particles. LMD offers huge improvements to this sample preparation step not only in speeding up the cutting of POIs, but also a completely automated particle isolation step.


Figure 62: Manual cutting around the POI. Notice that the POI is on a lexan detector from which an FT is used for verification. From [87])

4.2 Correlative Microscopy in Safeguards

To achieve these goals with LMD, major improvements needed to be made in the fission track method for safeguards. This meant a system needed to be devised for automating the relocation of particles between different instruments. Naturally, this depends on other factors such as the stage and microscope stability, etching quality and how deformed the detector was, but also on factors such as particle separation (addressed in Chapter 2). Ideally, such a system should find FTs on the overview image of the detector and automatically calculate the positions of the POIs on the catcher [11] [55] [87] .

To assign FTs to a POI, a correlative microscopy approach was developed in-house. Correlative microscopy is a technique that is well-established in the biological and materials sciences for using multiple instruments to study a single area or artefact of interest by using a set of markings for relocation [80] [88] [89] [90] [91] [92] [93] [94] [95]. It is a critical method for providing a complete assessment of particles from an environmental swipe sample since no single microscopy or mass spectrometry analysis can provide a comprehensive characterization of the sample [80]. Correlative microscopy has successfully been employed at the Seibersdorf Laboratories of the IAEA in relocation POIs between two optical microscopes, an LG-SIMS, a scanning electron microscope and a LA-ICP-MS device.
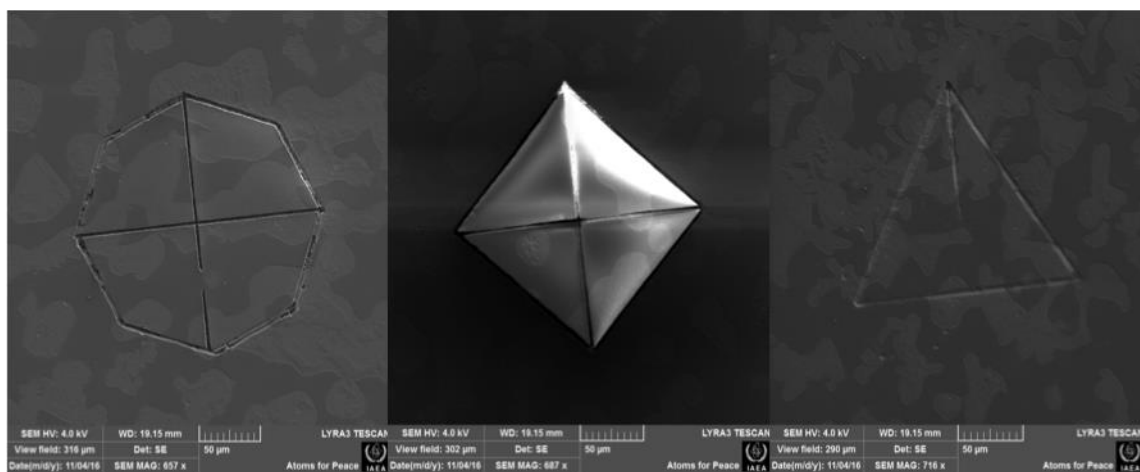
Figure 63: Fiducial markings imprinted on the detector using a LMD device. The shapes are inscribed in a circle of 100μm in diameter.

4.3 Relocation [96]

As was stated in the previous chapter, once the sample has been returned from the irradiation facility, a set of markings are imprinted on the sample catcher and detector before the detector is removed for etching. See figure 63 for images of the markings on an SSNTD detector.

The relocation principle employed in this work was devised by Uri Admon and Ernesto Chinea-Cano at the IAEA Laboratories and published in 2007 [11]. It is the so-called 3-point relocation algorithm and the mathematical details are as follows: [96] [11]

Let **A**, **B**, and **C** be three non-collinear fiducial points on the sample.

Let **O** and **O′** be two distinct Cartesian coordinate systems, corresponding to two instruments. It can be shown that any point **X** co-planar with **A**, **B**, and **C** may be expressed in both coordinate systems **O** and **O′** as the vector sums:

$$\vec{p} = \sum_{i=1}^{3} m_i \vec{r_i} \quad \text{(in coordinate system } \mathbf{O})$$

and

$$\vec{q} = \sum_{i=1}^{3} m_i \vec{s_i} \quad \text{(in coordinate system } \mathbf{O'})$$

where the components $\{m_i\}$ are independent of the coordinate system used and are of unit length such that $m_1 + m_2 + m_3 = 1$

Let $\{x_i, y_i\}$ and $\{u_i, v_i\}$ be the measured stage coordinates of the reference marks **A**, **B**, **C** in the source and in the target instruments, respectively. Considering that **A**, **B**, **C** and **X** are co-planar one can write:

$$\begin{pmatrix} x_p \\ y_p \\ 1 \end{pmatrix} = \begin{pmatrix} x_1 x_2 x_3 \\ y_1 y_2 y_3 \\ 1\ 1\ 1 \end{pmatrix} * \begin{pmatrix} m_1 \\ m_2 \\ m_3 \end{pmatrix} = R * \begin{pmatrix} m_1 \\ m_2 \\ m_3 \end{pmatrix}$$

(Eq. 1)
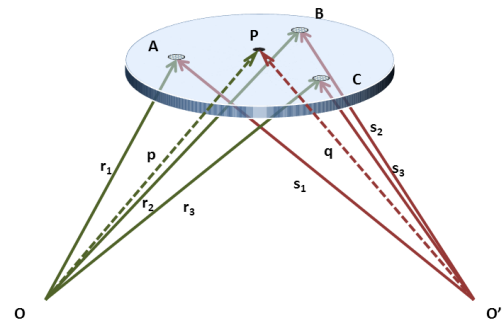
Figure 64: An illustration of the 6-point algorithm and how it is used to relocate FTs and corresponding POIs in the catcher-detector assembly using the three fiducial markings from Figure 56.

The reference marks matrix, **R**, is defined in this equation for later use.

The target stage coordinates of any given POI, $\{u_p, v_p\}$, can be calculated from its known source coordinates, $\{x_p, y_p\}$, by the relationship (see figure 64):

$$\begin{pmatrix} u_p \\ v_p \end{pmatrix} = \begin{pmatrix} u_1\,u_2\,u_3 \\ v_1\,v_2\,v_3 \end{pmatrix} \begin{pmatrix} m_1 \\ m_2 \\ m_3 \end{pmatrix} = \begin{pmatrix} u_1\,u_2\,u_3 \\ v_1\,v_2\,v_3 \end{pmatrix} \begin{pmatrix} x_1\,x_2\,x_3 \\ y_1\,y_2\,y_3 \\ 1\ 1\ 1 \end{pmatrix}^{-1} \begin{pmatrix} x_p \\ y_p \\ 1 \end{pmatrix} \qquad \text{(Eq. 2)}$$

Numerous implementations for the fiducial points, have been made. [97, p. S311] compared the use of unique dot/line patterns to the use of SEM reference grids. They found that the relocation by using patterns was both more accurate and more precise than in the case of using finder grids by using 87 and 92 simulated points respectively. In the first case, the average deviation of relocation was (5.8±2.6) μm and in the second case it was (7.1±5.6) μm. Another form of marking a sample is by means of e-beam lithography (surface patterning), ion deposition (Focussed Ion Beam Scanning Electron Microscope Gas Injection System or FIB-SEM-GIS) and laser micro-dissection [80]. The latter was used in our work and the LMD device was an MMI CellCut Plus System (based on a IX83 Olympus inverted microscope). The settings for sample marking were as follows: 15 μm/s cutting speed, 146.5 μm laser focus, 100% laser energy, repetition 5 times with Z-drill of 2 μm.

4.4 POI Isolation and Harvesting

After the fiducial points had been marked, the detector etched and the FTs found, the catcher is placed onto the harvester for particle isolation. Since the LMD is an inverted microscope, this sandwich was placed onto a Micro Slide (Corning Micro
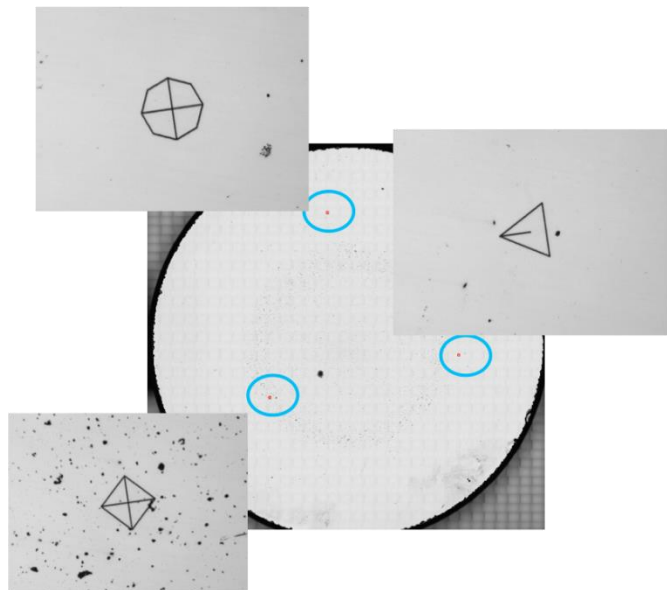
Figure 65: Typical fiducial markings on a glassy carbon planchet. These images were taken by the Zeiss Z2m optical microscope.

Slides, Corning Incorporated, NY, USA). See figure 41 for a reminder of the catcher-harvester sandwich and figure 66 for an overview of the sample flow (Chapter 4 discusses steps 6 and 7).
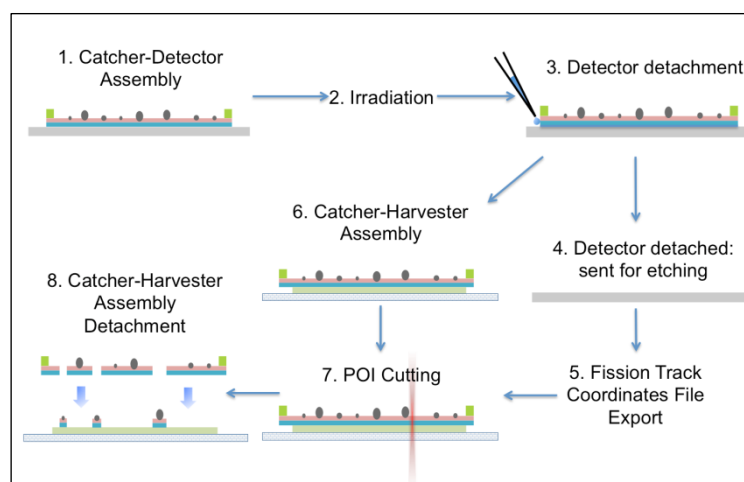
Figure 66: Diagram of sample flow

By re-measuring the fiducial markings in the LMD system and using the corresponding values of the fiducial marks on the detector, the coordinate table of the FTs can be re-computed for the second instrument. This new coordinate table is a list of POI coordinates in
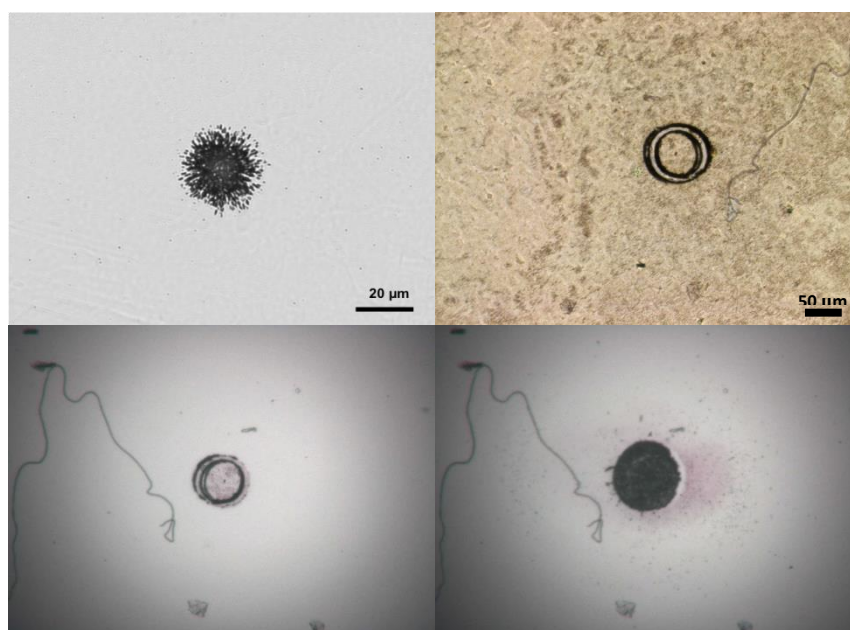
Figure 67: POI 3 from Sample 010: upper left the FT star (Zeiss Z2m image at 50x magnification); upper right: LMD image of corresponding particle (MMI IX83 with Olympus scope at 20x magnification); lower left: particle in laser ablation chamber before ablation; and lower right: after ablation.

the LMD [80]. Thus all POIs were relocated and then isolated and harvested by making circular (50 µm in diameter) cuts around each POI (as in figure 67).

Since the harvester material in contact with the catcher is silicone, as the laser cut the Mylar foil, (or Nucleopore filter) it would also melt the silicone material underneath, sticking the cutouts to the harvester as it dried and fixing them into place. To be able to trace back the POIs to their original FTs, the three fiducial markings were also re-burnt into the harvester.

Figure 67, from [16] shows one identified FT, its corresponding LMD cut-out (inverted image), the laser ablation relocated area and the resulting ablation crater of the same POI. One can clearly see the POI at the centre of both the cut-out Mylar and the harvested circle. Figure 68 is an SEM image of a cutout POI and figure 69 is an overview optical image of several cutouts. Figure 70 is an image of a whole harvester with fiducial marks.

In order to achieve 100% POI harvested after the detachment of the catcher and harvester assembly, the LMD cutting settings needed to be adjusted and varied slightly between Mylar and Nucleopore filter samples:

Cutting Parameters	Nucleopore Filter	Mylar foil
Cut velocity	15 µm/s	15 µm/s
Laser Focus	146.5 µm	146.5 µm
Laser energy	90%	90%
Repetition	7-10	2
Z-drill	1 µm	none

Table 6: LMD cutting settings for the two catcher substrate materials. Cutting through the Mylar foil was accomplished in fewer repetitions.

4.5 Harvesting Success Ratio and Relocation Accuracy [16]

The particle harvesting can be characterized in terms of two parameters for our purposes: success ratio and relocation accuracy. The success ratio is the total number of POIs harvested vs. the total number of FTs identified. The accuracy of FT-POI relocation accuracy can be understood as the total geometrical error between the true POI location on the catcher and

the calculated cut-out center (obviously, this error includes the error of assessing the FT position on the detector, as well as the true center of an FT source from an FT image). The recovery rate in the proposed procedure was between 96-100% in all samples. The average relocation accuracy, for 6 separate sample assemblies with a total of 282 POIs/FTs, was 12,1 ± 7,9 μm.

The relocation accuracy quoted in the literature from an optical microscope to an SEM is (5.8 ± 2.6) μm for points made with track membrane and (7.1 ± 5.6) μm with Maxtaform reference finder grids, respectively **[97, p. 309] [51, p. 254] [98, p. 2563]**.

All approaches for fiducial point marking are accurate enough to find the uranium-bearing particles in the second instrument for further analysis **[97, p. 309]**.
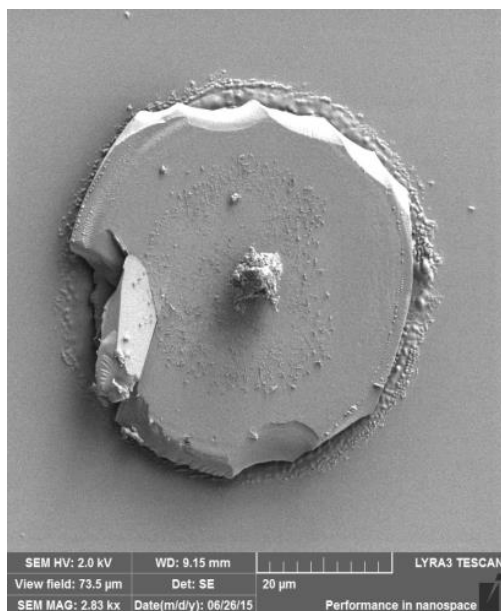
Figure 68: A POI cutout [80]
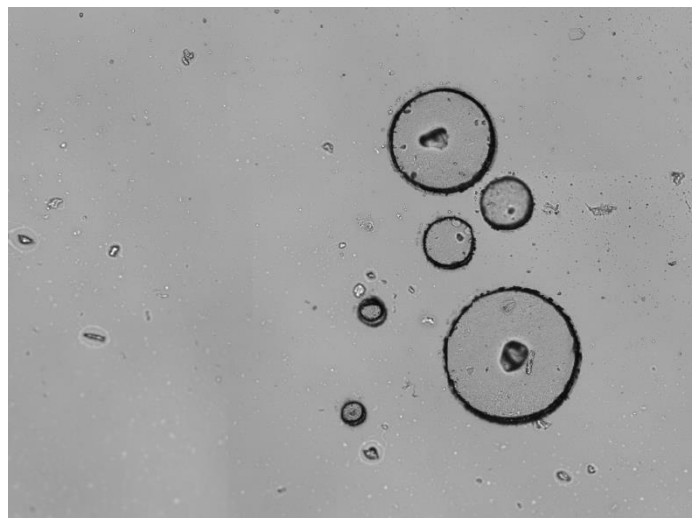
Figure 69: Overview image of several cuts under an optical microscope (4x magnification).
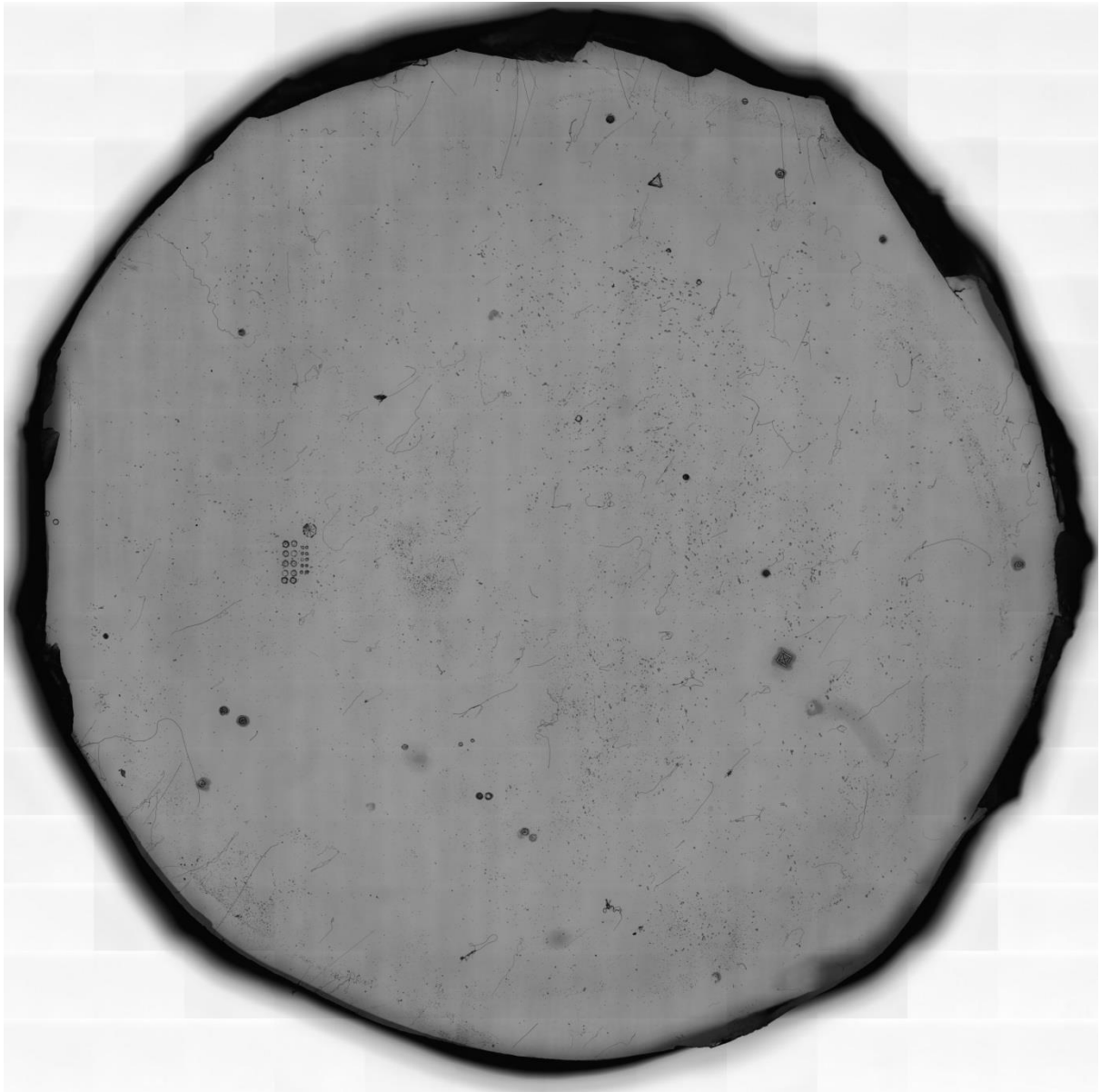
Figure 70: Overview of harvester with fiducial markings and POI cutouts

Chapter 5: Laser Ablation Inductively Coupled Plasma Mass Spectrometry of U-bearing Micron-sized POIs

This chapter starts with a description of the experimental setup for ablation of the POIs that were harvested in the previous chapter. The POIs were ablated at the Vienna University of Technology, Institute of Chemical Technologies and Analytics, Getreidemarkt 9, 1060 Vienna, Austria. The transient signal raw data was then exported for determining the isotope ratios of the POIs. Here, we summarize several data processing schemes in the LA-ICP-MS literature for treating transient signals and propose an alternative. This method was developed together with Stephen J. Walsh and Ernesto Chinea-Cano of the International Atomic Energy Agency, Seibersdorf Laboratories, Reaktorstrasse 1, A-2444, Austria. The manuscript for this approach has been sent to JAAS (Journal of Analytical Atomic Spectrometry) for review.

5.1 Sample Material [16]

The U-ore particulate material used for dispersal in Chapter 2 is the IAEA RGU-1 reference material ("Uranium ore in quartz"). A standard loading spoon for the disperser was created and the amount dispersed in each explosion was controlled (~ 40 µg or ~ 5µg per catcher). Sample particles were investigated prior to sample preparation by means of scanning electron microscopy (Lyra3, Tescan s.r.o) and it was found that the diameter range of the U-
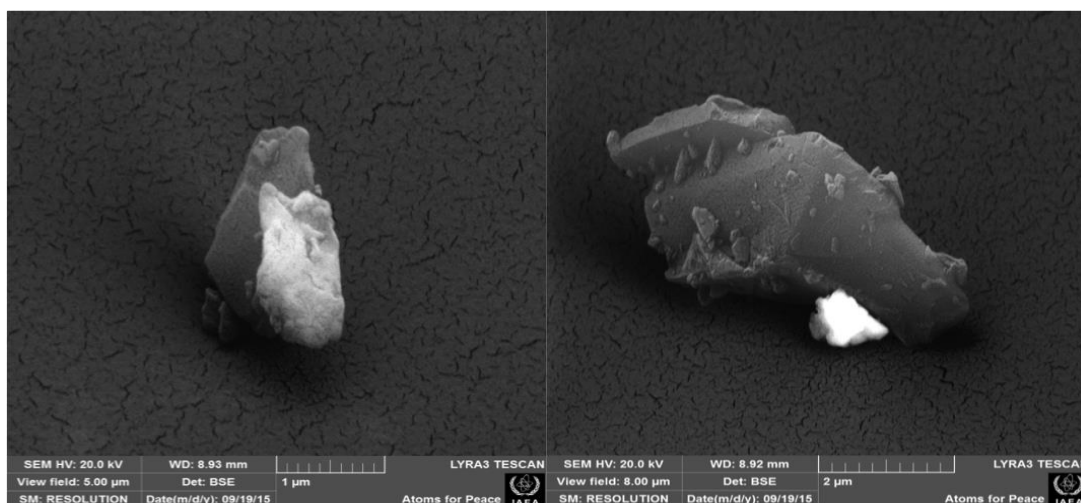
Figure 71: SEM BSE image of typical U-ore particles (white)
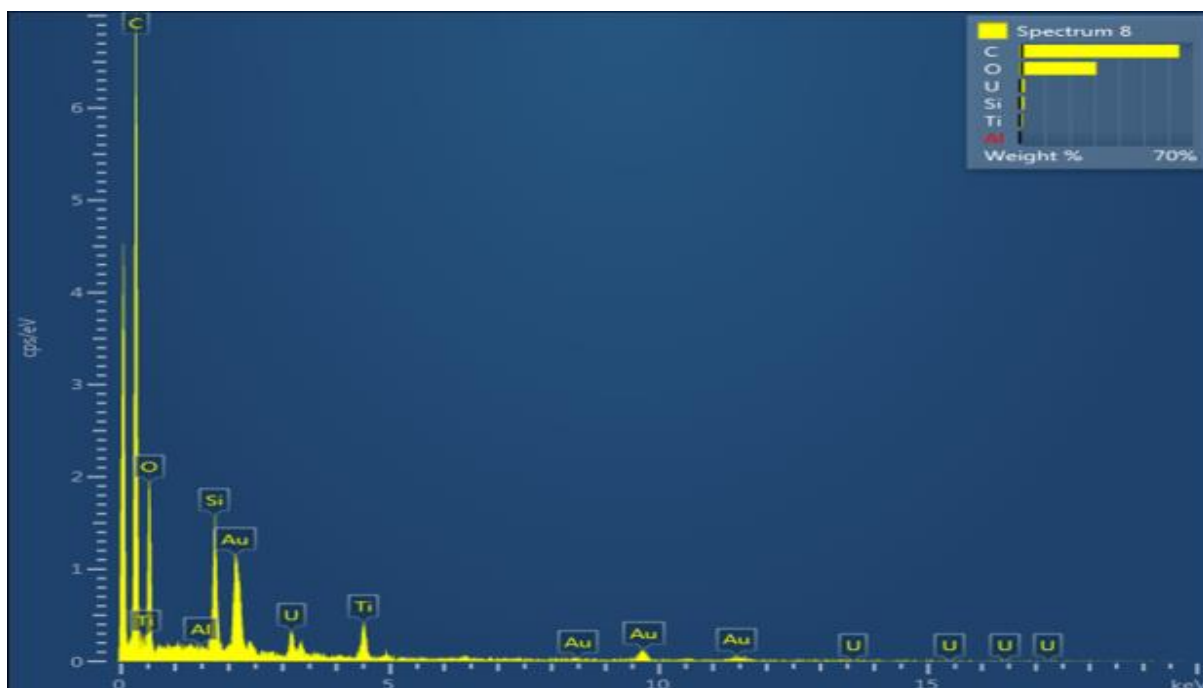
Figure 72: EDX spectrum of 1μm U-ore particle on a glassy carbon disc.

ore particles was 0.5-1.5 μm. Figure 71 shows two typical U-ore particles and Figure 72 is an

Energy Dispersive X-ray (EDX) spectrum collected from a single particle in a Tescan Lyra3

scanning electron microscope with an Oxford EDX detector, confirming the presence of

uranium in these particles.

5.2 LA-ICP-MS of POIs [99] [100]

The six harvesters with POIs were taken from the Seibersdorf Laboratories of the IAEA and

transferred to an LA-ICP-MS at Vienna University of Technology for micro-probing. The

coordinates of the POIs and fiducial marks were also recorded in the laser ablation chamber

for relocation. The LA-ICP-MS used was a New Wave Research, 213 NWR ESI laser attached

to a quadrupole ICP-MS (iCAP Q from Thermo Scientific). Table 7 and 8 show the LA and

ICP-MS instrumental parameters.

LA Parameters	
Number of shots	10
Spot size	80 μm
Repetition rate	10 Hz
Output energy	90% (21.5 mJ)
Carrier gas flow rate	0.8 l/min (He)
Make-up gas flow rate	0.8 l/min (Ar)

Table 7: LA instrumental parameters

ICP-MS Parameters	
Coolant gas flow rate	15.0 l/min
Auxiliary gas flow rate	0.8 l/min
RF power	1550W
Dwell time per isotope	10 ms
Cones	Ni
Measured Isotopes	U-235, U-238

Table 8: ICP-MS instrumental parameters

Before POI ablation, the LA-ICP-MS was auto-tuned using a continuous ablation (at the same instrumental parameters as in tables 7 and 8) of a NIST 612 glass reference material. This glass was also shot before and after the ablation of each series of 10 POIs as a within-run control. Note that a series of investigations using the NIST 612 glass was conducted to find the most suitable laser ablation and ICP-MS settings, after which the figures in tables 7 and 8 were used. The plasma of the ICP-MS was allowed to stabilize for an hour before each sample ablation cycle.

Nominal expectation for n(U-235)/n(U-238) isotope ratio in the POIs U-ore is 0.0072 (natural uranium). The NIST 612 certificate gives an information value for the isotope ratio n(U-235)/n(U-238) = = 2.388×10^{-3} [101] [100].

5.3 Standard Data Evaluation Approaches [100]

Data handling of transient signals comes with certain difficulties due to their short lifetime and low signal intensity compared to the measurement of e.g. long-lasting signals from high-abundance elements in mineral samples or reference materials. Moreover, transient signals, from single collector instruments especially, offer less precise isotope ratios due to internal variations of the signal during a measurement and so-called isotope ratio drifts reported by several authors [102] [103].

[102] conducted a thorough investigation into four transient signal evaluation strategies for LA-MC (Multi-Collector)-ICP-MS data. They ablated micrometer-sized uranium oxide

particles (of certified U-235/U-238 signatures) in order to compute U isotope ratios using the following evaluation strategies:

1. Point-by-point (PBP)

2. Integration

3. Linear regression slope

4. Finite mixture model

The point-by-point scheme averages the U isotope ratios that were derived from dividing individual, simultaneously (or quasi-simultaneously in the case of single collector instruments) acquired data points. No weighing of the influence of certain data points is given to signals of higher (or lower) intensity.

In the integration approach, an operator selects a peak area (time-window) for each isotope, which is then integrated. Each POI is dealt with individually and this approach therefore requires constant supervision.

The linear regression slope method calculates the U isotope ratios determining the slope of a linear regression line using the 'least squares' method of regression analysis. Weighted signal intensities are often applied here: the higher the signal, the larger the impact on the ratio for a given data point.

The fourth method – the finite mixture model – is similar to the linear regression slope method in that the isotope ratios are derived from the slopes of linear regression lines. POIs are assigned to populations with different isotopic compositions by combining measurement data with a theoretical model to estimate the most likely parameters that generated the observed data.

Each of these may address a certain data weakness better than the other. [102] argues that all evaluation strategies yield average U-235/U-238 isotope ratios which, within their

uncertainties, correspond to the certified values. The quality of this data can however be improved, and for this we build on the point-by-point method since it yielded the best precision and the smallest relative uncertainty for single collector transient signal data.

5.4 Estimating Isotope Ratios by the Integration Method [100]

Using a single collector LA-ICP-MS adds certain restraints on the data collected. Measuring several isotopes from a laser-ablation shot using a single-collector type ICP-MS instrument is done by means of a so-called peak-hopping mode. In this mode, the mass-spectrometer switches from detecting one isotope to detecting another in a fraction of a second, thus processing counts of two (or several) mass/charge ratios from a single ablation point quasi-simultaneously. This is the main difference between data from single vs. multi-collector ICP instruments: real simultaneous detection can only be achieved by the latter. Thus, single collector data will have gaps in the transient signal whereas these do not appear in multi-collector transient signals.

Another characteristic of ICP-MS data in general are fluctuations and spikes in the intensity of the recorded signals (see examples in figure 73). Such behavior in the raw data is more pronounced in single rather than multi-collector data due to the gaps in the records of the former. E.g. a spike may last during the recording of a single isotope, thus not being observed during the recording of another. Spikes occur due to issues such as plasma and laser ablation unevenness, particulate size distribution and particulate material not being fully ionized by the ICP [104]. This behavior cannot be completely avoided by using multi-collector ICP-MS instruments. To deal with chaotic signals, the mass spectrometry community typically ignores the first few seconds of recorded counts (the initial laser ablation 'peak') and uses only the stable ablation area in the evaluation (see top right graph in figure 73 where signals between cycle 490 to cycle 630 would typically be used and the initial peak from 445-460 would be ignored). This is excused largely due to presumed 'surface effects' and justified as a need for 'stabilization of the laser ablation' [105] [106]. This approach has as a consequence

a loss of the majority of the detected signal in the data processing step (the initial peak has the highest intensity). Following this pre-selection of relevant signal area, the raw data is calculated from the integrated (i.e. summed) intensities [107] [108]".

For single-particle laser ablation ICP-MS, the detected signals do not last long enough to reach a 'stable ablation' that normally follows the initial transient peak (note this difference in top graphs vs bottom graphs in figure 73). In such measurements, isotope ratios are calculated by dividing the integrated signal intensities of the isotopes using several averaged
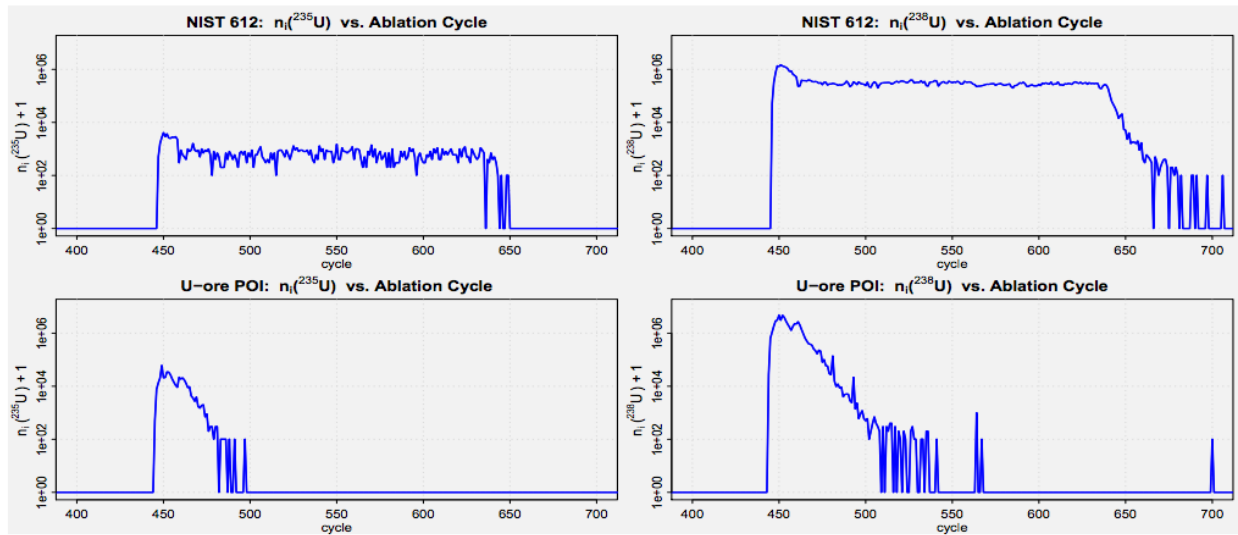
Figure 73: Typical transient ablation signals for 10 laser shots at 10 Hz frequency of NIST 612 and U-ore POIs. Top and bottom left are U-235 and top and bottom right are U-238 signals. [100]

(blocked) points. The ratios are averages of many raw data points within a single 'block' (a block contains all intensities in e.g. a 1 second window of a measurement). The integration is then performed using these data points by summing up the recorded individual block signal intensities. This approach is supposed to account to some degree for the erratic behavior of laser ablation signals, but should concurrently reduce the influence of small count rates on the overall calculated isotope ratio(s) [109]. Note that the length of a single block varies between publications and, to our best knowledge, there does not exist a single reference summarizing these differences.

Finally, to deal with possible background counts, a signal is recorded only if it is 'significant', i.e. statistically above the estimated detection limit. Each measurement is background

corrected: a period of about 2 seconds before the ablation commences is used to estimate the background count of the ICP- MS and this value is automatically subtracted from the ablation raw isotope intensities recorded by the ICP-MS device.

Note that the integration approach outlined here was used for evaluating signals measured in this work. In this scheme, as was previously discussed, the transient signal counts were integrated by simple summation of all recorded raw counts of each isotope measurement and these values were then divided for each POI (or NIST signal) in order to obtain an overall POI (or NIST) isotope ratio. No weighing or separation of data into blocks was done.

The greatest limitation to this approach for data reduction was that it had to be supervised: transient signals vary in length between POIs and an operator is required to pre-select data export windows (i.e. window lengths). In the following section, a new evaluation strategy is presented based on the point-by-point approach for data evaluation and compared to the simple integration approach.
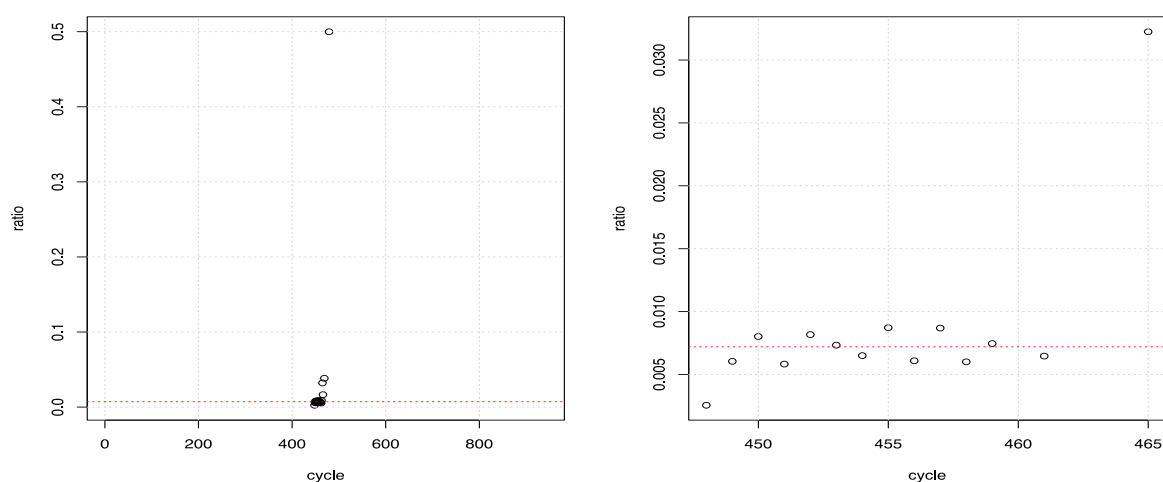
Figure 74: A measurement of a single POI: each circle corresponds to a ratio estimate from a single measurement cycle. The red line is the computed average. Note that the whole measurement comprises of approx. 800 cycles; relevant POI data corresponds to only a few of the cycles (right vs left graph above).
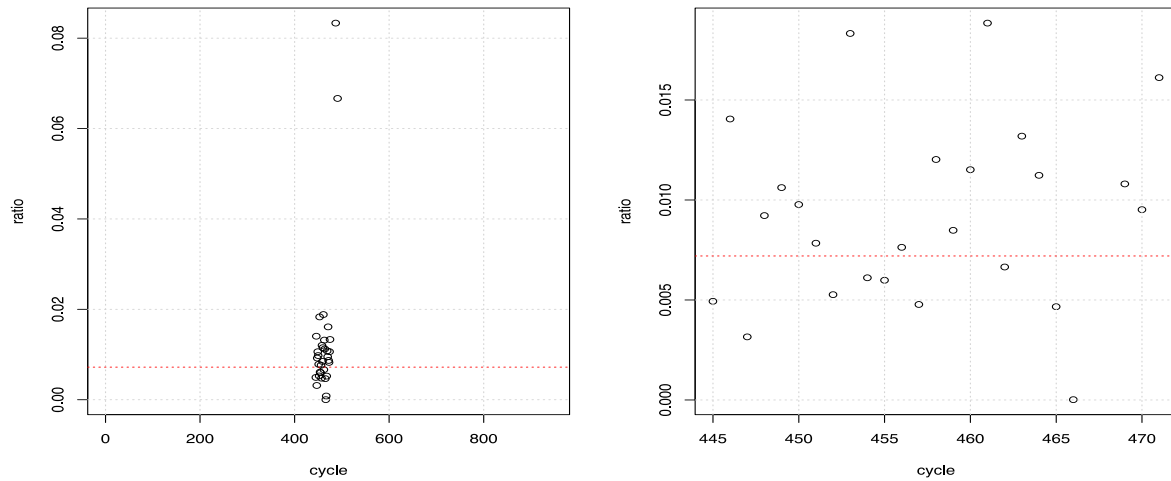
Figure 75: A second POI measurement without extreme values.
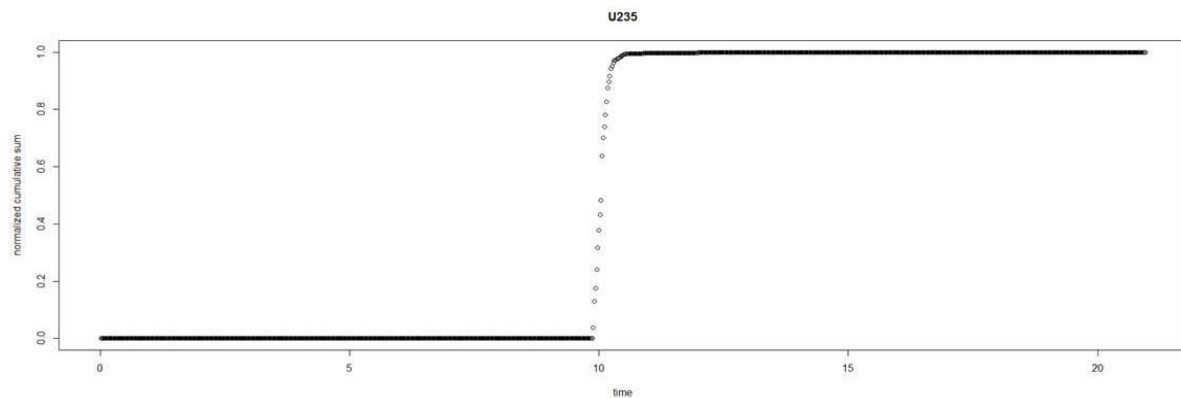
Figure 76: Cumulative sum function for the U-235 signal intensity. The x-axis is the time of signal acquisition and the y-axis represents the cumulative percentage of the acquired U-235 signal. Cycles between the 10-90% were labeled relevant for further statistical analysis.

5.5 Improving the Data Treatment [99] [100]

Data Reduction

To investigate data behaviour, an exploratory data analysis and model diagnostics was proposed in order to observe details and possibly identify patterns in data behaviour. Since the data is recorded in cycles of U-235 and U-238 measurements, the point-by-point approach to estimate statistical variables (mean, median, standard deviation etc) for each POI was used. This approach gives the evaluator a series of isotope ratio values for each POI instead of one final value as in the integration scheme. Errors in this case can be computed not just by assigning a $\sqrt{N}$ value (as is typically done in the integration method).

The LA-ICP-MS transient signals were reduced to n(U-235)/n(U-238) isotope ratio estimates via the point-by-point method [102]. Under this approach individual U-235 and U-238 counts within a single cycle of a measurement are divided to produce a series of estimates for the isotope ratio. Then, these ratio estimates across cycles of a POI or NIST measurement are summarized by appropriate statistics (see figures 74 and 75). Note that the open-source statistical programming language, R, was employed in our data analysis since it can be robustly used on large data sets, combating individually each POI isotope ratio measurement.

In the Median-Absolute-Deviation (MAD) approach [100], the median of the collected ratio estimates was used as the estimator of the isotope ratios of each ablation. This approach helps minimize the effect of sporadic extreme values (see outlier cycle for instance in figure 74), thus making the median of ratio estimates across all cycles a more robust and reliable estimator than the mean [102].

Additionally, a single measurement consists of around 800 cycles, hence only the cycles containing information on the ablation should be used in the evaluation. It is extremely time-consuming to re-visit each POI ablation signal and set the beginning and end of the 'relevant cycles'. Even when all laser ablation parameters are automated so that the ablation starts automatically, a slight variation is still observed in the total time it takes for the ablated fragments to reach the detector.
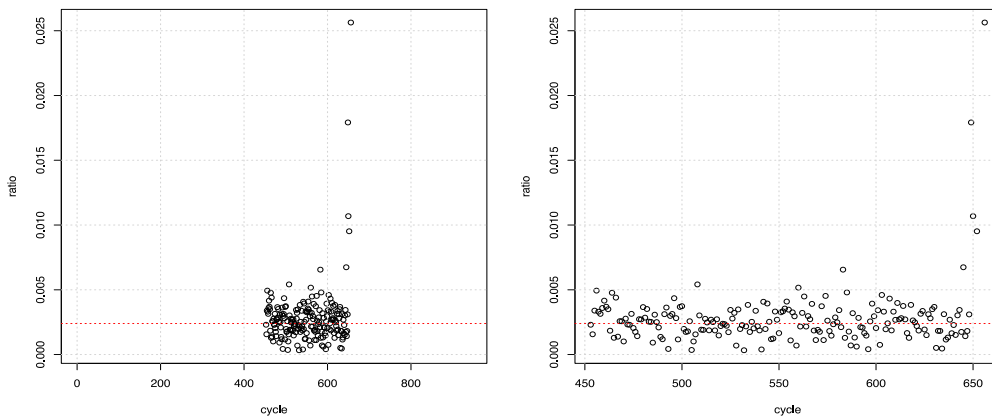
Figure 77: Relevant cycle data of a NIST 612 ablation.

Another limitation for assigning the beginning and end of relevant data cycles is that, because the U-235 isotope is less abundant, the U-235 signal will end before the U-238 signal does (the U-235 signal will reach the detection limit faster). Due to this and also the erratic behaviour of the beginning and ending of the recorded signals, only cycles belonging to the [0.1-0.9] range were used. This range was first applied to the minor isotope (U-235 signal) and then extended to the U-238 data set. To determine this range, a cumulative sum function on the minor isotope was found (see figure 76) and then ratios belonging to the [0.1-0.9] range were deemed relevant. For comparison, figure 77 depicts the 'relevant cycles' of a NIST 612 ablation which are greater in number, but also show a tailing effect. Note that the red dashed line in figures 74, 75 and 77 is the average, not the median value.

Breakdown of the Statistical Treatment of Ablation Data

To automate the statistical treatment of all signals using R, a generalised approach was developed. The main advantage, compared to standard ICP-MS (Thermofisher) software, as was discussed in the previous section, is that the time intervals for recording the relevant POI isotope ratio data are individually calculated for each POI in an automated manner. Here is a breakdown of the steps applied to each transient signal:

1. Export U-235 and U-238 spectrums individually;

2. On U-235 spectrum, apply the cumulative sum function and find the time interval between 10% and 90% of counts; This is the 'relevant data' window;

3. Subset both U235 and U238 on this interval;

4. For each cycle, calculate the U235/ U238 ratio;

5. Repeat for next cycle.

Applying Basic Statistics [100]

This scheme for raw data treatment outlined in the previous section thus resulted in a collection of isotope ratio estimates that could be summarized by appropriate statistics (the justification for this follows in the next section).

Specifically, isotope ratio measurements for every cycle i are computed by taking the ratio of U-235 and U-238 counts within that cycle [100]:

$$R_i = \frac{n_i(^{235}U)}{n_i(^{238}U)} \text{ for } i \in \{1,2,\dots,n_{cycle}\},$$

where n_{cycle} is the number of cycles that produce viable data. In the classical PBP approach the R_i are usually summarized, most often by the average, to produce an estimate of the isotope ratio for a given POI. This approach assumes that

$$R_i \sim N(\mu, \sigma)$$

meaning that the ratio estimates are independent and identically distributed Gaussian variables with mean μ and standard deviation σ. Note that μ and σ denote the true isotope ratio and measurement uncertainty of the POI under repeatability conditions [100] [110] [111] [112]. To apply to the observed measurements, denoted r_i, we can compute an estimate of both the sample mean $\hat{\mu}$ and the sample standard deviation $\hat{\sigma}$ by:

$$\hat{\mu} = \bar{r} = \frac{1}{n_{cycle}} \sum_1^{n_{cycle}} r_i$$

and

$$\hat{\sigma} = s = \sqrt{\frac{1}{n_{cycle} - 1} \sum_1^{n_{cycle}} (r_i - \bar{r})^2}$$

Following GUM principles [100] [113] [114] one may construct the final measurement result and confidence interval using the triple $\{\bar{r}, u(\bar{r}), k\}$ where the uncertainty of the average is $u(\bar{r}) = \frac{s}{\sqrt{n_{cycle}}}$ and the coverage factor is drawn from Student's t-Distribution with $df = n_{cycle} - 1$ degrees of freedom for a specified confidence interval $C = 1 - \alpha$, i.e. $k = t_{df,1-\frac{\alpha}{2}}$.

Thus, a standard error for each POI n(U-235)/n(U-238) can be computed based on corresponding robust statistics [115] [116] and this measure of uncertainty comprises variation in ablation under method repeatability conditions [100]. In such a way, the uncertainty estimation has been systematised.

5.6 Data Behaviour and Model Assumptions

[111] [100] are exemplary publications in analysing chemical measurement data by means of exploratory analysis and model diagnostics. The aim of such an approach is to familiarise the analyst with random and systematic structures in the data, thus estimating model parameters and the degree of consistency of the data with assumptions. This facilitates the identification of deviations in the data and enables one to update the model assumptions accordingly. Since we assume the data follow a Gaussian distribution, we can perform both diagnostics and exploratory analysis (parameter estimation) in a single step [100].

The proposed treatment of data from the previous sections is a valid approach to estimating isotope ratios of POIs only if the following assumptions are met [100]:

1. Computing the average from all cycles of a single POI ablation can be done only if the cycles are independent during the acquisition ("independent identically distributed" assumption). This means that each ratio at each cycle r_i is an estimate of the true ratio in the particle;

2. Ratios (according to the ISO Guide 35 [117]) are not Gaussian distributed. This should be considered and verified for all ablations;

3. Means and standard deviations are adversely affected by outliers and this should be investigated before drawing conclusions for the whole data set.

The first assumption was tested by means of an autocorrelation function plot of the consecutive cycle measurements for each ablation. Note that this was performed on the raw data set. Figure 78 [100] shows that the autocorrelation function at all lags is not significant, either for the NIST 612 or POI, thus confirming the assumption that the individual measurements are independent across all time cycles. This does not necessarily mean that the r_i's are truly independent, but it is not unreasonable to assume so. The left graphs from figure 79 and 80 are density histograms of individual measurements (of the same NIST 612 measurement in figure 77 and POI measurement in figure 75, respectively) with modes near the expectation values $\frac{n(^{235}U)}{n(^{238}U)} = 0.002388$ for NIST 612 measurements (the NIST 612 expectation value from [101] was used) and $\frac{n(^{235}U)}{n(^{238}U)} = 0.0072$ for POIs (natural uranium). The QQ-plots of the individual cycle isotope ratios compares the distribution of these to the assumed Gaussian distribution and is a clear indication that the measurements follow a
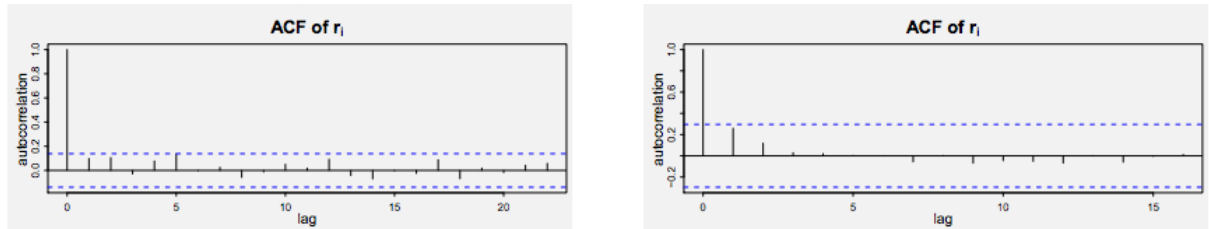
Figure 78: Autocorrelation function for NIST 612 (left) and a single POI measurement (right). [100]
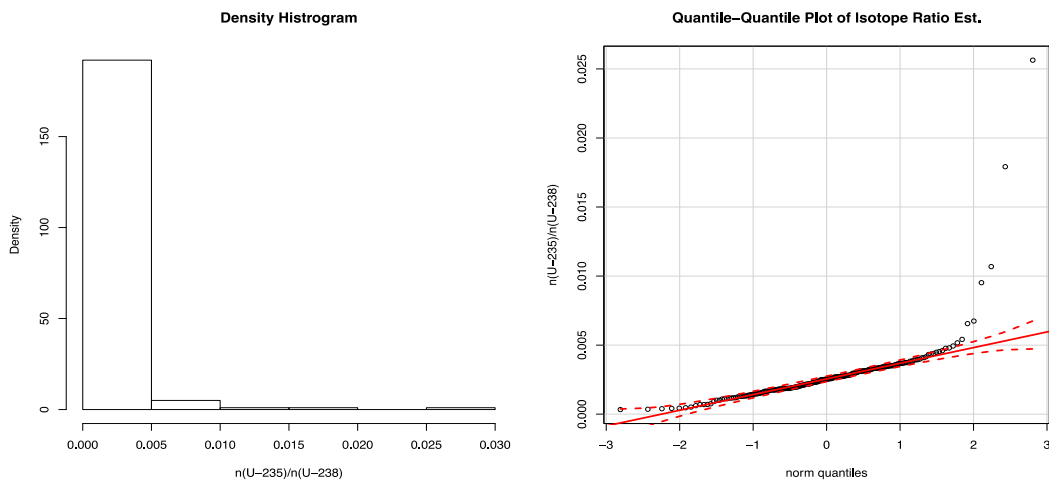
Figure 79: Cycle data of a NIST 612 ablation. Note the tailing towards the end of the ablation.

Gaussian distribution except for the clearly identified outlier(s). This is further evidence that the individual cycle ratios are a random set of variables (central limit theorem).
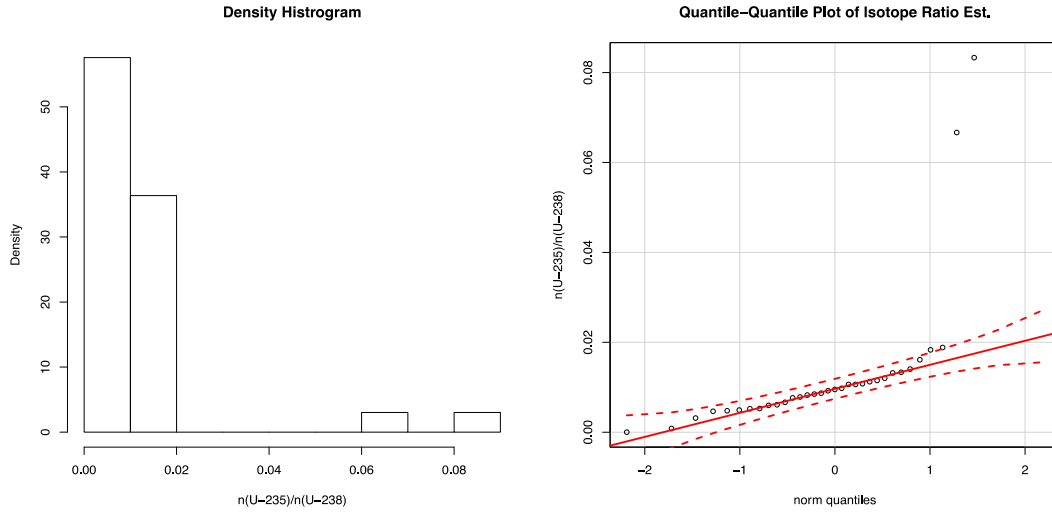
Figure 81: Cycle data of a POI ablation. Note the tailing towards the end of the ablation.

5.7 Median-Absolute-Deviation (MAD) Approach [100]

The MAD approach, as was mentioned briefly, makes use of the median to estimate the true mean μ of the (assumed) Gaussian distribution and makes use of the median-absolute-deviation to estimate the repeatability (im)precision σ. To find the median of a series, the individual cycle isotope ratio measurements must first be ordered in ascending order:

$$\{r_{(1)}, r_{(2)}, \dots, r_{(n_{cycle})}\}$$

where $r_{(1)} < r_{(2)} < \cdots < r_{(n_{cycle})}$. Thus, the median is the middle value of the series of cycle measurements, and is taken as the estimate of the isotope ratio of the POI:

$$\hat{\mu}_{robust} = \tilde{r} = \begin{cases} r_{(\frac{n_{cycle}+1}{2})} & if\ n_{cycle}\ is\ odd \\ \dfrac{r_{(\frac{n_{cycle}}{2})} + r_{(\frac{n_{cycle}}{2}+1)}}{2} & if\ n_{cycle}\ is\ even \end{cases}$$

An estimate of the repeatability precision $\hat{\sigma}$ can therefore be made by:

$$\hat{\sigma} = 1.253 \times b_{n_{cycle}} \times MAD_{r_i}$$

where 1.253 accounts for the median being a less efficient estimator of μ than the sample mean [118], $b_{n_{cycle}}$ is a bias correction factor for small n_{cycle} [115] with values given in [119] as follows: $\{b_2 = 1.196, b_3 = 1.495, b_4 = 1.363, b_5 = 1.206, b_6 = 1.200, b_7 = 1.140, b_8 = 1.129, b_9 = 1.107\}$, and $b_{n_{cycle}} = \frac{n_{cycle}}{n_{cycle} - 0.8} \; for \; n_{cycle} \geq 10$.

Furthermore, $MAD_{r_i} = 1.4826 \times med(|r_i - med(r_i)|)$ where 1.4826 is a bias correction used to make MAD_{r_i} a consistent estimator of σ.

As before, after completing these calculations, the final isotope ratio estimate, the uncertainty, and the coverage factor are summarized:

$$\{\hat{\mu}_{robust} = \tilde{r}, u(\bar{r}) = \frac{\hat{\sigma}_{robust}}{\sqrt{n_{cycle}}}, k\}$$

where the coverage factor k was drawn from Student's t-Distribution with $df = n_{cycle} - 1$ degrees of freedom for a specified confidence interval $C = 1 - \alpha$, i.e. $k = t_{df, 1 - \frac{\alpha}{2}}$.

Thus, this approach is more robust to outliers, it accommodates small sample size (small number of relevant cycle data) with appropriate adjustments to uncertainty and accommodates additional uncertainty due to using a less efficient estimator (median instead of mean) [100].

5.8 LA-ICP-MS Results [16] [100]

In figure 81 the n(U-235)/n(U-238) ratio estimates with 95% confidence interval for four analytical runs ($n(POI)$ = 126) are presented. Nominal expectation n(U-235)/n(U-238) = 0.0072 is indicated as the vertical red dashed line. In figure 82 the n(U-235)/n(U-238) ratio estimates with 95% confidence interval for measurements of NIST 612 reference material in the same four analytical runs are shown. Information value n(U-235)/n(U-238) = 2.388 × 10−3 is indicated as the vertical blue dashed line [101]. In both cases the majority n(U-235)/n(U-238) estimates are consistent with their expected values with 95% confidence.

		Consistent with Expectation	
Material	**number of measurements**	**at 95% confidence**	**at 99% confidence**
U-Ore (POI)	126	116 (92%)	125 (99%)
NIST 612	22	19 (86%)	22 (100%)

Table 9: Number and proportion of U-ore POI and NIST 612 measurements consistent with nominal expectations at 95% and 99% confidence. [16]

In Table 9 the proportion of U-ore POI and NIST 612 measurements consistent with nominal expectations at both 95% and 99% confidence levels is presented. A large percentage of U-ore POI and NIST 612 measurements are deemed consistent with expectations at 95% confidence (92% and 86% of all measurements respectively). Nearly all (99% and 100% respectively) U-ore POI and NIST 612 measurements are consistent with expectations at 99% confidence (see figures 83 and 84 for POI and NIST 612 ablation MAD vs intergration method results with uncertainties depicted). These results emphasize the success of LA-ICP-MS measurements on particles under the sample preparation procedure presented in previous chapters **[16]**.
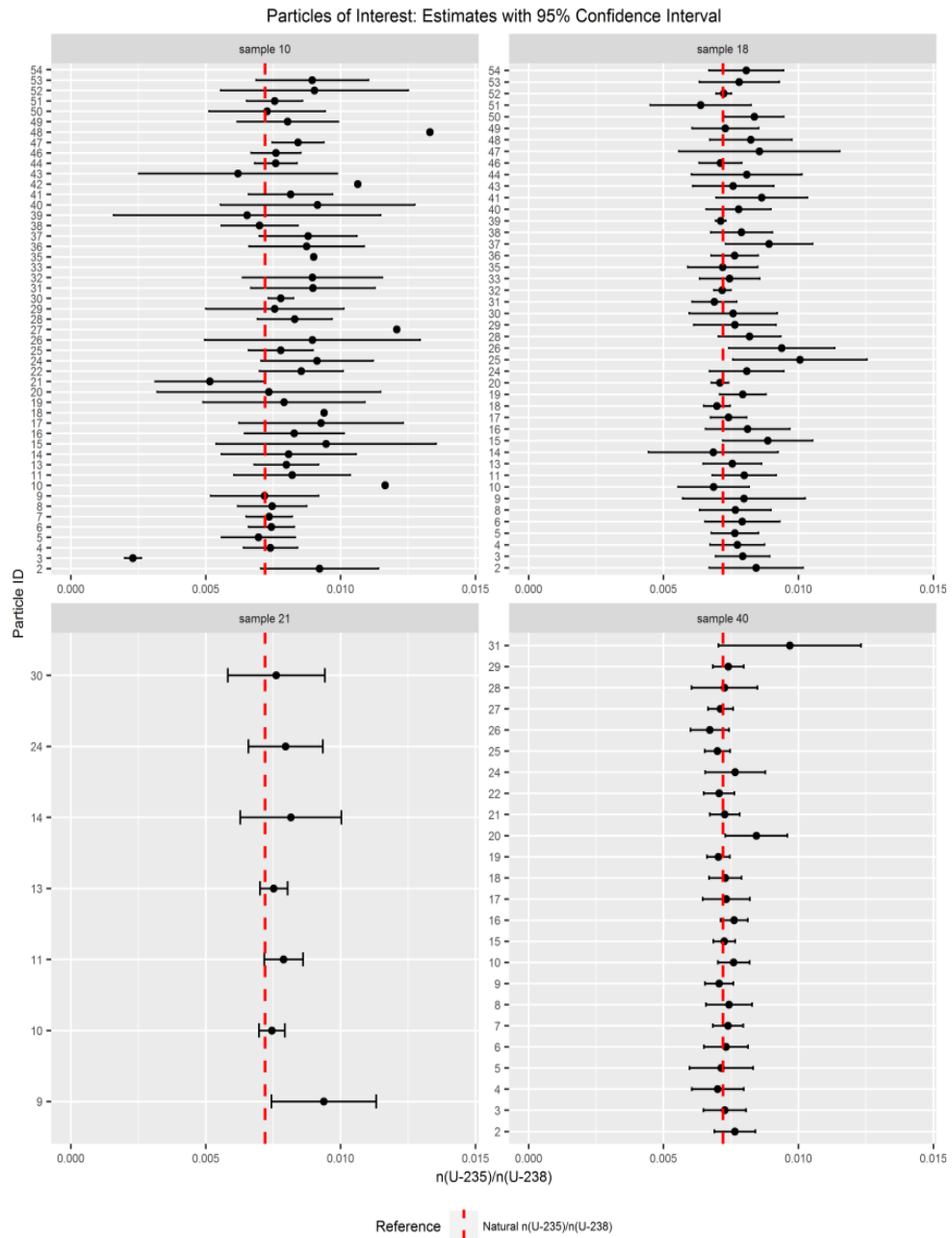
Figure 81: Calculated ratios and their uncertainties for LA-ICP-MS measurements of U-ore particles. [16]
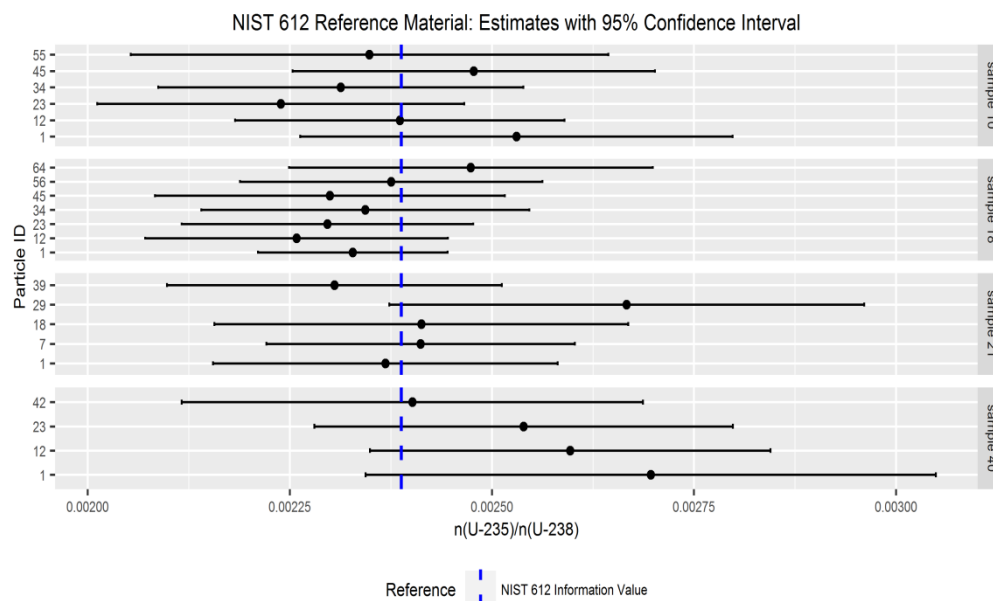
Figure 82: Calculated ratios and their uncertainties for LA-ICP-MS measurements of NIST 612 values. The same laser settings were used as for the particle ablations [16]
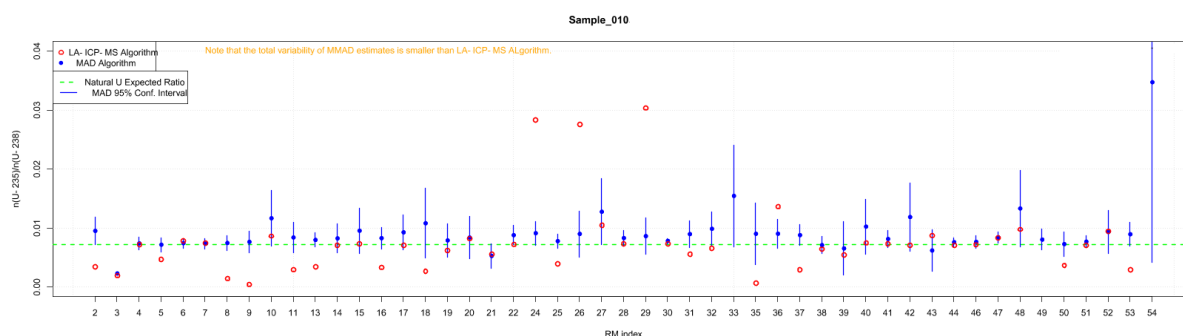
Figure 83: A comparison between integrated instrument data (red) and improved statistical model (blue) is depicted for U-orevalues in a single sample. Note that the standard uncertainty typically used for integrated data - $\sqrt{N}$ - is not depicted here since it would go off of the chart. [100]
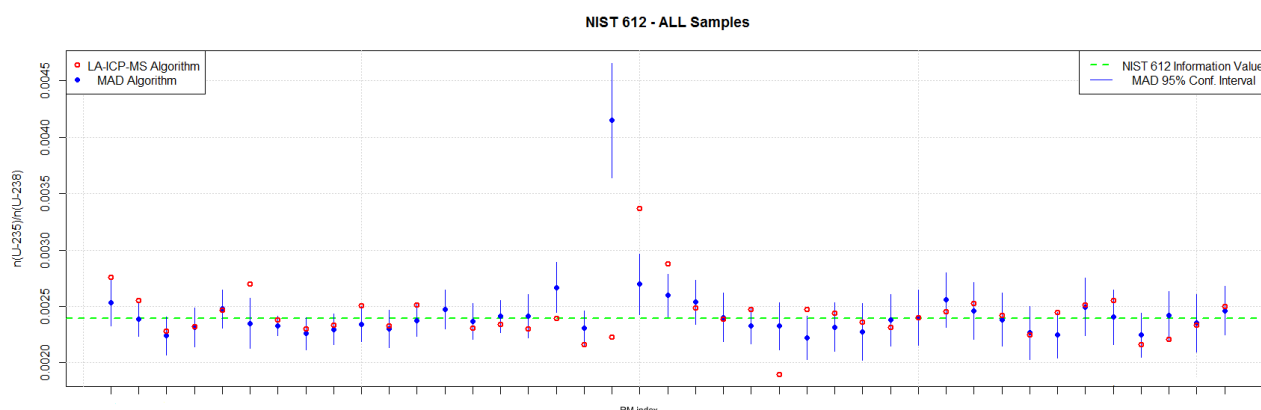
Figure 84: A comparison between integrated instrument data (red) and improved statistical model (blue) is depicted for NIST 612 values in all samples. Note that the standard uncertainty typically used for integrated data - $\sqrt{N}$ - is not depicted here since it would go off of the chart. [100]

Comparison of MAD and Integration Method [100]

As was stated previously, for comparison, the simplest method for isotope ratio measurements (the integration method), was compared to the new MAD algorithm. The integration of the transient signals was done by defining a time window in the ICP-MS software and then summing the total number of counts for each isotope. This window varied between 1-2 seconds – which was enough for the whole transient signal for both isotopes to be fully counted. A background count was taken prior to each ablation and subtracted from the total counts automatically by the native software. See figure 85 for a depiction of a single POI ablation measurement with a 1 second time window from which the U-238 and U-235 values were taken, as well as the highlighted (subtracted) background area.
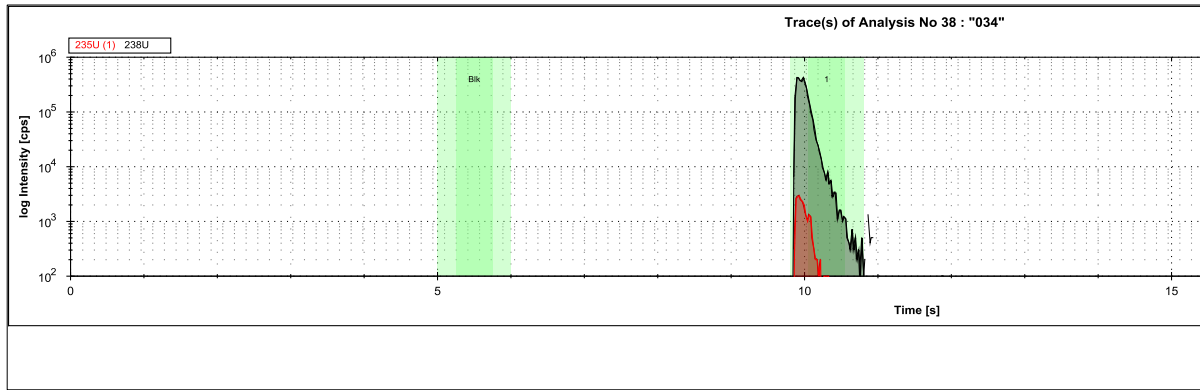

Figure 85: Transient signal of POI ablation with integration window depicted in green. U-238 counts are black, U-235 are red.

To compare two estimation procedures, statistical figures such as the bias, standard deviation and root mean-squared-error were used. These are defined as:

$$Bias(\hat{\theta}) = \overline{\overline{\theta}} - \theta_R$$

$$Var(\hat{\theta}) = \frac{1}{n-1}\sum_{i=1}^{2}(\widehat{\theta}_i - \overline{\overline{\theta}})^2$$

Where n represents the number of estimates from the procedure and I the index of the estimates

$$SD(\hat{\theta}) = \sqrt{Var(\hat{\theta})}$$

Such that for a measurand θ with reference value θ_R and a procedure which estimates $\hat{\theta}$, the bias of the procedure is estimated as the deviation of the average result from the reference; the imprecision of the procedure is the variance; the imprecision of the procedure on the scale of measurement is the standard deviation. From this the mean-squared-error and thus the root mean-squared-error can be calculated.

$$MSE(\hat{\theta}) = Bias^2(\hat{\theta}) + Var(\hat{\theta})$$

$$RMSE(\hat{\theta}) = \sqrt{MSE(\hat{\theta})}$$

Values closer to zero indicate better measurement performance. In figures 86 and 87 comparative graphs of the human supervised integration approach vs. the robust PBP unsupervised approach are presented. Figure 86 shows the isotope ratio measurements under the integration (red points) and the robust PBP (blue points, MAD algorithm) data reduction approach for 123 measurements of U-ore POIs. The dashed line is the natural uranium expectation value. The second graph shows the % relative difference vs the natural uranium expectation for the two data reduction approaches. The third graph shows the % relative difference again, but scaled to only 100% thus excluding the outliers from the integration approach. A general tendency for the robust PBP to exhibit smaller and less variable errors is apparent.

Similarly, figure 87 shows 21 measurements of the NIST 612 glass reference material where the dashed line is the certificate information value [101]. The bottom graph shows the % relative difference vs. the information value contrasting the two data approaches.
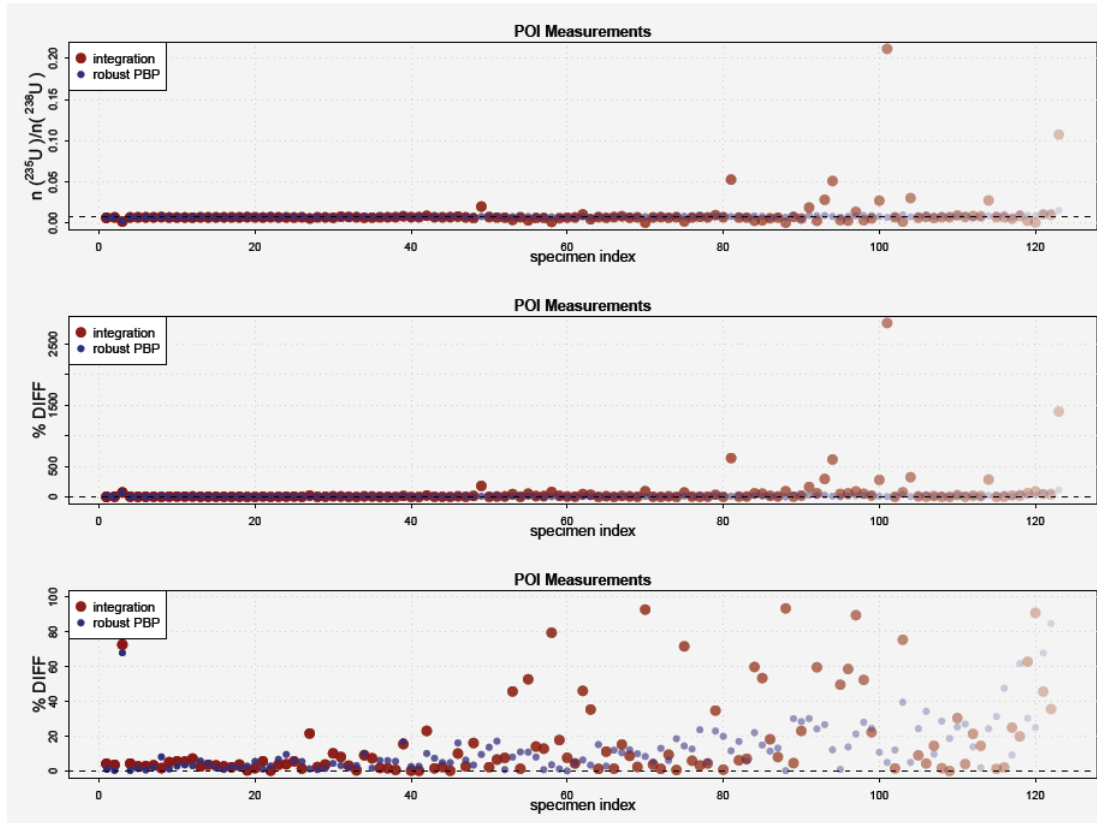
Figure 86: The integration method isotope ratio values for each POI from a single sample are shown in red dots and those from the MAD algorithm are depicted in blue. [100]
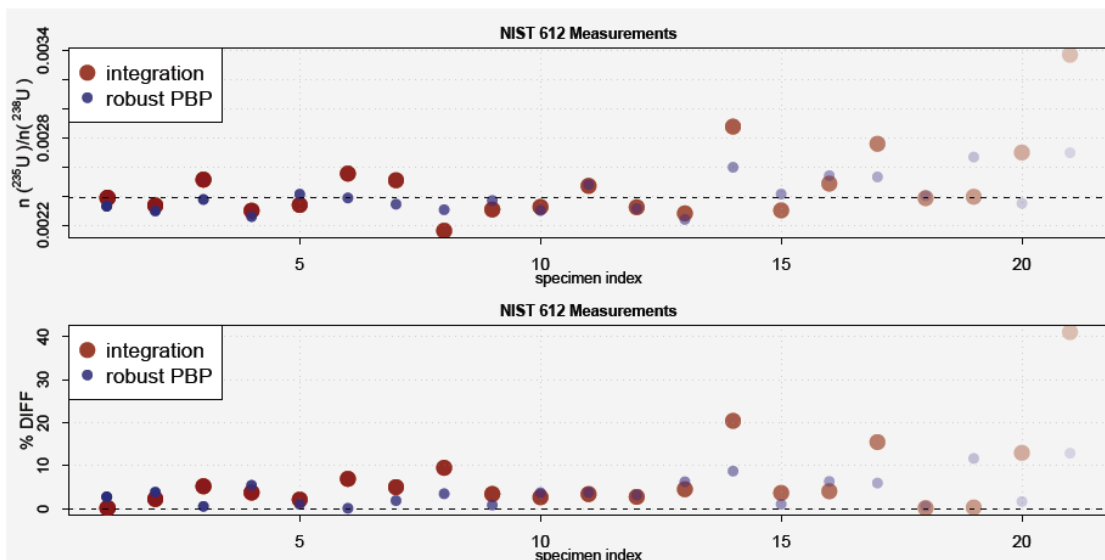
Figure 87: NIST 612 isotope ratio measurements comparison between integration (red) and MAD algorithm (blue). Note that the dashed line is a the expected value for U-ore (natural uranium). [100]

The graphics indicate that both data reduction approaches seem reasonable, producing most estimates with smaller than 20% relative difference. However, it can be seen that the errors of estimates under the robust PBP data reduction approach tend to be smaller and less variable than the integration approach, which is confirmed by the performance summary statistics presented in Table 10. The robust PBP approach (by means of the MAD algorithm) achieved a 2.2 times smaller total error than the integration approach. [100]

Material	Approach	bias	SD	RMSE
NIST 612	integration robust PBP	0.0000909 0.0000213	0.0002676 0.0001294	0.0002827 0.0001311
U-Ore (POI)	integration robust PBP	-0.000656 0.000737	0.001997 0.001114	0.002102 0.001335

Table 10: Performance figures of the integration and robust PBP data reduction approaches for 21 NIST 612 and 114 U-ore POIs.

5.9 Other Results

Particle Contamination

After combining all particle ablation estimates into a single data set, it was found there was one POI whose isotope ratio did not match that of the rest of the particles, or that of natural uranium. This POI had a U-235/U-238 isotope ratio of 0.00253 ± 0.000103 (4% uncertainty), which is a typical depleted uranium ratio value. Therefore, it is apparent that this particle was a contamination and by tracking back, it was found that the particle was implanted before irradiation since it had a matching FT. See figure 88 for a depiction of the whole data set and figure 89 for the FT image of this POI. We concluded that this was due to performing the sample preparation in non-clean lab environments, in several places at the laboratories where DU particles were handled beforehand.
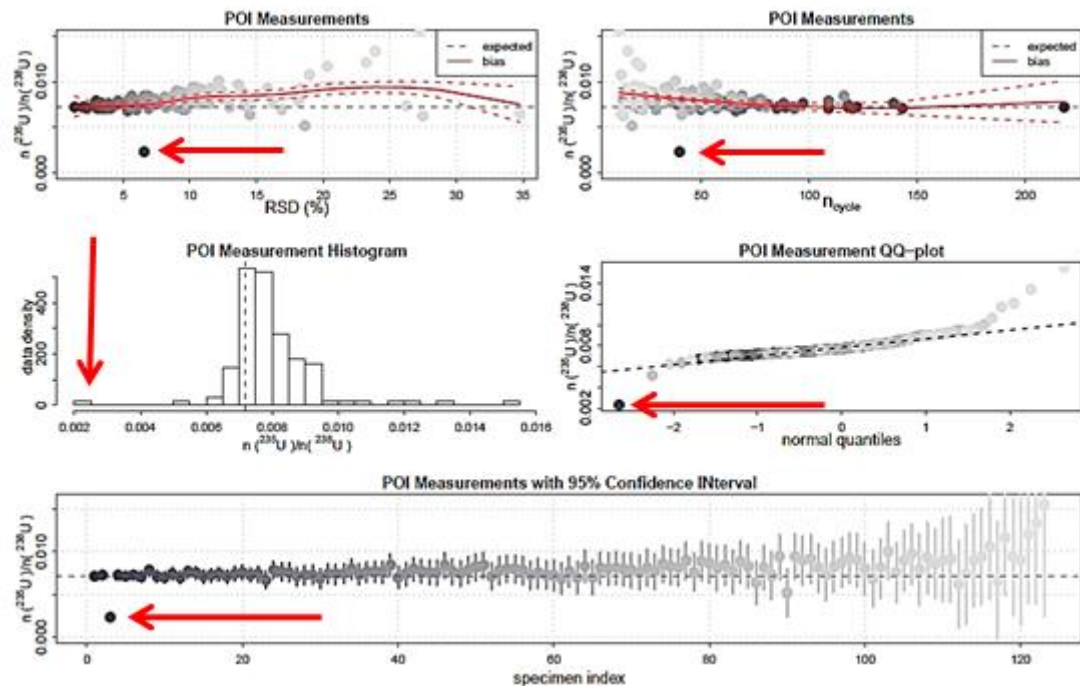
Figure 88: Outlier particle identified as probable contamination.
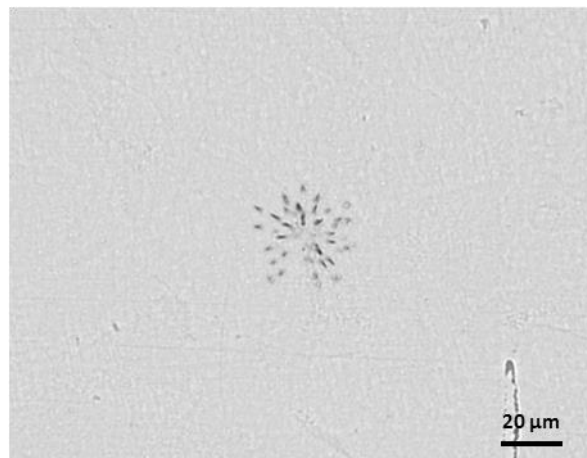
Figure 89: FTs of depleted uranium particle. Note that this is not distinguishable from FTs of a natural uranium particle (see FTs in figure 51).

FT Density vs. U-235

Previous publications show that a linear relationship between the number of counted fission tracks and a POI's enrichment exists **[20] [120]**. However, it can be argued that such a relationship may be affected by the particle size and/or total U-235 content (since this is the fissionable isotope). In other words, a variation of FT internal density (differing number of individual tracks) can be observed from particles of the same enrichment. In this way, using the LA-ICP-MS signal as a normalizing factor, the different U-235 containing particles could potentially be distinguished since they would fall onto separate enrichment lines. To test this hypothesis, 20 POIs from a single sample were investigated.
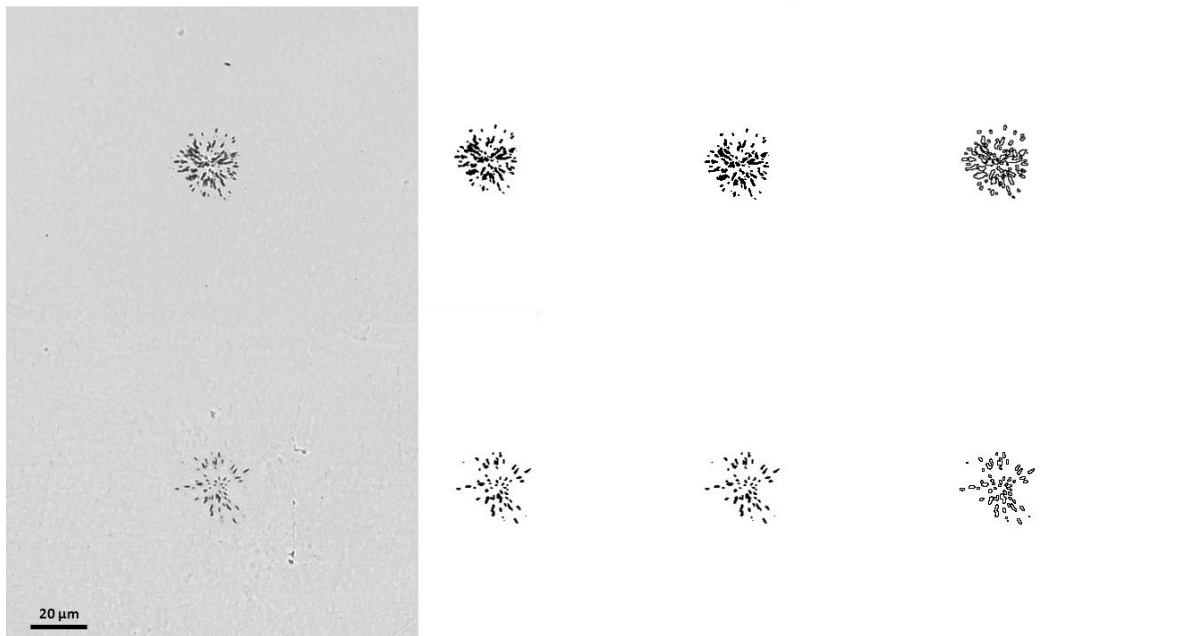
Figure 90: Top and bottom rows are images depicting operations in FIJI. From left to right: original image; thresholded (default); Watershed; Analyze particles operation. The top image resulted in 59 fission tracks counted and the bottom in 49. The bottom is about the limiting amount for which individual tracks are still distinguishable by the software. Top area of FTs = 130 μm² and bottom FT area = 70 μm².

The raw images were input to ImageJ and then thresholded to clear the background. The Analyse Particles functionality on these FT images was used to segment out individual tracks (and possibly cut out overlapping tracks). The number of tracks found on each image was plotted against the number of counts detected from their originating POIs in the LA-ICP-MS. A linear correlation between the number of tracks and the total U-235 counts for each particle was found for low activity FTs where nearly all individual tracks could be distinguished from the background (mainly due to their low number). In the case of FTs with a well-developed omphalos, this linear relationship fails (figure 91.). Nevertheless, for those POIs. a linear correlation between their FT track area and the U-235 counts was confirmed (figure 92).
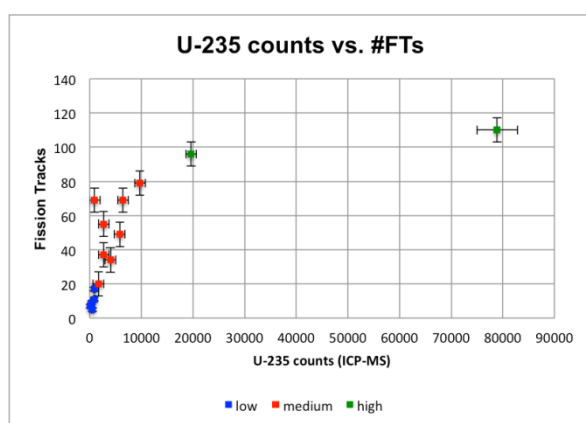
Figure 91: U-235 counts vs. Number of Fission Tracks in Sample 010. The linear relationship fails for dark centroid stars.
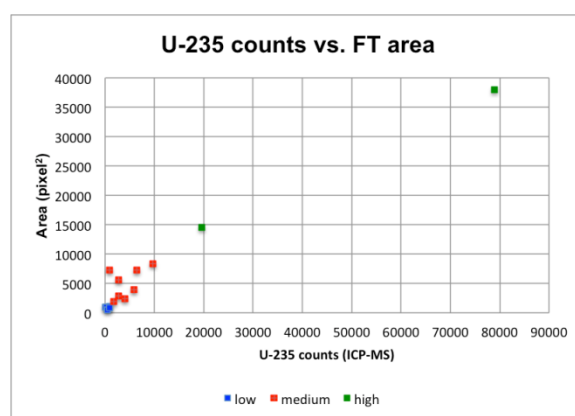
Figure 92: Linear relationship between particles' U-235 counts and their FT star areas.

Chapter 6: Conclusion [16] [26] [80] [86]

The analysis of Environmental Samples (ES) collected from nuclear facilities is an important tool for Safeguards (SG) at the International Atomic Energy Agency (IAEA). Microparticles from ESs are routinely individually screened for their actinide content and then microprobed using a range of techniques. In general, two main approaches are used: probing a large number of particles to identify the actinide-containing micro artefacts (Particles of Interest – POIs) during the data analysis step; or sifting and identifying the POIs before analysis in order to submit only a small number of particles for detailed processing. In this work, the fission track (FT) method was used to identify POIs. Therefore, as part of this monograph, detailed systematic modifications to the Fission Track method for single particle identification for safeguards was presented.

In Chapter 2, an in-depth discussion of current sample preparation techniques used at analytical laboratories for the extraction and handling of micron-sized dust particles was evaluated. The conclusion of this study was that the a shock-wave based particle dispersion device that was designed and constructed as part of this work showed the least biased results for particle re-distribution. Particles of a wider size distribution compared to other methods could be re-sampled and the average inter-particle distance using this method facilitated the sampling of the largest number of particles for further analysis steps. Chapter 3 presented fundamental improvements to the fission track methodology, including, as far as the author is aware of, the first attempt to standardize the FT method for micron particle analysis. Specifically, the details of the sample preparation and micron particle handling were discussed. These include:

1. Construction of a catcher and harvester assembly for facilitating the handling of micron particles during irradiation, detector from catcher detachment; FT identification and coordinate export for particle-of-interest relocation and isolation;

2. Fundamental considerations undertaken prior to SSNTD material selection;

3. Etching optimization;

Chapter 4 provided the details of a correlative microscopy methodology by which means the fission tracks were used to find particles-of-interest. Moreover, a laser-micro-dissection device was used to relocate POIs and cut them out from the original sample, embedding these onto a silicone-based harvester for further handling. The resulting procedure is semi-automated.

Chapter 5 described the need for a modified treatment of transient signals collected by a ns LA-ICP-MS device (New Wave Research, 213 NWR ESI laser attached to a quadrupole ICP-MS iCAP Q device from Thermo Scientific). The short lifetime of 1μm ablated isotope-ratio signals from natural uranium particles required a modified approach to the data analysis. For this, a modified treatment was devised based on the PBP method that achieves an operator-independent evaluation of isotope ratios in POIs.

Thus, a list of achievements of this work includes:

1. Dispersion of particles using a shock-wave disperser device to achieve an even distribution (even inter-particle dispersion that apparently is not biased towards particles of a certain size range);

2. Use of thin membranes as catchers to hold dispersed particles and minimise and standardize the distance from the particles to the SSNTD surface;

3. Use of a fixing medium for holding dispersed particles on the foil;

4. Use of thick detectors to minimise detector deformation due to irradiation and etching;

5. Use of low gamma background irradiation positions to decrease detector deformation (such as milkiness and other etching artefacts);

6. Optimise detector etching by using an accelerated etching approach;

7. Use of a laser to mark fiducial points for locating FTs and modifying existing relocation algorithms to find corresponding POIs;

8. Employ large area imaging of a 2.5 x 2.5 cm^2 SSNTD detector;

9. Automate the export of FT coordinates and import these to LMD, LA-ICP-MS and other microprobe devices;

10. Use of a silicone-based harvester material for isolating particles from a single sample. Several harvester materials can be used for isolating POIs from a single sample. This way, multiple microprobe techniques can be used for the evaluation of each sample;

11. Automate the isolation of corresponding relocated POIs from surrounding matrix particles using a laser micro-dissection device;

12. Develop a novel approach to transient signal handling,that considers the empirical nature of the signal to assign measurement uncertainties;

Using this novel approach, 1 μm sized U-ore particles could be identified, isolated and microprobed within 3 days upon receipt from the irradiation facility. The greatest delay to this method is the irradiation step: transport (1 day each to and from the facility); irradiation handling 1 day; cooling and clearing for transportation 7 days. Thus, the total analysis time for the proposed method is 12 days. In a single sample, 68 POIs were isolated and microprobed, the microprobing itself taking 2 hours (including ICP-MS tuning and plasma stabilisation). The POI isolation and transfer recovery rate is close to 100%. This proposed analytical procedure for a standardised isolation and transfer of safeguards particles-of-interest was found to be successful and can be further automated. We appear to have made surprisingly good measurements of a small amount of uranium ore material: most estimates are with 95% confidence consistent with expected values. The method overall had a small positive bias.

Future Work

This monograph is a collection of improvements aimed primarily towards the complete automation of the fission track method for POI handling. A semi-automated POI isolation and harvesting method using a laser-micro-dissection device was achieved as well as an operator independent data analysis. Correlative microscopy for micron-sized particles was successfully implemented and used to identify fission tracks for tagging safeguards particles-of-interest. The method was tested on a single uranium ore material.

Further development of this work could include:

1. Testing of the method to differentiate uranium particles of different source material; Possibly test the success rate of detecting sub-micron POIs;

2. Use of other SSNTD materials and/or plastics as detectors;

3. Use of a new irradiation channel with higher flux to decrease the total irradiation time;

4. Fully automate the fission track recognition algorithm to make use of fiducial points in order to assign coordinates to each FT of a sample;

5. Fully automate the relocation and isolation of FTs and POIs in a single instrument;

6. Use the FT method for POI identification developed to compare microprobe techniques;

7. Add modifications in order to be able to easily transfer particles onto a TIMS filament;

8. Develop further the transient signal data analysis scheme in R for safeguards;

9. Application of the Fission Track – LMD approach with LA-Multi-Collector-ICP-MS and the comparison of these data with single collector ICP-MS.

References

[1]   "Preamble to the Charter of the United Nations," [Online]. Available: http://www.un.org/en/documents/charter/preamble.shtml. [Accessed 11 November 2014].

[2]   "Manhattan Project," Nuclear Files, [Online]. Available: http://www.nuclearfiles.org/menu/key-issues/nuclear-weapons/history/pre-cold-war/manhattan-project/. [Accessed 5 November 2014].

[3]   P. Goldschmidt, "The IAEA Safeguards System Moves into the 21st Century," *Supplement to the IAEA Bulletin, Volume 41, No 4,* p. 15, 12 1999.

[4]   IAEA, "IAEA Safeguards Glossary," 2002. [Online]. Available: http://www-pub.iaea.org/MTCD/publications/PDF/nvs-3-cd/PDF/NVS3_scr.pdf. [Accessed 11 2014].

[5]   D. Brady and L. Rappoport, "Policy-capturing in the field: The nuclear safeguards problem," *Organizational Behavior and Human Performance,* vol. 9, no. 2, pp. 253-266, 1973.

[6]   B. Johnson, "Nuclear Power Proliferation: Problems of International Control," *Energy Policy,* vol. September, pp. 179-194, 1977.

[7]   B. Clark and G. B. Cook, "The Safeguards Analytical Laboratory," IAEA, [Online]. Available: http://www.iaea.org/sites/default/files/17606082427.pdf. [Accessed 17 11 2014].

[8]   IAEA, "IAEA Safeguards in 1981," *The Environmentalist,* vol. 2, no. 4, pp. 345-346, 1982.

[9]   R. Kreger, "IAEA Iraq Inspections: Lessons Learned and Future Implications," Center for Nonproliferation Studies, 4 6 2014. [Online]. Available: http://www.nonproliferation.org/iaea_iraq_inspections-lessons-learned-and-future-implications/. [Accessed 14 11 2014].

[10]   D. Donohue, "Strengthening IAEA Safeguards Through Environmental Sampling and Analysis," *Journal of Alloys and Compounds,* Vols. 271-273, pp. 11-18, 1998.

[11]   U. Admon, E. Chinea-Cano, D. Wegrzynek, M. Bogovac and A. Markowicz, "Isolated Particles Handling and Research," in *Hot Particles Released from Different Nuclear Sources*, Yalta, Crimea, 2007.

[12]   D. Donohue, "Strengthened Nuclear Safeguards," *Analytical Chemistry,* vol. 74, no. 1, pp. 28A-35A, 2002.

[13]   M. J. Kristo, "Nuclear Forensics," in *Hanbook of Radioactivity Analysis*, Academic Press (Elsevier), 2012, pp. 1281-1304.

[14]   Z. Macsik, *Analysis of Actinides in Safeguards Swipe Samples by Radiometric and Mass Spectrometric Methods (PhD Dissertation),* Budapest: Eötvös Loránd University of Sciences, Budapest Chemistry Ph.D. School, 2012.

[15]   N. Vajda and C.-K. Kim, "Determination of Transuranium Isotopes (Pu, Np, Am) by Radiometric Techniques: A Review of Analytical Methodology," *Analytical Chemistry,* vol. 83, pp. 4688-4719, 2011.

[16]   N. Dzigal, E. Chinea-Cano, S. Walsh and A. Limbeck, "Revisiting the Fission Track Method for the Analysis of Particles in Safeguards Environmental Samples," *Talanta,* 2016.

[17]   S. Baude and R. Chiappini, "Isotopic measurements on micrometric particles: the French experience to detect fissile material," CEA, Service Radioanalyses, Surveillance, Environnement, 2001. [Online]. Available: http://www-pub.iaea.org/MTCD/publications/PDF/ss-2001/PDF%20files/Session%2010/Paper%2010-05.pdf. [Accessed 18 11 2014].

[18]   O. Stetzer, M. Betti, J. van Geel, N. Erdmann, J.-V. Kratz, R. Schenkel and N. Trautmann,

"Determination of the U-235 content in uranium oxide particles by fission track analysis," *Nuclear Instruments and Methods in Physics Research Section A: Accelerators, Spectrometers, Detectors and Associated Equipment,* vol. 525, no. 3, pp. 582-592, 2004.

[19] M. Kristo, "Nuclear Forensics," in *Handbook of Radioactivity Analysis*, Elsevier Academic Press, 2012, pp. 1281-1304.

[20] O. Stetzer, M. Betti, J. van Geel, N. Erdmann, J. Kratz, R. Schenkel and N. Trautmann, "Determination of the U-235 content in uranium oxide particles by fission track analysis," *Nuclear Instruments and Methods in Physics Research Section A: Accelerators, Spectrometers, Detectors and Associated Equipment,* vol. 525, no. 3, pp. 582-592, 2004.

[21] L. Sangély, "Comparison between vacuum impactor and liquid extraction techniques for sample preparation," in *CGM on Particle Analysis on Environmental Samples for Safeguards*, Toronto, 2009.

[22] C.-G. Lee, K. Iguchi, F. Esaka, M. Magara, S. Sakurai, K. Watanabe and S. Usuda, "Influence of uranium enrichment on the etching rate of polycarbonate fission track detector containing uranium," *Nuclear Instruments and Methods in Physics Research Section B: Beam Interactions with Materials and Atoms,* vol. 245, no. 2, pp. 440-444, 2006.

[23] Y. Park, K. Song, H. Pyo, M. Lee, K. Jee and W. Kim, "Investigation on the fission track analysis of uranium-doped particles for the screening of safeguards environmental samples," *Nuclear Instruments and Methods in Physics Research Section A: Accelerators, Spectrometers, Detectors and Associated Equipment,* vol. 557, no. 2, pp. 657-663, 2006.

[24] B. Salbu, M. Burkitbaev, G. Strømman, I. Shishkov, P. Kayukov, B. Uralbekov and B. Rosseland, "Environmental impact assessment of radionuclides and trace elements at the Kurday U mining site, Kazakhstan," *Journal of Environmental Radioactivity,* vol. 123, pp. 14-27, 2013.

[25] C. G. Lee, K. Iguchi, J. Inagawa, D. Suzuki, F. Esaka, M. Magara, S. Sakurai, K. Watanabe and S. Usuda, "Development in fission track-thermal ionization mass spectrometry for particle analysis of safeguards environmental samples," *Journal of Radioanalytical and Nuclear Chemistry,* vol. 272, pp. 299-302, 2007.

[26] N. Dzigal and E. Chinea-Cano, "On the Dispersion of Particles on Flat Substrates for Microprobe Analysis Techniques," *Journal of Nuclear Materials Measurements,* vol. 44, no. 2, pp. 62-75, 2015.

[27] F. Esaka and M. Magara, "Secondary ion mass spectrometry combined with alpha track detection for isotope abundance ratio analysis of individual uranium-bearing particles," *Talanta,* vol. 120, p. 3490354, 2014.

[28] C.-G. Lee, D. Suzuki, F. Esaka, M. Magara and T. Kimura, "Combined application of alpha-track and fission-track techniques for detection of plutonium particles in environmental samples prior to isotopic measurement using thermo-ionization mass spectrometry," *Talanta,* vol. 85, no. 1, pp. 644-649, 2011.

[29] F. Esaka, C.-G. Lee, M. Magara and T. Kimura, "Fission track–secondary ion mass spectrometry as a tool for detecting the isotopic signature of individual uranium containing particles," *Analytica Chimica Acta,* vol. 721, pp. 122-128, 2012.

[30] T. Shinonaga, F. Esaka, M. Magara, D. Klose and D. Donohue, "Isotopic analysis of single uranium and plutonium particles by chemical treatment and mass spectrometry," *Spectrochimica Acta Part B,* vol. 63, pp. 1324-1328, 2008.

[31] F. E. J. I. K. I. C.-G. L. S. S. K. W. S. U. Konomi Esaka, "Application of Fission Track Technique for the Analysis of Individual Particles Containing Uranium in Safeguard Swipe Samples," *Japanese Journal of Applied Physics,* vol. 43, no. 7A, pp. L915-L916, 2004.

[32] M. M. Fumitaka Esaka, "Secondary ion mass spectrometry combined with alpha track detection for isotope abundance ratio analysis of individual uranium-bearing particles," *Talanta,* vol. 120, p. 3490354, 2014.

[33] S. Woelfl, M. Magesb and F. Encinac, "Cold plasma ashing improves the trace element

detection of single," *Spectrochimica Acta Part B,* vol. 58, pp. 2157-2168, 2003.

[34] F. Esaka and M. Magara, "Secondary ion mass spectrometry combined with alpha track detection for isotope abundance ratio analysis of individual uranium-bearing particles," *Talanta,* vol. 120, pp. 349-354, 2014.

[35] P. Lukes, F. Fernandez, J. Gutierrez-Aceves, E. Fernandez, A. U.M., P. Sunka and A. Loske, "Tandem shock waves in medicine and biology: a review of potential applications and successes," *Shock Waves,* 2015.

[36] B. Oudheusden, A. J. P. Joebsis, F. Scarano and S. L.J., "Investigation of the unsteadiness of a shock-reflection interaction with time-resolved particle image velocimetry," *Shock Waves,* vol. 21, no. 5, pp. 397-409, 2011.

[37] Z. Zong, Z. Li and J. Dong, "Solving the sod shock tube problem using localized differential quadrature (LDQ) method," *Journal of Marine Science and Application,* vol. 10, no. 1, pp. 41-48, 2011.

[38] D. Rogg, D. Hermann and G. Adomeit, "Shock-induced flow in regular arrays of cylinders and packed beds," *International Journal of Heat and Mass Transfer,* vol. 28, no. 12, pp. 2285-2298, 1985.

[39] "CADFEM," [Online]. Available: http://cadfem.en.softonic.com/.

[40] IAEA, "Report on Intercomparison IAEA/Soil7 of the Determination of Trace Elements in Soil," IAEA, Vienna, 1984.

[41] J. Schindelin and I. &. F. E. e. a. Arganda-Carreras, "Fiji: an open-source platform for biological-image analysis," *Nature methods 9(7),* vol. 9, no. 7, pp. 676-682, 2012.

[42] K. Barthel, "Interactive 3D Surface Plot," 2008. [Online]. Available: http://imagej.net/plugins/surface-plot-3d.html.

[43] W. Rasband, "Dynamic Profiler," 2003. [Online]. Available: http://rsb.info.nih.gov/ij/plugins/dynamic-profiler.html.

[44] P. Carl, "Azimuthal Average," 2007. [Online]. Available: http://rsb.info.nih.gov/ij/plugins/azimuthal-average.html.

[45] R. Wayne, "Concentric Circles," 2007. [Online]. Available: http://rsb.info.nih.gov/ij/plugins/concentric-circles.html.

[46] D. Prodanov, "Granulometric Filtering," 2005. [Online]. Available: http://fiji.sc/Granulometric_Filtering.

[47] J. Schindelin and L. P. Chew, "Delaunay Voronoi," 2006. [Online]. Available: http://fiji.sc/Delaunay_Voronoi.

[48] G. Matheron, Randoms sets and integral equation, New York: Wiley, 1978.

[49] C.-Y. Wu, "Aerosol Transport," University of Florida, [Online]. Available: http://aerosol.ees.ufl.edu/aerosol_trans/section09_d.html.

[50] J. Schindelin and P. Chew, "Delaunay Voronoi," 2006. [Online]. Available: http://fiji.sc/Delaunay_Voronoi.

[51] S.-L. Guo, B.-L. Chen and S. Durrani, "Solid-State Nuclear Track Detectors," in *Handbook of Radioactivity Analysis*, Academic Press (Elsevier), 2012, pp. 233-298.

[52] P. Price and R. Walker, "Chemical etching of charged-particle tracks in solids," *Journal of Applied Physics,* vol. 33, pp. 3407-3412, 1962.

[53] R. Fleischer, P. Price, R. Walker and E. Hubbard, "Track registration in various solid state nuclear track detectors," *Physics Review,* vol. 133A, pp. 1443-1449, 1964.

[54] M. Pollard and C. Heron, Archaeological Chemistry, Cambridge: RSC Publishing, 2008.

[55] A. Weiss, I. Halevy, N. Dzigal, E. Chinea-Cano and U. Admon, "Fission Track Detection using Automated Microscopy," *Journal of Nuclear Engineering and Radiation Science,* 2017.

[56] M. Kraiem, S. Richter, H. Kühn and Y. Aregbe, "Development of an improved method to perform single particle analysis by TIMS for nuclear safeguards," *Analytica Chimica Acta,* vol.

688, pp. 1-7, 2011.

[57] K. Esaka, F. Esaka, J. Inagawa, K. Iguchi, C. Lee, S. Sakurai, K. Watanabe and S. Usuda, "Application of fission track technique for the analysis of individual particles containing uranium in safeguard swipe samples," *Japanese Journal of Applied Physics, Part 2: Letters,* vol. 43, no. 7A, pp. L915-L916, 2004.

[58] M. Lee, J. H. Park and K. Song, "Investigation on the nuclear track techniques for the screening of the fissile nuclides in swipe samples," *Radiation Measurements,* no. 46, pp. 409-412, 2011.

[59] K. Iguchi, L. C. K.T. Esaka, J. Inagawa, F. Esaka, T. Onodera, H. Fukuyama, D. Suzuki, S. Sakurai, K. Watanabe and S. Usuda, "Study on the etching conditions of polycarbonate detectors for particle analysis of safeguards environmental samples," *Radiation Measurements,* vol. 40, pp. 363-366, 2005.

[60] E. Enkelmann, T. A. Ehlers, G. Buck and A.-K. Schatz, "Advantages and challenges of automated apatite fission track counting," *Chemical Geology,* Vols. 322-323, pp. 278-289, 2012.

[61] R. Fleisher and P. Price, "Tracks of charged particles in high polymers," *Science,* vol. 140, pp. 1221-1222, 1963.

[62] P. Joshirao, C. Vyas, K. T. P. Kalsi and V. K. Manchand, "Determination of Alpha Activity in Organic Solvents using CR-39," *Applied Radiation and Isotopes,* vol. 78, pp. 68-71, 2013.

[63] M. Misdaq, H. Khajmi, F. Aitnouh, S. Berrazzouk and W. Bourzik, "A new method for evaluating uranium and thorium contents in di€fferent natural material samples by calculating the CR-39 and LR-115 type II SSNTD detection eff • ciencies for the emitted alpha particles," *Nuclear Instruments and Methods in Physics Research B,* vol. 171, pp. 350-359, 2000.

[64] R. Fleisher and P. Price, "Tracks of charged particles in high polymers," *Science,* vol. 140, pp. 1221-1222, 1963.

[65] R. Fleisher, P. Price and R. Walker, "Solid-State Track Detectors: Applications to Nuclear Science and Geophysics," *Annual Review of Nuclear Science,* vol. 15, pp. 1-28, 1965.

[66] A. Donard, F. Pointurier, A.-C. Pottin, A. Hubert and C. Pecheyran, "Determination of the isotopic composition of micrometric uranium particles by UV femtosecond laser ablation coupled with sector-field single- collector ICP-MS," *J. Anal. At. Spectrom. ,* 2016.

[67] S. Repetsky and et al., "Electron and atomic structure of polymers: Implication for nuclear tracks formation," *Rad. Measurements ,* vol. 40, pp. 204-212, 2005.

[68] R. Shweikani and et al., "Effects of Gamma Irradiation on the Bulk and Track Etching Properties of Cellulose Nitrate (DAICEL 6000) and CR-39 Plastics," *Nucl. Tracks Radiat.Meas.,* vol. 22, no. 1-4, pp. 153-156, 1993.

[69] E. Khan, N. Ali and e. al., "Study of the etching characteristics of Na2CO3-mixed NaOH solution," *Radiation Measurements,* vol. 40, p. 299–302, 2005.

[70] M. B. A.K. Galwey, Thermal Decomposition of Ionic Solids: Chemical Properties and Reactivities of Ionic Crystalline Phases, Elsevier, 1999, p. 187.

[71] D. Nikezic and K. N. Yu, "Formation and growth of tracks in nuclear track materials," *Materials Science and Engineering,* pp. 51-123, 2004.

[72] F. Esaka, K. T. Esaka, C. Lee, M. Magara, S. S., S. Usuda and K. Watanabe, "Particle isolation for analysis of uranium minor isotopes in individual particles by secondary ion mass spectrometry," *Talanta,* vol. 71, no. 3, p. 1011–1015, 2007.

[73] P. Baiocchi and et al., "Calibration with Relativistic and Low Velocity Ions of a CR39 Nuclear Track Detector35," *Rad. Measurements,* vol. 25, pp. 145-150, 1995.

[74] F. Leonardi, M. Caresana, M. D'Alessandro, R. Mishra, S. Tonnarini, R. Trevisi and M. Veschetti, "An extended study of the etching characteristics of CR-39 detectors," *Radiation Measurements,* vol. 44, pp. 787-790, 2009.

[75] M. Matiullah, S. Rehman, S. Rehman and W. Zaman, "Discovery of new etchants for CR-39 detector," *Radiation Measurements,* vol. 39, pp. 337-343, 2005.

[76] Y. Shen, Y. Zhaoa, S. Guo, J. Cui, Y. Liu, J. Li, J. Xu and H. Zhang, "Study on analysis of isotopic ratio of uranium-bearing particle in swipe samples by FT-TIMS," *Radiation Measurements* , vol. 43, pp. 299-302, 2008.

[77] F. Pointurier, A. Hubert and A. Pottin, "Performance of laser ablation: quadrupole-based ICP-MS coupling for the analysis of single micrometric uranium particles," *Journal of Radioanal Nucl Chem,* no. 296, p. 609–616, 2013.

[78] S. Balestra, M. M. Cozzi, G. Giacomelli, R. R. Giacomelli, M. Giorgini, A. Kumar, G. Mandrioli, S. Manzoor, A. Margiotta, E. Medinaceli, L. Patrizii, V. Popa, I. Qureshi, M. Rana, G. Sirri, M. Spurio, V. Togo and C. Valieri, "Bulk etch rate measurements and calibrations of plastic nuclear track detectors," *Nuclear Instruments and Methods in Physics Research Section B: Beam Interactions with Materials and Atoms,* vol. 254, no. 2, pp. 254-258, 2007.

[79] I. Simakin, I. Vlasova and S. Kalmykov, "Digital image analysis of the etched a-tracks in CR-39," *Radiation Measurements,* vol. 50, pp. 212-217, 2013.

[80] N. Dzigal and E. Chinea-Cano, "Correlative Microscopy Techniques for the Analysis of Particles in Safeguards Environmental Samples," *Journal of Physics: Conference Series,* vol. 644, 2015.

[81] G. Isenberg, W. Bielser, W. Meier-Ruge and E. Remy, "Cell surgery by laser micro-dissection: A preparative method," *Journal of Microscopy,* 1976.

[82] M. R. Emmert-Buck, R. S. P. C. R. Bonner, Z. Qhuang, S. R. Goldstein and R. L. L. A. Weiss, "Laser Capture Microdissection," *Science,* vol. 274, pp. 998-1001, 1996.

[83] R. Bonner, M. Emmert-Buck, K. Cole, T. Pohida, R. Chuaqui, S. Goldstein and L. Liotta, "Laser Capture Microdissection: Molecular Analysis of Tissue," *Science,* pp. 1481-1483, 1997.

[84] D. Frumkin, A. Wasserstrom, S. Itzkovitz, A. Harmelin, G. Rechavi and E. Shapiro, "Amplification of multiple genomic loci from single cells isolated by laser micro-dissection of tissues," *BMC Biotechnology,* 2008.

[85] S. Hernandez and J. Lloreta, "Manual Versus Laser Micro-dissection in Molecular Biology," *Ultrastructural Pathology,* vol. 30, no. 3, 2006.

[86] N. Dzigal and E. Chinea-Cano, "Laser-Assisted Sampling Techniques in Combination with ICP-MS: A Novel Approach for Particle Analysis at the IAEA Environmental Samples Laboratory," International Atomic Energy Agency, Vienna, Austria, 2014.

[87] U. Admon, E. Chinea-Cano, N. Dzigal, I. Halevy, E. Boblil, T. Elkayam, A. Weiss and K. Vogt, "Advancements in Particle Analysis Procedures and their Application to the Characterization of Reference Materials for Safeguards," in *Safeguards Symposium, IAEA, 2014*, Vienna, Austria.

[88] A. Sartori, R. Gatz, F. Beck, A. Rigort, W. Baumeister and J. Plitzko, "Correlative microscopy: Bridging the gap between fluorescence light microscopy and cryo-electron tomography," *Journal of Structural Biology,* vol. 160, no. 2, pp. 135-145, 2007.

[89] J. Plitzko and A. L. A. Rigort, "Correlative cryo-light microscopy and cryo-electron tomography: from cellular territories to molecular landscapes," *Current Opinion in Biotechnology,* vol. 20, no. 1, pp. 83-89, 2009.

[90] P. Kempen, M. Kircher, A. de la Zerda, C. Zavaleta, J. Jokerst, I. Mellinghoff, S. Gambhir and R. Sinclair, "A correlative optical microscopy and scanning electron microscopy approach to locating nanoparticles in brain tumors," *Micron,* vol. 68, pp. 70-76, 2015.

[91] C. Fona and B. Humbel, "Correlative microscopy," *Archives of Biochemistry and Biophysics,* 2015.

[92] D. Kong and J. Loncarek, "Correlative light and electron microscopy analysis of the centrosome: a step-by-step protocol," *Methods in Cell Biology,* p. online, 2015.

[93] Carl Zeiss, "Correlative microscopy in materials analysis," *Tools & Techniques,* vol. 12, no. 10, p. 47, 2009.

[94] A. Fejfar, M. Hyvl, A. Vetuschka, P. Pikna, Z. Hajkova, M. Ledinsky, J. Kocka, P. Klapetek, A. Maskova, J. Vyskocil, J. Merkel, C. Becker, T. M. S. Itoh, M. Foldyna, L. Yu and P. Roca i

Cabarrocas, "Correlative microscopy of radial junction nanowire solar cells using nanoindent position markers," *Solar Energy Materials and Solar Cells,* vol. 135, no. EMRS 2014 Spring Meeting – Advanced materials and characterization techniques for solar cells II, pp. 106-112, 2015.

[95] M. Herbig, P. Choi and D. Raabe, "Combining structural and chemical information at the nanometer scale by correlative transmission electron microscopy and atom probe tomography," *Ultramicroscopy,* vol. 153, pp. 32-39, 2015.

[96] U. Admon, E. Chinea-Cano, D. Wegrzynek, H. Aigner, A. Marcowitz and D. Donohue, "Single Particles Handling and Analyses," in *Radioactive Particles in the Environment*, D. Oughton and V. Kashparov, Eds., Springer, 2009, pp. 15-55.

[97] S.-L. Guo, Y. Zhao, Y. Shen, G. Liu, J. Li and C. Wang, "Mathematical and technical procedures of relocation of microscopic aerosol particles for chemical and isotopic analysis," *Radiation Measurements,* vol. 43, no. Supplement 1, pp. 309-312, 2008.

[98] D. Donohue, A. Ciurapinski, J. Cliff, F. Ruedenauer, T. Kuno and J. Poths, "Microscopic studies of spherical particles for nuclear safeguards," *Applied Surface Science,* vol. 255, p. 2561–2568, 2008.

[99] N. Dzigal, E. Chinea-Cano, S. Walsh and A. Limbeck, "Revisiting the Fission Track Method for the Analysis of Particles in Safeguards Environmental Samples," *Talanta,* 2016.

[100] S. Walsh, N. Dzigal, E. Chinea-Cano and A. Limbeck, "Simple robust estimation of uranium isotope ratios in individual particles from LA-ICP-MS measurements," *Journal of Analytical Atomic Spectroscopy,* 2017.

[101] A. Duffin, G. L. Hart, R. Hanlen and G. Eiden, "Isotopic analysis of uranium in NIST SRM glass by femtosecond laser ablation MC-ICPMS," *Journal of Radioanalytical and Nuclear Chemistry,* vol. 296, no. 2, 2012.

[102] S. Kappel, S. Boulyga, L. Dorta, D. Gunther, B. Hattendorf, D. Koffler, G. Laaha, F. Leisch and T. Prohaska, "Evaluation strategies for isotope ratio measurements of single particles by LA-MC-ICPMS," *Anal Bioanal Chem,* vol. 405, no. DOI 10.1007/s00216, p. 2943–2955, 2013.

[103] T. Pettke, F. Oberli, A. Audetat, U. Wiechert, C. Harris and C. Heinrich, "Quantification of transient signals in multiple collector inductively coupled plasma mass spectrometry: accurate lead iso- tope ratio determination by laser ablation of individual fluid inclu- sions," *Journal Analalytical Atomic Spectrometry,* vol. 26, pp. 475-492, 2011.

[104] Z. Varga, "Application of laser ablation inductively coupled plasma mass spectrometry for the isotopic analysis of single uranium particles," *Analytica Chimica Acta ,* vol. 625, pp. 1-7, 2008.

[105] N. LaHaye, S. Harilal, P. Diwaker and A. Hassanein, "The effect of laser pulse duration on ICP-MS signal intensity, elemental fractionation, and detection limits in fs-LA-ICP-MS," *J. Anal. At. Spectrom.,* vol. 28, p. 1781, 2013.

[106] L. Koch, M. Walle, R. Dietiker and D. Gunther, "Analysis of Laser-produced Aerosoles by Inductively Coupled Plasma Mass Spectrometry: Transport Phenomena and Elemental Fractionation," *Anal. Chem,* no. 80, pp. 915-921, 2008.

[107] F. Pointurier, A. Pottin and A. Hubert, "Application of Nanosecond-UV Laser Ablation-Inductively Coupled Plasma Mass Spectrometry for the Isotopic Analysis of Single Submicrometer-Size Uranium Particles," *Anal. Chem,* no. 83, pp. 7841-7848, 2011.

[108] S. Bürger, S. S.D. Balsley, S. Baumann, J. Berger, S. Boulyga, J. Cunningham, S. S. Kappel, A. Koepf and J. Poths, "Uranium and plutonium analysis of nuclear material samples by multi-collector thermal ionisation mass spectrometry: Quality control, measurement uncertainty, and metrological traceability," *International Journal of Mass Spectrometry,* vol. 311, pp. 40-50, 2012.

[109] S. Kappel, S. Boulyga and T. Prohaska, "Direct uranium isotope ratio analysis of single micrometer-sized glass particles," *Journal of Environmental Radioactivity,* vol. 113, pp. 8-15, 2012.

[110] J. C. f. G. i. Metrology, "JCGM 200:2012 International vocabulary of metrology - Basic and

general concepts and associated terms (VIM), 3rd Edition," JCGM, 2012.

[111] S. Walsh, Z. Macsik, D. Wegrzynek, T. Kriger and S. Boulyga, "Model diagnostics for detecting and identifying method repeatability outliers in precision studies: application to a homogeneity study under a two-stage nested ANOVA," *Journal of Analytical Atomic Spectrometry,* vol. 31, pp. 686-699, 2016.

[112] S. Walsh, A. Venzin, D. Wegrzynek and C. Mansoux, ", Proceedings of the American Nuclear Societies Advances in Nuclear Nonproliferation Technology and Policy Conference," Santa Fe, NM, 2016.

[113] I. o. f. standarization, "2009 Uncertainty of measurement - Part 1: Introduction to the expression of uncertainty in measurement," International organization for standarization technical report, 2009.

[114] JCG, " Evaluation of measurement data - Guide to the expression of uncertainty in measurement," Joint Committee for Guides in Metrology, JCGM 100:2008, 2008.

[115] P. Rousseeuw and S. Verboven, "Robust estimation in very small samples," *Computational Statistics and Data Analysis,* no. 40, pp. 741-758, 2002.

[116] P. Rousseeuw and C. Croux, "Alternatives to the Median Absolute Deviation," *Journal of the American Statistical Association ,* vol. 88, no. 424, pp. 1273-1283, 1993.

[117] I. R. M. C. (REMCO), "ISO Guide 35 (Third Edition): Reference materials - General and statistical principles for certification," International Organization for Standardization, 2006.

[118] I. 13528:2015(E), "Statistical methods for use in proficiency testing by interlaboratory comparison," International Organization for Standardization, 2015.

[119] M. Abu-Shawiesh, F. Al-Athari and H. Kittani, "Confidence Interval for the Mean of a Contaminated Normal Distribution," *Journal of Applied Sciences,* vol. 9, no. 15, pp. 2835-2840, 2009.

[120] M. Pollard and C. Heron, Archaeological Chemistry, Cambridge: RSC Publishing, 2008.

[121] P. Oliveira, "Uranium," in *The Elements*, Turtleback Books, 2001, pp. 1216-1248.

[122] A. Ioffe, "Encyclopedia of Espionage, Intelligence, and Security," Gale, 2004. [Online]. Available: http://militero.files.wordpress.com/2010/10/espionage-intelligence-and-security-encyclopedia-of-volume-3.pdf. [Accessed 10 11 2014].

[123] P. Oliveira, "Plutonium," in *The Elements*, 2001, pp. 1254-1278.

[124] K. E. F. ,. I. J. I. K. L. C.-G. S. S. W. K. U. S. Esaka, "Application of fission track technique for the analysis of individual particles containing uranium in safeguard swipe samples," *Japanese Journal of Applied Physics, Part 2: Letters,* vol. 43, no. 7A, pp. L915-L916, 2004.

[125] P. Hypes, W. Geist and S. Peter, "Analytical Techniques in Nuclear Safeguards," in *Handbook of Radioactivity Analysis*, 3 ed., M. F. L'Annunziata, Ed., Academic Press (Elsevier), 2012, pp. 1243-1280.

[126] R. Higgy and D. Fischer, "Detection of Reprocessing Activities Using Environmental Sampling," in *IAEA Safeguards Symposium*, Vienna, 2014.

[127] R. Fleischer, P. Price and R. Walker, "Solid-State Track Detectors: Applications to Nuclear Science and Geophysics," *Annual Review of Nuclear Science,* vol. 15, pp. 1-28, 1965.

[128] Y. Chen, Y. C. Z. Shen, Y. Zhao, S. Guo, J. Cui and Y. Liu, "Studies on analyzing single uranium-bearing particle by FT-TIMS," *Radiation Measurements,* vol. 50, pp. 43-45, 2013.

[129] A. El Farrash, H. Yousef and A. Hafez, "Activity concentrations of 238U and 232Th in some soil and fertilizer samples using passive and active techniques," *Radiation Measurements,* vol. 47, pp. 644-648, 2012.

[130] F. Esaka, M. Magara, D. Suzuki, Y. Miyamoto, C.-G. Lee and T. Kimura, "Isotope ratio analysis of individual sub-micrometer plutonium particles with inductively coupled plasma mass spectrometry," *Talanta,* vol. 83, pp. 569-573, 2010.

[131] C.-G. Lee, D. Suzuki, Y. Saito-Kokubu, F. Esaka, M. Magara and T. Kimura, "Simultaneous

determination of plutonium and uranium isotope ratios in individual plutonium–uranium mixed particles by thermal ionization mass spectrometry," *International Journal of Mass Spectrometry,* vol. 314, pp. 57-62, 2012.

[132] A. Kerkápoly, N. Vajda and T. Pintér, "Film autoradiography used for hot particle identification," *Journal of Radioanalytical and Nuclear Chemistry,* vol. 265, no. 3, pp. 423-429, 2004.

[133] J. Pálfalvi, J. Szabó and I. Eördögh, "Detection of high energy neutrons, protons and He particles by Solid State Nuclear Track Detectors," *Radiation Measurements,* vol. 45, pp. 1568-1573, 2010.

[134] J. Szabó and J. Pálfalvi, "Calibration of solid state nuclear track detectors at high energy ion beams for cosmic radiation measurements: HAMLET results," *Nuclear Instruments and Methods in Physics Research A,* vol. 694, pp. 193-198, 2012.

[135] O. Bondarenko and e. al., "Application of SSNTD for Maintenance of Radiation and Nuclear Safety of the Sarcophagus," *Rad. Measurements,* vol. 30, pp. 709-713, 1999.

[136] U. Admon, D. Donohue, H. Aigner, G. Tamborini, O. Bildstein and M. Betti, "Multiple-Instrument Analyses of Single Micron-Size Particles," *Microscopy and Microanalysis,* vol. 11, pp. 354-362, 2005.

[137] N. Lloyd, R. Parrish, M. Horstwood and S. R. N. Chenery, "Precise and accurate isotopic analysis of microscopic uranium-oxide grains using LA-MC-ICP-MS," *J. Anal. At. Spectrom.,* vol. 24, pp. 752-758, 2009.

[138] K. Esaka, F. Esaka, J. Inagawa, K. Iguchi, C. Lee, S. Sakurai, K. Watanabe and S. Usuda, "Application of Fission Track Technique for the Analysis of Individual Particles Containing Uranium in Safeguard Swipe Samples," *Japanese Journal of Applied Physics,* vol. 43, no. 7A, pp. L915-L916, 2004.

[139] Z. Varga, "Application of laser ablation inductively coupled plasma mass spectrometry for the isotopic analysis of single uranium particles," *Anal Chim Acta,* vol. 625, pp. 1-7, 2008.

Curriculum Vitae

Email: naida.dzigal89@gmail.com

naida.dzigal@student.tuwien.ac.at

FORMAL EDUCATION

2012 – present	**Vienna University of Technology (TU Wien)**, Doctoral programme in Natural Sciences (PhD Candidate)
2007 – 2011	**Imperial College London**, M. Sci Physics
2009 – 2010	Erasmus Exchange Year at Ruprecht-Karls-Universität Heidelberg with a focus on atomic physics and lasers at the Synthetic Quantum Systems Group
2005 – 2007	**Vienna International School**, Vienna, Austria (IB Diploma program)
	HL subjects: Mathematics, Physics, Computer Science;
	SL subjects: A1 English, B German, ITGS, Further Mathematics;
2004 – 2005	**De la Salle Schule**, Strebersdorf, Vienna, Austria
2003 – 2004	**Druga gimnazija** Sarajevo, BiH

WORK EXPERIENCE

2012 – 2015	**International Atomic Energy Agency** Environmental Samples Laboratory, Department of Safeguards 3.5 years of practical experience in micron particle analysis, image analysis, optical and electron microscopy, mass spectrometry, and related techniques;
Summer 2010	**UNICEF BiH** Internship
Summer 2009	**IAEA, Vienna, Austria** Internship
June 2009	**deltaDot, London** Internship

LANGUAGES

Fluent	English, Bosnian (Croatian/Serbian), German
Limited use	Spanish, French

OTHER

Computer Skills   Proficient in word processing, spreadsheets, presentation and desktop publishing, data mining, internet research and email; Programming languages studied include Java and C++; Other software and programming languages: R, ImageJ + Fiji, CADFEM, SQL, Adobe InDesign

Awards

- TUtheTOP 2016-2017
- WiNner of the Year 2013 and 2015 (awarded by Women in Nuclear IAEA)
- Safeguards Symposium E-poster Winner 2014 (for Techniques in Environmental Sample Analysis);

Societies & Other

- Women in Nuclear IAEA (Executive Committee and Events Team Leader 2012-2015);
- International Science Fair Judge 2013, 2014, 2015;
- CTBTO Diplomacy and Public Policy Course 2013;
- IAEA Ski Club Member;
- INMM, EMS, ASEM, IOP and EMAS Member;

PUBLISHED ARTICLES AND PARTICIPATION IN CONFERENCES

1. "Simple robust estimation of uranium isotope ratios in individual particles from LA-ICP-MS measurements", S. Walsh, N. Dzigal, E. Chinea-Cano and A. Limbeck, JAAS, March 2017 (submitted).

2. "Fission Track Detection using Automated Microscopy", A. Weiss, I. Halevy, N. Dzigal, E. Chinea-Cano, U. Admon, Journal of Nuclear Engineering and Radiation Science, March 2017 (submitted).

3. "Revisiting the Fission Track Method for the Analysis of Particles in Safeguards Environmental Samples," N. Dzigal, E. Chinea-Cano, S. Walsh and A. Limbeck., Talanta, February 2017.

4. "The Application of Correlative Microscopy in the Identification of Uranium-bearing Microparticles", N.Dzigal, E.Chinea-Cano, U.Admon, A.Weiss, EMAS Workshop, Marcoule, France, May 2016.

5. "Correlative Microscopy Techniques for the Analysis of Particles in Safeguards Environmental Samples", N. Dzigal, E. Chinea-Cano, Journal of Physics: Conference Series 644, June 2015.

6.   "On the Dispersion of Particles on Flat Substrates for Microprobe Analysis Techniques", N. Dzigal, E. Chinea-Cano, Journal of Nuclear Materials Management, January 2015.

7.   "Technical Aspects of the Verification of Non-Proliferation: The Role of the Safeguards Analytical Laboratory", N. Dzigal, NPT Academic Symposium, New York, April 2015.

8.   "Laser-Assisted Sampling Techniques in Combination with ICP-MS: A Novel Approach for Particle Analysis at the IAEA Environmental Samples Laboratory", N. Dzigal and E. Chinea-Cano, IAEA Safeguards Symposium, October 2014, Vienna, Austria.

9.   "Advancements in Particle Analysis Procedures and their Application to the Characterization of Reference Materials for Safeguards," U. Admon, E. Chinea-Cano, N. Dzigal, I. Halevy, E. Boblil, T. Elkayam, A. Weiss and K. Vogt, Safeguards Symposium, IAEA, October 2014, Vienna, Austria.

Table of Contents